Dissertation for the degree of Doctor of Philosophy

# High Throughput Phenotyping Methods of *Mentha arvensis* L. Grown under Various LED Lights

**Le Anh Tuan**

**Department of Agriculture Science**
**The Graduate School**
**Jeju National University**

**February 2024**

# High Throughput Phenotyping Methods of *Mentha arvensis* L. Grown under Various LED Lights

A Dissertation submitted to the graduate school of Jeju National University in partial fulfillment of the requirements for the degree of Doctor of Philosophy in Agricultural Science under the supervision of

**Young Suk Chung**

The dissertation for the degree of Doctor of Philosophy by

**Le Anh Tuan**

has been approved by the dissertation committee.

December 2023

| | |
|---|---|
| Chairman | Yong-Chull Jeun |
| Member | In-Jung Kim |
| Member | Jin-Hyun Ahn |
| Member | Jong-Eun Park |
| Member | Yong-Suk Chung |

**Contents**

## List of Abbreviations

2D: Two-dimensional

3D: Three-dimensional

ANN: Artificial neural network

Anth: Anthocyanin index

ARI1: Anthocyanin reflectance index 1

CCD: Charge-coupled device

CCI: Chlorophyll content index

Chl: Chlorophyll

CNN: Convolutional neural network

CRI1: Carotenoid reflectance index 1

CT: Computed tomography

CWSI: Crop water stress index

DBSCAN: Density-based spatial clustering of applications with noise

DCNN: Deep convolutional neural network

DW: Dry weight

ETR: Electron transport rate

EWT: Equivalent water thickness

Faster R-CNN: Faster region convolutional neural network

Flav: Flavonol index

FMC: Fuel moisture content

$F_v/F_m$: Maximal quantum yield of PSII

FW: Fresh weight

GCW: Guard cell width

GCL: Guard cell length

GCA: Guard cell area

HTP: High-throughput phenotyping

ICP: Iterative closest point

LA: Leaf area

LAI: Leaf area index

LED: Light-emitting diode

LiDAR: Light Detection and Ranging

LIF: Laser-induced fluorescence

LSD: Fisher's least significant difference

Mask R-CNN: Mask region-based convolutional neural network

MVS: Multi-view stereo

NBI: Nitrogen balance index

NDVI: Normalized difference vegetation index

NIR: Near-infrared

OCT: Optical coherence tomography

PA: Plant

PAM: Pulse amplitude modulation area

PCH: Plant convex hull

PLSR: Partial least squares regression

PMT: Photomultiplier tube

PPFD: Photosynthesis photon flux density

qN: Non-photochemical fluorescence quenching coefficient

qP: Photochemical fluorescence quenching coefficient

RDR: Reflectance difference ratio

RGB: red, green, blue

RWC: Relative water content

SD: Stomatal density

SFM: Structure from motion

Suc: Sucrose content

SPA: Stomatal pore apertures

Sta: Starch content

SVR: Support vector regression

TLA: Total leaves area

TPC: Total phenolics content

UAVs: Unmanned aerial vehicles

VIs: Vegetation indices

YOLO: You only look once

## List of Figures

## List of Tables

## 초록

LED (Light-emitting diodes)는 식물의 광형태학적, 생화학적 또는 생리적 반응을 유도하고 작물 생산을 증가시키기 위해 실내 재배에 널리 적용되어 왔다. 광은 식물의 품종, 처리 기간, 광도 및 스펙트럼에 따라 식물에게 다양한 영향을 미친다. 본 연구의 목적은 청색광과 적색광의 다른 비율이 *Mentha arvensis* L. (야생 민트)의 생장, 광합성 활동, 바이오매스 및 대사산물 축적에 미치는 영향을 조사하는 것이다. 이를 위해 본 연구는 여러 가지 고전적인 방법과 고처리량 표현 방법을 사용하여 최적의 야생 민트 생산을 위한 적절한 LED사용 방법에 대한 생장 모델링을 평가했다. 결과는 단일 청색광이 광합성의 빛의존적 반응에서 빛 에너지 흡수를 자극하고 화학 에너지로 전환시켰음을 보여주었다. 그러나 이 처리는 탄소 고정 반응의 생성물을 감소시켜 바이오매스 축적 및 야생 민트 식물의 발달을 억제했다. 반면, 단일 적색광에서 재배된 야생 민트 식물은 광반응 단계를 낮은 수준으로 유지하며 바이오매스 축적을 증가시키고 생장 속도를 향상시키며 형태 발달을 개선하는 경향을 보였다. 엽록소 함량 지수와 광계II의 최대 양자 수율 사이에는 강한 양의 상관관계가 있었으며, 이러한 특성은 광화학적 형광 소진 계수, 전자 수송 속도 및 플라보놀 지수와는 약한 양의 상관관계를 가지고 있었다. 본

연구는 또한 식물 대사산물과 질소 균형 지수, 생체중, 건물중, 자당 함량, 전분 함량 및 총 페놀 함량을 포함한 식물 대사산물 간에 강한 양의 관계가 있음을 발견했다. 그러나 기공 특성, 광합성 및 식물 대사산물 간에는 유의한 관계가 없었다. 이러한 결과는 *Mentha arvensis* L.의 광환경 변화에 대한 뚜렷한 생리학적 반응을 나타냈다. 특히 30%의 청색광과 70%의 적색광 스펙트럼의 조합은 야생 민트 식물의 광합성 생산성, 바이오매스 및 2차 대사산물을 크게 향상시켰다. 이 연구의 결과는 LED 기술이 야생 민트 재배 과정에서 선호하는 생리활성 물질의 생장과 축적을 조절하는 데 잠재력을 가지고 있음을 강조하며, 생산 수요를 충족하기 위한 실내 허브 재배 프로토콜의 개선에 기여될 수 있다.

**Abstract**

Light-emitting diodes (LEDs) have been widely applied in indoor cultivation to enhance crop production and induce targeted photomorphogenic, biochemical, or physiological responses in plants. The effect of light quality on plants varies depending on species, treatment durations, light intensities, and spectrum. The aim of this study was to investigate the impact of different ratios of blue and red LED light on growth, photosynthetic activity, as well as plant biomass and metabolite accumulation of *Mentha arvensis* L. (Wild Mint). To achieve this, the study employed several conventional and high-throughput phenotyping methods to evaluate growth modeling alternative LED light strategies for obtaining optimal Wild Mint production. The results showed that mono-blue LED stimulated light energy absorption and converted it into chemical energy in the light-dependent reactions of photosynthesis. Nevertheless, this treatment reduced the products of the carbon fixation reaction, thereby inhibiting biomass accumulation and the development of the Wild Mint plant. In contrast, Wild Mint plants grown under mono-red LED maintained the light reaction phases at a low level and tended to increase biomass accumulation, enhance growth rate, and improve morphology development. A strong positive correlation was found between the chlorophyll content index and the maximal quantum yield of photosystem II, these traits have a low positive correlation with the photochemical fluorescence quenching coefficient, electron transport rate, and the flavonol index. The study also found that plant metabolites have a strong positive relationship with plant biomass, including the nitrogen balance index, fresh weight, dry weight, sucrose content, starch content, and total phenolics content. However, no significant relationship was found between stomatal traits, photosynthesis, and plant biomass. These results revealed distinct physiological responses of *Mentha arvensis* L. to changes in light environments. Notably, the combination of a 30% blue and 70% red LED spectrum significantly enhanced photosynthesis productivity,

biomass, and secondary metabolites in the Wild Mint plant. The findings of this study emphasize the potential of LED technology in manipulating the growth and accumulation of desirable bioactive compounds during Wild Mint plant cultivation, contributing to the refinement of indoor herb cultivation protocols to meet production demands.

## Introduction

By 2050, the human population is predicted to reach 9.7 billion, which will require crop production to be double the present levels to meet the projected demand (Ray et al., 2013). However, the current agricultural output growth rate fails to reach the demanding growth. Furthermore, the productivity of up to 40% of crop cultivation land has been hibernated (Fischer and Edmeades, 2010). The greatest challenge to ensure global food security is climate change due to the increasing of carbon footprint, which leads to various adverse weather conditions (Altieri and Nicholls, 2013; Hunter et al., 2017). Global warming impacts are different depending on geographical regions, further complicating the effort of finding solutions. Developing countries are especially susceptible to the changing climate due to limited available resources as well as unproductive cultivation methods (Altieri and Nicholls, 2013). Therefore, the increasing of crop production requires targeted sustainable methods for different agro-ecological regions by adopting modern techniques for plant breeding, cultivation, and crop management (Chawade et al., 2018). The ultimate goal is to generate high productivity and tolerance crop cultivars in the target environments.

To improve plant yield and quality, studies investigating the association between genotypic and phenotypic information are crucial. The development of next-generation sequencing technologies has enabled the acquisition of high-resolution genetics information at lower cost. Obtaining plant phenotypic information with high-throughput and resolution and low cost has become a bottleneck to facilitate these studies. Plant phenotypes are results of the complex, multi-layer interaction between genotype and a multitude of envirotype (Xu, 2016). Therefore, comprehensive and accurate phenotypic information can provide insight into gene functions and regulatory networks as well as accelerated plant breeding pipelines (Cheng et al., 2020). In addition, the development of automated monitoring systems to determine plant health

is also important to ensure agricultural production. For both goals, field-based high-throughput phenotyping tools are required (Zhang et al., 2023). With the technological advances in imaging sensors, image analysis as well as machine learning, plant phenotypic traits include morphological, physiological and biochemical can be accurately acquired at various levels ranging from cell, tissue, organ and whole plants to field populations of plants (Jin et al., 2022).

## 1. History and development

The term 'phenotype' originated from the Greek phaeno and typos, which mean show and type respectively. Phenotype was described by Wilhelm Johannsen as "all types of organisms can be distinguished by direct inspection or with finer methods of measurement or description'' (Johannsen, 1911). In 1949, the term 'phenome' was first defined as a complementary with genome as the whole set of phenotypic entities expressed by a cell, tissue, organ, organism, or species (Davis, 1949). Phenotypic studies can be traced back to the 1990s in the context of studying complex human disease. The new discipline phenomics has been established as a key complement of genomics in order to identify the association between genes and clinical endpoints (Schork, 1997). Phenomics can be characterized as the systematic measurement and analysis of qualitative and quantitative traits, including clinical, biochemical, and imaging methodologies, for the refinement and characterization of a phenotype (Shahzad et al., 2022). In term of plant science, plant phenotyping refers to the set of methodologies and protocols for quantitatively evaluate plant's anatomical, ontogenetical, physiological and biochemical traits at various scales ranging from cells to even populations (Walter et al., 2015).

As the results of complicated interactions between genetics and external factors, crop phenotypes present as a challenge to accurately evaluate. The combining effects of genotypes and envirotypes influence plants on various levels, ranging from structural, functional to content traits. These internal properties are in turn expressed as crop external phenotypes such as

morphology, biomass, and productivity (Li et al., 2021). Crop phenomics research require the incorporation of various disciplines, including agronomy, life sciences, information science, math, and engineering sciences to discover multifaceted phenotypic information of plant growth and development in a complex environment.

Traditional phenotyping methods were based on the appearance, taste, and touch of the crop, which are time-consuming, labor-intensive and even destructive to sample large populations (Li et al., 2021). Phenotyping efficiency has been highly recognized as the key factor that restricts the progression of applied genetics, especially in different environments (Guzman et al., 2015). Moreover, conventional phenotyping fails to apprehend physiological and biochemical properties in term of plant basic mechanisms, which can provide insight into patterns of genetics and biology. Hence, to address these limitations, various automated high-throughput phenotyping platforms with the assist of technological advances have been developed since 2000 and became common tools in commercial or research teams. These phenotyping systems, in combination with artificial intelligence, have largely overcome the problems of traditional methods. The novel tools provide advantages with respect to levels of throughput, resolution, cost as well as applicability under various field conditions.

A high-throughput phenotyping platform is a combination of a data acquisition equipment, a control terminal, and a data analysis platform (Xiao et al., 2022). Phenotypic data are mainly obtained through non-invasive imaging and spectroscopy techniques for quantitative studies of complex traits, such as growth, tolerance, resistance, architecture, physiology, yield, and the basic measurement of individual quantitative parameters that form the basis for more complex traits (Chen et al., 2014; Li et al., 2014). One of the first high-throughput phenotyping platforms is the PHENOPSIS, which was developed in 2006 by Apilogic for *Arabidopsis thaliana* (Granier et al., 2006). Another example is the in-house GROWSCREEN system (Walter et al.,

2007) that was used for analyzing phenotypes of different plant species. Both systems used a camera that is moved over the plants to capture images. Other platforms targeting various plant species were also developed, including LemnaTec 3D Scanalyzer system for rice (*Oryza saltiva*) (Hairmansis et al. 2014); HyperART for barley (*Hordeum vulgare*), maize (*Zea mays*), tomato (*Solanum lycopersicum*) and rapeseed (*Brassica napus*) (Bergsträsser et al. 2015); PhenoBox for *Brachypodium* and tobacco (*Nicotiana tabacum*) (Czedik-Eysenberg et al. 2018) or PhénoField for wheat (*Triticum aestivum*) (Beauchêne et al. 2019). Besides, phenotyping techniques have also been developed for different targets, such as micro-computed tomography (micro-CT) imaging and microscopic imaging for cells and tissues (Faulkner et al., 2017; Mele and Gargiulo, 2020; Zhang et al., 2021), visible light imaging or X-ray imaging for seeds (Baek et al., 2020; Ligterink and Hilhorst, 2017; Medeiros et al., 2020), near-infrared spectroscopy and time-domain pulsed nuclear magnetic resonance (NMR) for biochemical contents (Anderson et al., 2019; Jasinski et al., 2016; Melchinger et al., 2018). The characteristics and potential applications of high-throughput phenotyping techniques at organs, individual plant and canopy have also been well documented (Yang et al., 2013; Zhang Y and Zhang N, 2018).

In addition to imaging techniques, other methods were also applied for plant phenotyping, including positron-emission tomography (Brezovcsik et al., 2020; Qu et al., 2016) or microwave resonator (Dadshani et al., 2015; Sydoruk et al., 2016). Moreover, high throughput phenotyping techniques can also be used in combination for providing more comprehensive and accurate results. Some examples include the combination of RGB (red, green, blue) camera with various sensors for yield estimation (Herrero-Huerta et al., 2020; Maimaitijiang et al., 2020) and biochemical and biophysical parameters quantification (Maimaitijiang et al., 2017). Generally, high-throughput phenotyping tools provide a large set of data for accurately and efficiently evaluating plant performances. The obtained data can be extracted/processed using

various algorithms. With the advancement of computer technology development, deep learning presents outstanding advantages on a wide range of plant phenotyping tasks. Detailed information of applying deep learning in plant phenotyping can be found in several previous reviews (Mochida et al., 2019; Singh et al., 2018). It is foreseeable that applying deep learning in plant phenotyping is an inevitable trend, and there will be more research in this field in the future.

## 2. Photosynthetic and high-throughput photosynthetic

The global carbon cycle is a key aspect of life, which generally comprises of carbon reservoirs (stocks) and the dynamic transfer of carbon between them (fluxes) (Green and Byrne, 2004). Plant photosynthesis represents the major flux that drives global carbon cycle (Friedlingstein et al., 2019). Photosynthetic activities extensively depend on various factors, including plant species, plant functional types, plant development stages or the external conditions (Beer et al., 2010). As the natural process to convert water and $CO_2$ into biomass by utilizing light energy, photosynthesis plays a crucial role in plant productivity. Previous studies on the mechanism of photosynthesis have resulted in key insights that photosynthesis was inefficient at leaf to canopy scales. Particularly, the conversion rates of the intercepted radiation into biomass for both C3 and C4 crop species were found to be only a fifth of the theoretical maximum (Zhu et al., 2010). Therefore, improving photosynthesis has been considered as a promising strategy for increasing crop production to meet the global demand (Long et al., 2015; Ort et al., 2015). For this purpose, accurate and rapid techniques to characterize variations of photosynthetic capacity over a range of spatial and temporal scales are of importance.

Traditionally, photosynthetic activities are quantified by gas exchange techniques at the leaf level, which are found to be low-throughput, time-consuming and labor-intensive. Furthermore, agronomic traits are based on canopy-scale processes and therefore require

canopy-scale measurements (Fu et al., 2022). High-throughput phenotyping tools, which can overcome the limitations of traditional methods for evaluating photosynthesis in the context of crop breeding, have emerged as potential solutions (Furbank et al., 2019). Various high-throughput phenotyping platforms, either with indoor or outdoor settings, have been developed to address the limitations of conventional methods (Bai et al., 2019; Bandopadhyay et al., 2020; Meacham-Hensold et al., 2020; Salter et al., 2018; Zhang et al., 2020). These platforms employed sensor-based non-invasive phenotyping to characterize plant growth and photosynthesis over time. Commonly used sensors including RGB (red, green, blue), hyperspectral, thermal, and fluorescence sensors while monochrome sensors, Raman spectroscopy, and tomographic sensors are less frequentetly used (Tanner et al., 2022). These phenotyping tools have greatly facilitated the mechanistic understanding of photosynthetic physiology and the improvement of productivity via photosynthesis (Siebers et al., 2021). In this section, we provide an overview of the current development of high-throughput photosynthetic phenotyping techniques and their application in plant breeding pipelines.

### *2.1 Morphological traits in leaf*

As the primary photosynthetic organs in plants, the leaves are optimally designed and adapted for photosynthesis to occur. Via photosynthesis, leaves convert absorbed light energy into organic matters and generate resources required for plant metabolism. Hence, leaves play crucial roles in determining the growth rate and health conditions of the plants. Leaf morphological traits include area, inclination angle, number, thickness, and phenology. The leaf morphology varies greatly as the results from both internal (genotype) and external (environmental) factors (Zhang et al., 2023). Leaf morphological features directly influence whole-leaf photosynthesis through effects on light capture at the leaf surface, as well as via its propagation and attenuation within the leaf. Therefore, leaf morphology is considered as an

important factor to evaluate plant photosynthetic capacity.

Leaf area is a major morphological trait that influences crop productivity and economic values, especially for species whose leaves are the end products. Leaf area can be studied at different scales, varying from a single leaf to a whole plant population. A common parameter for studying leaf area is the leaf area index (LAI) – the ratio of the total leaf area of a plant population to the land area it covers (Fang and Liang, 2008). LAI reflects the total leaf size, canopy structure as well as light energy utilization, which can be employed to estimate plant growth and yield (Duchemin et al., 2008; Gaso et al., 2021). Single leaf area can be easily obtained by several techniques. One of the simplest methods is employing two-dimensional (2D) imaging and a reference object of known size to estimate the leaf area of a single leaf (Guo et al., 2014). The most accurate leaf-area prediction model was based on the combination of two parameters leaf length and leaf width (Fanourakis et al., 2021). Multiple advancements can also be applied to improve the accuracy of leaf area estimation. For example, a visible-light imaging system accompanied by a power-function model can be used to predict leaf area from side view average projection area (Jiang et al., 2015). The accuracy of this model was evaluated by investigating the influence of various factors, including side view projections, top view projections area, texture, and morphological features.

Three-dimensional (3D) models can also be employed to address the limitations of 2D images such as leaf curl or camera view angle. The 3D point clouds are generated from acquired plant images using various types of cameras including visible light camera (Su et al., 2019), RGB-D (Red, Green, Blue-Depth) camera (Yau et al., 2021), and LiDAR (Berk et al., 2020; Li and Xue, 2023). The methods for constructing 3D point clouds include structure from motion (SFM) (Itakura and Hosoi, 2018), multi-view stereo (MVS) (Li et al., 2020) and iterative closest point (ICP) (Hosoi and Omasa, 2015), which serve for different types of cloud construction.

Preprocessing steps such as filtering and de-noising (depth threshold or statistical filtering) on the reconstructed 3D point cloud is commonly carried out to optimize the cloud (Zhang et al., 2021). From this, a single leaf can be clustered and segmented. Common algorithms for point-cloud clustering and segmentation include K-means clustering (Zhang et al., 2021), region growth (Li et al., 2020), density-based spatial clustering of applications with noise (DBSCAN) (Xu et al., 2020), and watershed algorithm (Itakura and Hosoi, 2018). Finally, the leaf surface is built using Delaunay triangulation (Zhang et al., 2021), least squares (Hosoi and Omasa, 2015) and other methods. The leaf area is measured by the surface grid of the reconstructed leaf grid model from the point clouds.

Estimation of the total leaf area for a group of plants, which usually based on LAI, required a more complicated set up and model. LAI values can vary depending on factors such as vegetation types, canopy structures and environmental conditions. For estimating LAI, remote sensing imaging technology is widely employed. The popular systems include unmanned aerial vehicles (UAVs) or manned aircraft carrying imaging sensors, satellites data or laser scanning, which provide different utilities and limitations that can be applied for various schemes or purposes. Several satellites have been used for this purpose such as the Sentinel-2 (Kaplan and Rozenstein, 2021) or the Landsat 5 TM and 7 ETM+ (Kinane et al., 2021). The imaging instruments are also flexible based on the field conditions, the weather and other factors to optimize the model and reduce the errors while obtaining images. Many researchers have employed UAVs due to their advantages of flexible operation and low cost compared to the manned aircraft or satellite systems. The UAVs are accompanied by one or various imaging sensors such as RGB (Liu et al., 2021a; Sakar et al., 2021), multispectral (Liu et al., 2021a;b) and thermal cameras (Liu et al., 2021a; Wang et al., 2021) to acquire plant canopy images containing color, spectral and thermal information. Prediction models will be established based

on the obtained imaging data using several methods such as multiple linear regression, artificial neural network (ANN) (Sakar et al., 2021), random forest (RF), extreme gradient boosting (XGBoost) (Liu et al., 2021b; Zhang et al., 2021), partial least squares regression (PLSR), support vector regression (SVR) or deep learning (Liu et al., 2021a).

One of the most commonly used vegetation indices (VIs) for estimating LAI is the normalized difference vegetation index (NDVI). NDVI quantifies vegetation by measuring the difference in absorption/reflection rate between the near-infrared light that vegetation strongly reflects and the red light that vegetation strongly absorbs (Rulinda et al., 2012). The canopy reflectance is strongly affected by various factors such as the growth stages, the canopy structure, the leaf inclination angle or the leaf surface characteristics. Therefore, some imaging systems require the application of radiometric correction to calculate the true reflectance of plants. For plants species with varying phenological traits during different growth stages, phenology highly affects LAI estimation, which lead to the establishment of phenology-specific models (Zhang et al., 2023). 3D point clouds can also be applied for measuring LAI of plant populations. A previous study has employed UAVs carrying RGB and multispectral cameras to obtain imaging data at various angles and calculate the LAI of the forest canopy from the generated 3D point clouds (Lin et al., 2021).

In addition to multispectral imaging, hyperspectral cameras are also useful for estimating LAI. The high-resolution images obtained by hyperspectral imaging sensors provide rich and complex hyperspectral information from a wide range of wavebands that can be used to construct prediction models for LAI (Huang et al., 2022; Jiang et al., 2022). Compared to multispectral images, hyperspectral images contained more data regarding vegetation indices to be extracted. In exchange, these advantages also negatively affect the accuracy and efficiency of the LAI due to the presence of low correlation indices among the full data set (Zhang et al.,

2023). A method to avoid this limitation is employing feature band selection, which has been proved to effectively improve the accuracy of the estimation model (Jiang et al., 2019).

Another important leaf morphological trait that can be measured using high-throughput phenotyping techniques is the leaf inclination angle. This trait is determined as the angle between the leaf axis and the horizontal. The leaf inclination angle directly controls the amount of light that can be absorbed by the leaf, therefore affecting plant growth and biomass production (Hu et al., 2019). Factors that govern the leaf inclination angle include the shape, size, softness, and curvature, which lead to the diversity of methods to measure this trait. Depending on plant species, the leaf angle can either be directly determined from side-view captured images or estimate with several leaf features in consideration (Zou et al., 2014).

Quantification of plant leaf angle mainly involves measurement in 3D space, which is based on the 3D point clouds of leaves. The workflow and methods for constructing 3D point clouds are similar to that for measuring leaf area. From the constructed leaf surface, the leaf inclination angle can be extracted by calculating the ratio of a single leaf to the leaf area (Zhang et al., 2021), finding the angle between the leaf normal and the z axis (Hosoi and Omasa, 2015; Li et al., 2020; Xu et al., 2018) or using a voxel-based 3D image processing method (Itakura and Hosoi, 2018).

The number of leaves is one of the key visual traits that indicate the plant's current status and growth stages (Dobrescu et al., 2017). High-throughput phenotyping techniques based on modern imaging technology and machine learning provide high-precision, time- and labor-saving methods for leaf counting. Existing leaf counting methods can be divided into two categories: deep learning and image processing. While image-based leaf counting must face the problems of leaf occlusion and uneven in situ growth of the leaf, employing deep learning can extract the intrinsic information from plant images despite the complex structure (Fan et al.,

2022). Several commonly used deep learning models for estimation of plant leaf number include the convolutional neural network (CNN) (Jiang et al., 2019), Faster R-CNN (Miao et al., 2021; Zhou et al., 2021), Mask R-CNN (Lou and Lv, 2022; Zhou et al., 2021) or deep convolutional neural network (DCNN) (Praveen Kumar and Domnic, 2020) models. Target species for the current leaf counting models are mainly corn (Jiang et al., 2019; Lou and Lv, 2022; Miao et al., 2021; Zhou et al., 2021), sorghum (Miao et al., 2021) and rosette plants (Praveen Kumar and Domnic, 2020; Ubbens et al., 2018).

The use of deep learning for leaf counting is mainly based on RGB, fluorescent or near-infrared (NIR) imaging. The network is applicable for a variety of plant species and field conditions (Giuffrida et al., 2018). Basically, there are two ways to obtain leaf numbers using deep learning: (1) directly counting as a holistic regression problem or (2) estimation as a sub-product from leaf detection and segmentation (Fan et al., 2022). For direct counting method, the machine learning based regression model only requires the leaf number annotations, which is easier compared to the segmentation-based methods. Various counting frameworks have been proposed, which employed different deep learning models and data collection (Dobrescu et al., 2017; da Silva and Goncalves, 2019; Ubbens et al., 2018). Beside these methods, several segmentation-based methods for leaf count have also been developed (Aich and Stavness, 2017; Kumar and Domnic, 2019; Ren and Zemel, 2017; Romera-Paredes and Torr, 2016). However, for segmentation or detection-based method, only successfully segmented leaves can be counted, which will result in reduced accuracy in case of imperfect detection/segmentation. This limitation can be solved by employing segmented binary images to guide the learning of leaf counting, which will not count directly from segmented image (Fan et al., 2022). Detailed information regarding two approaches can be found in previous literature (Buzzy et al., 2020; Fan et al., 2022; Lu et al., 2021).

Leaves' thickness reflects the influence of environment on plants, which leads to the diversity phenotype among species, regions and altitudes. Leaf thickness is determined by plant anatomy, including the number, size, and arrangement of leaf cells (Afzal et al., 2017). Thick leaves are better in maintaining water potential under limited water supply, which is tightly associated with plant survivability under arid, high-irradiance environments (Poorter et al., 2009). Measurement of leaves thickness provides plant stress monitoring, which allows timely management for better plant growth and development (Zhang et al., 2018). Despite its importance, leaves thickness could not been measured effectively due to the complex, time-consuming and labor-intensive nature of the conventional methods. This morphological trait can only be obtained frequently in recent studies due to the advancement of imaging technologies.

Tomography-based methods are commonly used for estimating leaves' thickness. For example, soybean leaf area and thickness were measured using computed tomography (CT) (Pfeifer et al., 2018). Another example is the application of optical coherence tomography (OCT) – a newly developed imaging technology for estimating leaf thickness on the basis of 3D OCT images of biological tissues (de Wit et al., 2020). Beside tomography, several other methods have also been applied in predicting/measuring leaf thickness, such as partial least squares regression (Buitrago et al., 2018), digital thickness gauge (Ahn et al., 2020) or magnetic field sensor (Afzal et al., 2017).

Beside the aforementioned morphological traits, plant phenology is another important factor that affects plant growth and development. Plant phenology refers to the timing of plant life cycle events such as leaf bud burst, flowering, and fruiting (Stucky et al., 2018). Plant phenology is tightly associated with carbon, nutrients, and water availability, reflecting plant adaptation to external and climatic changes. The advancement in technologies has provided the

foundation for the development of plant phenology prediction models. These models are useful for seeking insight regarding the relationship between various factors and phenology (Anderson et al., 2016; Lei et al., 2013; Xie et al., 2018). The current status of phenology research based on modern imaging sensors and data processing has been carefully reviewed in a previous study (Zhang et al., 2023).

### *2.2 Leaf biomass*

One of the ultimate goals of plant biological research is to generate new cultivars with improved performance and yield under various external conditions. In this regard, the leaf biomass is a crucial trait, which indicates the plant growth rates and net production. Study on leaf biomass can be traced back to the 1980s, when soybean leaf biomass was assessed using spectral data (Holben et al., 1980). From then, several models/methods have been proposed, aiming to evaluate this performance-related trait in both woody plants (Le Maire et al., 2008; Mediavilla and Escudero, 2003) or crop species (Friedl et al., 1994; Giltelson et al., 2003). The development of new imaging technologies as well as imaging/data processing methods has enabled the high-throughput evaluation of leaf biomass in a high-precision, time- and labor-saving manner.

There are several methods that can be employed for leaf biomass estimation, depending on the requirement of the study. One of the most used methods is the estimation of biomass based on normalized difference vegetations index (NDVI), which can be obtained from hyperspectral imaging sensors. This method has been applied for a wide range of crops, including maize (Gitelson et al., 2001), wheat (Serrano et al., 2000) and soybeans (Kross et al., 2015).

### *2.3 Leaf pigment contents*

The leaf comprises of various pigments such as chlorophyll, carotenoid, or anthocyanin,

among which chlorophyll is the main pigments for photosynthesis. Chlorophyll mediates leaf light energy absorption, thus directly affecting the plant photosynthetic rate (Gao et al., 2018). Furthermore, chlorophyll can also indicate the plant health status, as this type of pigment tends to be degraded under stressful conditions (Li et al., 2021). Therefore, the leaf chlorophyll content is an important physiological trait for monitoring plant growth and development as well as yield prediction. Traditional techniques for estimating chlorophyll contents include spectrophotometry and chlorophyll meter. Spectrophotometry measures the absorbance of chlorophyll of grinding samples in a specific wavelength range, which is destructive, complex and inefficient. On the other hand, chlorophyll meter can only provide data at a certain point of the leaves and requires the average value from multiple measurement in various parts of the leaves to obtain a representative chlorophyll content value. Additionally, these methods are impractical on large scales and in field conditions. Therefore, various techniques employing modern technology have been developed to quickly, accurately estimate chlorophyll contents at different scales in a non-destructive manner.

RGB imaging, PLSR or ridge regression have been proved to be reliable methods for measuring leaf chlorophyll content based on the color features of captured images. Several studies on different plant species such as apple (Cheng et al., 2017), lettuce (Pérez-Patricio et al. 2018), tomato (Sun et al., 2019) or sorghum (Zhang et al., 2022) have successfully employed these methods. Multi-angle imaging and a stable light condition can greatly enhance the accuracy of chlorophyll estimation from image data, as these factors directly influence the obtained images (Pérez-Patricio et al. 2018).

One-dimensional spectral data is also useful for determining leaf chlorophyll contents. The common technique is building a prediction model based on spectral information. Though spectral imaging technology can provide comprehensive and rich information regarding leaf

phenotype, spectral preprocessing is required to solve issues such as noise and spectral baseline shift. Employing feature band extraction algorithms (Jiang et al., 2022) or second derivative-partial least squares regression (2-Der-PLSR) (Wang et al., 2019) proved to significantly improve the prediction performance in estimating leaf chlorophyll content. Several external factors that can affect spectral-based chlorophyll content prediction models include soil, light, and leaf structure. The impacts of these factors can be effectively diminished by utilizing vegetation indices obtained from two or more corresponding spectral bands. Vegetation indices reflect the essential characteristics of the spectra that vary depending on different pigment classes, which is able to reduce large volume of data into a single viable value (Hallik et al., 2017). Employing vegetation indices in chlorophyll prediction model has shown to be more effective compared to single relevant band prediction model (Guo et al., 2019; Zhang et al., 2021).

Beside the aforementioned factors, leaf morphological traits such as leaf inclination angle and leaf surface characteristics can also affect the reflectance spectrum of plant leaves. The reflectance difference ratio (RDR), the improved MDATT index (IMDATT) and other indexes have been employed to overcome the impacts of these factors on chlorophyll content linear regression model (Li et al., 2019; Zhao et al., 2019). Vertical leaf position is another factor that needs to be considered in chlorophyll content prediction model. Generally, chlorophyll content is positively correlated at first and then negatively correlated with the increase of leaf positions. This is due to the shading effect of upper layer leaves on the bottom layer, as well as the fact that the leaves in the top layer are not fully developed. Therefore, it is necessary to study plant chlorophyll content in the context of leaf vertical distribution. Wu et al. (2021) employed a hyperspectral system that collects spectral information from various angles. The obtained data is used to estimate the correlation between vegetation indices and the leaves vertical positions,

which can provide insight into the optimal monitoring angle for predicting chlorophyll content of different leaf layers at various growth stages.

Due to plant complex and diverse 3D morphology, plant phenotypic information can be obtained more accurately using 3D point clouds. However, conventional 3D point clouds of plants only provide color and coordinate information, which cannot be employed to effectively estimate chlorophyll content. To address this limitation, Sun et al. (2019) proposed a combined system of RGB, depth and multispectral images of plants at different angles. The obtained data is used to construct a multispectral 3D point cloud, which provides vegetation indices information to establish a prediction model for leaf chlorophyll content in a spatial distribution context.

Remote sensing technology displayed advantages over ground-based imaging technology, as they often have higher throughput and flexibility in a wide range of time and space. Satellite remote sensing and UAV remote sensing are the two most commonly used technologies for measuring plant chlorophyll content. These technologies can be combined with various imaging sensors, including multispectral camera (Ali et al., 2020; Li et al., 2018; Xu et al., 2021), RGB camera (Li et al., 2018) and hyperspectral camera (Cao et al., 2020; Hoeppner et al., 2020) coupled with various platform/models to provide reliable prediction on chlorophyll content.

Finally, chlorophyll information can also be obtained from chlorophyll fluorescence signals, which were measured based on pulse amplitude modulation (PAM) technologies. Chlorophyll fluorescence information is obtained in a light environment to estimate photochemical and non-photochemical quenching. This method has also been widely used in measuring chlorophyll content (Campbell et al., 2021). Overall, chlorophyll prediction models can be constructed from various types of data depending on the purpose and availability of the study.

Besides chlorophyll, high-throughput phenotyping systems are able to provide information regarding other leaf pigments. By employing different VIs such as anthocyanin reflectance index 1 (ARI1) and carotenoid reflectance index 1 (CRI1), the content of various pigments in leaves can be accurately estimated using similar manner as chlorophyll content (Tayade et al., 2022).

*2.4 Leaf water content*

Leaf water content reflects the water status of the leaves, which can govern the plant growth environment and soil water potential. Furthermore, water supplies electrons for the light reaction during photosynthesis. Leaf water content therefore can provide important insight into plant current health and final yield. Leaf water content is conventionally calculated the difference between leaves fresh and dried weights. Other indicators are for leaf water content include relative water content (RWC), equivalent water thickness (EWT), fuel moisture content (FMC) and crop water stress index (CWSI) (Zhang et al., 2023).

Hyperspectral imaging is one of the most common techniques for estimating leaf water content. Hyperspectral sensors are able to capture thousands of bands per pixel, ranging from the visible (400-700 nm), near infrared (700-1000 nm) to short-wave infrared (1000-2500 nm), providing comprehensive information regarding leaf phenotypes (Ge et al., 2019). Currently, hyperspectral-based high-throughput phenotyping systems focus on identifying different VIs by combining multiple spectral. Though requires complex preprocessing steps to filter the viable data, hyperspectral imaging produces normalized difference vegetation index (NDVI) values that are effective for checking the leaf water content. This method has been employed to study leaf water contents in various plant species, including cotton (Yi et al., 2013), soybean (Kovar et al., 2019), wheat (Yang et al., 2021) or maize (Gao et al., 2019). By combining image and spectral information, parameters that are highly correlated with plant leaf water can be

identified. For example, canopy structure (Zhu et al., 2019), leaf parts (Murphy et al., 2019) or leaf vertical positions (Kong et al., 2021) were found to affect the accuracy of leaf water content prediction models.

Previous studies indicated that leaf water spectral absorption has higher sensitivity in the infrared bands than other bands (Jin et al., 2017; Torres et al., 2019). Therefore, infrared imaging is also widely employed, providing an effective, real-time and non-invasive monitoring method for leaf water content in plants. For example, NIR signals were found to be proportional with water content in barley (Chen et al., 2014). Another study constructed a prediction model of leaf water content based on leaf spectral reflectance in SWIR domain (Zhang et al., 2019). Overall, NIR imaging enables rapid, non-destructive analysis of leaf water content, providing essential information for monitoring vegetation growth and forecasting final productivity.

Another commonly used technique in leaf water content studies is thermal imaging (or infrared thermal imaging). This method generates the image based on radiation emitted by the object, which is proportional to the object's temperature. Thermal sensors can detect changes in leaf temperature caused by transpiration, therefore estimating temperature-related features such as water content (Ishimwe et al., 2014). Various studies have employed this method to effectively predict leaf water content in different plant species (Arshad et al., 2018; Swain et al., 2012; Ullah et al., 2014).

Beside the aforementioned methods/techniques, some new approaches are also proposed for measuring leaf water content (Farinas et al., 2019). For example, leaf water status can be reliably predicts using linear regression model based on $\tau \cdot LA$, which are estimated by THz-QCL and RGB image respectively (Pagano et al., 2019). Data from THz-QCL can also be used to determine other water-related leaf traits such as the leaf water layer or RWC (Li et al., 2020).

### *3.5 Leaf stomatal traits*

Stomata are the specialized gates present in the epidermis of plant cells, through which plant leaves exchange gases with the environment. Stomata plays an essential role in plant growth and development by regulating the balance between leaf water status and carbon fixation. Factors that affect stomata activities include morphology, density, and sensitivity to external stimuli (Lawson and Matthews, 2020). Stomata are dynamically regulated by various external factors such as drought, heat, salinity, light. In nature, stomata display diversity morphology and characteristics depending on the plant species (Franks and Farquhar, 2007), which enable plants to adapt to a wide range of environmental conditions (Liu et al., 2018; Liu et al., 2022). Given the current global climate changes, stomata flexibility made them primary targets for improving crop survivability and productivity.

Traditional approach to determine stomatal traits involving tissue collection and imaging following by manually phenotyping traits of interest. The most commonly used method for stomatal phenotyping is the nail polish method, which is extremely time-consuming, costly and impractical in large populations. This method requires applying nail polish on the leaf surface, drying and carefully peeling off the polish to get the leaf imprint, following by examining under a light microscope for images to determine stomatal traits. Beside the prolonged process, the nail polish method also presents several limitations that can negatively affect the accuracy of phenotyping process such as the unavoidable presence of air bubbles that interfere with stomata imaging (Millstead et al., 2020). Altogether, stomatal phenotyping using leaf imprints is time-consuming and inconsistent, which limits the maximum number of samples that can be analyzed together and prevents this method from being employed for large mapping populations or diversity panels (Pathoumthong et al., 2023).

To address the issues with conventional methods, several new techniques have been

introduced. To reduce the time taken for samples imaging, many researchers currently employed simple light-field or other manual stage microscopes (Fetter et al., 2019; Jayakody et al., 2017). These technologies are sufficient to examine small numbers of stomata. However, major drawbacks of these approaches include the limitations in leaf area for imaging and the requirement of manual operation for refocusing the microscopes. Therefore, fast imaging methods requiring minimal manual effort are of necessity. For example, Millstead et al. (2020) has proposed the automatic microscope slide scanner to image nail polish imprints. This technology allows the rapid collection of high-quality images from entire samples with minimal manual effort. Another example is the application of optical topometric for a rapid and non-destructive measuring of leaf surface at nanometer scale (Ferguson et al., 2021; Xie et al., 2021). The obtained images will undergo several image processing steps before being used to extract stomatal traits. Additionally, thermal or spectral imaging can also be employed to monitor stomatal activities. Overall, there are still limitations present in current imaging technologies for stomata phenotyping and the development of new approaches for data collection would greatly facilitate stomata-related studies.

Besides imaging technologies, machine learning is being exploited to automatically analyze stomatal features. Though displays low explanatory power, machine learning tends to provide more accurate estimations (Houshmandfar et al., 2021). There are two types of machine learning models: supervised and unsupervised learning. The basic difference between the two categories is the requirement of data labeling. Therefore, supervised learning is often used in various regression and classification problems, while unsupervised learning is employed for identifying outliers and classification (Zhang, 2023). Due to their different natures, supervised learning is the most prevalent method for agricultural research. A supervised learning model basically begins with the model training for automatic feature extraction from preprocessed raw

images. Subsequently, the trained model can identify, classify, quantify, and predict the phenotypic traits of interest (Singh et al., 2018). In terms of stomata phenotyping, the input images were first labeled as stomata and/or pavement cells and randomly split into a training set for model training and validation. Various types of algorithm can be used to build accurate stomata detection models, such as general one-stage object detection algorithms, single shot multiBox detector (SSD, Sakoda et al., 2019) and you only look once (YOLO, Casado-García et al., 2020), and two-stage object detection algorithm, real-time object detection with Faster R-CNN (Li et al., 2019) and mask region-based CNN (Mask R-CNN, Bheemanahalli et al., 2021). These models have been successfully employed for stomata studies in different plant species such as rice, soybean, wheat, maize, or sorghum.

Machine learning-based methods for stomata phenotyping significantly reduced the required time and labor compared to conventional methods. Several studies have indicated the strong correlations between predicted results from machine learning and manual measurements across species. For example, the computer-predicted values of stomata traits in maize displayed positive correlation with those manually obtained results (Xie et al., 2021). Another study on sorghum also indicated the significant association between manual and predicted measurements of stomatal complex area (Bheemanahalli et al., 2021). These results suggested the reliability and accuracy of automated computer predicted methods. However, machine-learning based stomata phenotyping is currently limiting to one species in isolation, and a comprehensive practical model for predicting stomata across different plant species is required.

### *2.6 Chlorophyll-a fluorescent*

Chlorophyll (chl) fluorescent is defined as the emission of photons from excited chl a molecule. Chl fluorescent is widely used as an indicator of energy conversion in photosynthetic organisms such as plants, algae, and bacteria. After being hit by a photon, chl molecules absorb

the light energy and enter excited state, which is very unstable and require the releasing of excess energy. There are three different competing ways for chl a molecule to return to a non-excited state, including heat dissipation, photochemical utilization of energy and fluorescence emissions. Depending on the physiological status of the photosynthetic apparatus, the contribution of each process will vary (da Silva et al., 2007). The advancement of technologies has facilitated chl fluorometry developing into various types, which can basically divide into passive and active chl fluorescent (Candrero-Mateo et al., 2016). Passive methods measure emission under actinic light, while active methods stimulate fluorescence emission using dedicated light sources. Active fluorescence techniques are the prevalent methods for studying fluorescence emission spectra.

One of the most commonly used active fluorescence techniques is laser-induced fluorescence (LIF). In LIF, samples enter an excited state with a laser, and the emitted fluorescence is subsequently captured by a photodetector. Depending on the laser and detecting systems, LIF can be categorized into excitation and emission LIF. The fluorescence emission when samples return from excited to non-excited state is detected by a photomultiplier tube (PMT). In excitation LIF, a tunable laser is used to produce various excitation wavelengths, which enable the resolve of vibrational structure of the excited state. A bandpass filter is required in excitation LIF to remove scattered laser light before emission detection by PMT. On the other hand, emission LIF employed a fixed pump wavelength, and a monochromator is utilized to analyze sample emission in the detection wavelength. LIF can be conducted remotely, hence preferably used for phenotyping in the field. LIF was applied in various plant studies for different purposes, such as estimating overall photosynthetic activities during a defined period of time (Astafurova et al., 2001; Zuev et al., 2009), differentiating plant species (Richards et al., 2003; Saito et al., 2000) or estimating the maturity (Brach et al., 1977).

Active fluorescence employing PAM techniques allows the estimation of various photosynthetic-related traits such as the quantum efficiency of photosystem II, the electron transport rate or the non-photochemical quenching. PAM fluorometry can distinguish between the photochemical (qP) and non-photochemical use of light energy using the light-doubling technique (da Silva, 2016). PAM fluorometry measures basal fluorescence ($F_0$) with a weak pulse of light, followed by saturating light to establish the maximal fluorescence ($F_m$). The effective quantum yield of photosystem II can be estimated using the fluorescence index $\Delta F/F_m$, which indicate the difference between the maximum fluorescence and the steady-state fluorescence of light-adapted samples (Genty et al., 1989). The physiological status of the photosynthetic apparatus directly affects $F_0$ value, and this dependent relation is also affected by external factors (Serôdio et al., 2001). Healthy leaves of various plant species were found to have a very constant $F_v/F_m$ value of approximately 0.832 ± 0.004 (Bjorkman and Demmig, 1987). PAM was widely applied in various plant species including crops, such as maize (Stefanov et al., 2022), rice (Jiang et al., 2023), wheat (Jia et al., 2023) or lettuce (Kumar et al., 2021).

Another variation of PAM fluorometry is the imaging-PAM fluorometry that has been applied widely in plant phenotyping. Conventional and imaging PAM techniques employed different technologies to detect fluorescence signal. While normal PAM fluorometry uses a photodiode or phototube, a charge-coupled device (CCD) camera is used in imaging-PAM fluorometry. Depends on the purpose, imaging-PAM fluorometry can measure PS II photochemical efficiencies at the microscopic level (Oxborough and Baker, 1997; Oxborough et al., 2000) or mapping of fluorescent parameters over large areas (Hill et al., 2004; Scholes et al., 1996). As chlorophyll fluorescent techniques play a major role in plant phenotyping, various commercial flatforms have been introduced to provide high-throughput phenotyping

capabilities for plant breeders. Some notable flatforms include LemnaTec (Germany) or Photon System Instruments (Czech Republic).

Various high-throughput phenotyping (HTP) methods are being developed so far. The current study reviewed recently developed HTP methods and platforms for screening traits related to photosynthesis that play a pivotal role in determining crop production. This would be helpful to those who are interested in researching photosynthesis for enhancing crop yield.

## Chapter I. *Mentha arvensis* L. growth under different combinations of LEDs light

### 1. Introduction

Mentha species, a member of the Lamiaceae family, is one of the most ancient and widely beloved herbs globally (Bahadori et al., 2018; Fatih et al., 2017). It was originally described and first named in 1789 by Jussieu, who assigned it to the Lamiaceae family (Fatih et al., 2017). Among five basic Mentha species, *Mentha arvensis* L. commonly referred to as Corn Mint, Wild Mint, or Field Mint, is a renowned herbaceous, with a remarkable ability to adapt to diverse environmental conditions from temperate regions of Europe and western and central Asia, east to the Himalayas and eastern Siberia, and North America (Ellis, 1960; Fatih et al., 2017; Rehman et al., 2016). Leaves of *Mentha arvensis* L., which are a rich source of essential oils, are central to its distinctive aroma and flavor profile. In traditional medicine systems, *Mentha arvensis* L. has been esteemed for its therapeutic properties, including its role in alleviating digestive discomfort and its potential as an anti-inflammatory and analgesic agent. Nowadays, *Mentha arvensis* L. is of huge economic value and is widely used in the food, pharmaceutical, beverage, perfume, cosmetic, and tobacco industries (Dar et al., 2014; Naeem et al., 2012; Rao, 1999; Rashid et al., 2023).

Since the early 20th century, when human knowledge of photosynthesis began (Rabinowitch and Livingston, 1946), manipulating photosynthetic production has been widely used to enhance crop yields. Research on photosynthetic yield primarily focuses on changes in plant biomass, such as fresh or dry weight, reflecting cumulative photosynthetic activity throughout a plant's life. These measurements are typically determined at the end of harvesting (Van Bel et al., 2003). Various laboratory techniques involve measuring photosynthetic organs by monitoring changes in $CO_2$ or $O_2$ levels using electrodes within isolated chambers and a conventional recording spectrophotometer (Hunt, 2003). In addition to these methods,

photosynthetic efficiency in certain environments can also be evaluated by quantifying its products, such as sucrose and starch, or by assessing components integral to the photosynthesis process, including plant pigments and rates of water vapor loss (Beadle et al., 1985; Hind, 1985; Yue et al., 2021).

Among various environmental factors, the quality of light exerts a significant influence on photosynthesis. Therefore, it stands as an important element in the regulation of plant development and protection, serving as a critical sensory signal that enables plants to adapt to external stimuli (Liu and Van Iersel, 2021; Rahman et al., 2021). In higher plants, the blue and red light regions within the visible light spectrum, characterized by wavelengths ranging from 380-750 nm (known as photosynthetically active radiation or PAR), are the two light regions that most notably affect the photosynthesis process (Chen and Blankenship, 2011; Rabinowitch and Govindjee, 1965). Red light plays a crucial role in shaping the development of the photosynthetic system and can enhance the accumulation of photosynthetic products by moderating photosynthetic translocation. Meanwhile, blue light has vital effects on chloroplast development, chlorophyll formation, and the regulation of stomatal opening (Zhang et al., 2020b). The utilization of a gradient of light colors proves to be a potent tool for assessing how plants respond to variations in light quality (Lejeune et al., 2022).

The revolution and development of light-emitting diodes (LEDs) have enabled researchers to delve deeper into the mechanisms of light's effect on photosynthetic activity. These LED technologies are increasingly gaining attention, especially with the development and expansion of indoor farms. They are gradually replacing traditional artificial lighting sources due to several advantages, including higher energy efficiency, precise light spectrum emission, lower heat emission, longer lifespan, and environmental friendliness (Jou et al., 2015; Kozai et al., 2016; Olle and Viršile, 2013). Numerous investigations have indicated that altering the

wavelength and intensity of LED light may serve as a means to control plant metabolism, ultimately facilitating the production of functionalized foods (Hasan et al., 2017; Jung et al., 2021). Additionally, LEDs can be flexible, and convenient integration into electronic systems facility make them easily customized and controlled to simulate natural light conditions, which allows to cultivation of a wide variety of crops and medicinal plants (Jou et al., 2015; Ma et al., 2021).

Several studies reported that changes in light quality can enhance essential oils in Pepper Mint (*Mentha piperita* L.), Japanese Mint (*Mentha arvensis* L.), Mexican Mint (*Plectranthus amboinicus* (Lour.) Spreng.) and Sweet Mint (*Mentha spicata*) (Fahlén et al., 1997; Nguyen and Saleh, 2019; Nishioka et al., 2008; Noguchi and Amaki, 2016). Furthermore, changing the LED light spectrum triggered the change in oil composition and the accumulation of monoterpenes in Mint species (Maffei and Scannerini, 1999; Nguyen and Saleh, 2019; Ueda et al., 2021). Nevertheless, an exploration of the impacts of LEDs lighting on Wild Mint plant growth within smart farm environments has yet to be reported. Thus, the current study is designed to determine the effect of various LEDs lights on *Mentha arvensis* L. traits relative to growth and important secondary metabolite: phenolics. It would be helpful to enhance the yield and to increase the important chemical content in this plant.

## 2. Material and methods

### *2.1 Plant material and experiment design*

10-days-old *Mentha arvensis* L. plants (Wild Mint plants) was grown in a hydroponic system (Figure 2.1). The hydroponic nutrition was provided from Hoptri Hydro Leafy medium (Hoptri Investment Corporation, Vietnam) (Table 2.1). The growth conditions were controlled at 27 ± 2°C with a relative humidity of 65 ± 5%, 6.8 ± 0.2 pH, and 50 µmol photon $m^{-2}$ $s^{-1}$ using a fluorescent lamp with 12 hours of light and 12 hours of dark (12/12) photoperiod.

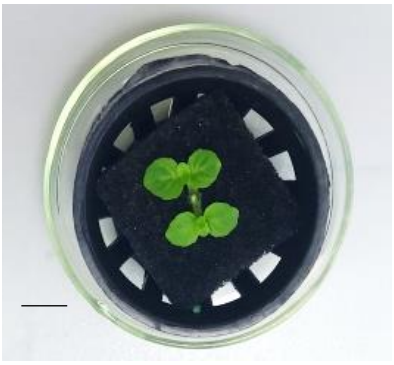

**Figure 2.1** 10-days-old *Mentha arvensis* L. plant in hydroponic system. *Cross bar: 1cm.*

**Table 2.1** Component of a Hoptri Hydro Leafy mixture media.

| Elements | Part A | Part B | A+B |
|---|---|---|---|
| Nitrogen ($NH_4NO_3$, $KNO_3$) | 15% | 6% | 10,5% |
| Phosphorus ($P_2O_5$) | | 9% | 4,5% |
| Potassium ($K_2O$) | 15% | 26% | 20,5% |
| Calcium ($CaCl_2$. $2H_2O$) | 12% | | 6% |
| Magnesium ($MgSO_4$. $7H_2O$) | | 3% | 1,5% |
| Fe (FeNaEDTA) | | 4000 ppm | 2000 ppm |
| Mn ($MnSO_4$. $4H_2O$) | | 1100 ppm | 550 ppm |
| B ($H_3BO_3$) | | 400 ppm | 200 ppm |
| Cu ($CuSO_4$. $5H_2O$) | | 100 ppm | 50 ppm |
| Zn ($ZnSO_4$. $7H_2O$) | | 400 ppm | 200 ppm |
| Mo ($Na_2MoO_4$. $2H_2O$) | | 50 ppm | 25 ppm |
| S | | 4% | 2% |

*2.2 Light treatment*

The Wild Mint plants were grown in the indoor hydroponic system for 4 weeks under four light sources: 100% blue (B), 30% blue and 70% red (B3R7), 100% red (R), and cool white LEDs (W), 12/12 photoperiod, at the same PPFD 150 μmol photon.$m^{-2}$ $s^{-1}$.

LEDs light tubes were provided by Smart Agriculture Lighting Technology, Republic of Korea. The emission spectra from light sources were measured with a PG200N (UPRtek, Taipei, Taiwan) (Figure 2.2).

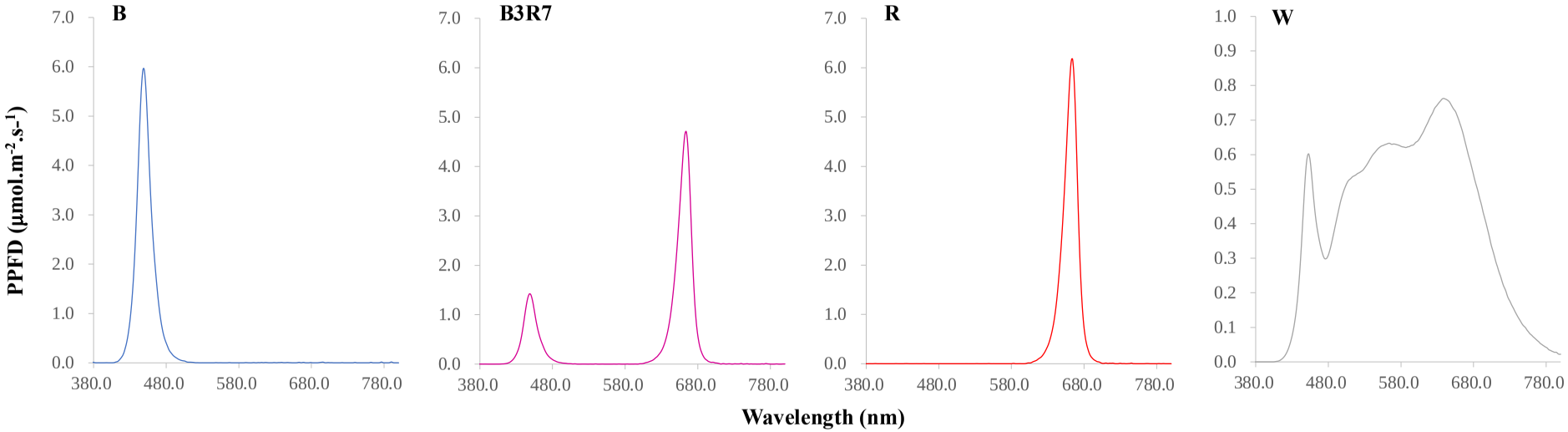


**Figure 2.2** The spectrum of photosynthesis photon flux density of light treatments that were used in this study. All LEDs light treatments were controlled at the same PPFD 150 µmol photon $m^{-2}$ $s^{-1}$.

*2.3 Number of leaves and auxiliary bud*

The number of leaves and auxiliary buds on the main stem were monitored over the cultivation time, by counting all the pairs of leaves or auxiliary buds from the base of the plant.

*2.4 Plant height*

The plant height was measured over the cultivation time, using a digital ruler, starting from the "shoot base" point (where the main stem of the plant emerges from the growing media, this is typically the point where the plant starts growing upward) to the leaf base of the highest fully developed leaf.

*2.5 Fresh and dry weight*

The fresh and dry weight of plants were determined at the end of harvest time. Each plant was separated and weighed for its fresh weight using an HR-202i balance (A&D Company, Limited, Japan). For the dry weight determination, the plants were dried in an electric drying oven (UNB 500, Memmert, Germany) at 40°C for three days until a constant mass was achieved.

*2.6 Extract and determine total sugar content*

*Preparation of sucrose standard curve:*

Sucrose was dissolved in distilled water to prepare sucrose solutions with concentrations ranging from 10 to 320 mg/L. One milliliter of each sucrose solution was mixed with 1 ml of 5% phenol and 5 ml of concentrated sulfuric acid, shaken well, allowed to cool, and its absorbance was measured at a wavelength of 490 nm to establish the standard curve (Coombs et al., 1985).

*Extraction and quantification of total sugars:*

Different plant organs (roots, stems, leaves) were isolated and stored in a refrigerator at -20°C (to stop leaf metabolism immediately). One gram of samples was ground in absolute

ethanol and then boiled in the water bath for 15 minutes. The mixture was then centrifuged at 4,000 rpm for 5 minutes, and the extract was collected. The residue after centrifugation underwent the following steps twice: mixed with 80% ethanol, heated under reflux for 15 minutes, centrifuged at 4,000 rpm for 5 minutes, and the extract was collected. After the ethanol had completely evaporated, distilled water was added to make up a total volume of 50 ml. One milliliter of the diluted extract was reacted with 1 ml of 5% phenol ($C_6H_6O$) and 5 ml of concentrated sulfuric acid ($H_2SO_4$), and its absorbance was measured at a wavelength of 490 nm. The total sugar content (mg/g fresh weight) in the sample was determined based on the sucrose standard curve (Coombs et al., 1985).

*2.7 Extract and determine starch content*

*Preparation of glucose standard curve:*

Glucose was dissolved in distilled water to prepare glucose solutions with concentrations ranging from 10 to 320 mg/L. One milliliter of each glucose solution was mixed with 1 ml of 5% phenol and 5 ml of concentrated sulfuric acid, shaken well, allowed to cool, and its absorbance was measured at a wavelength of 490 nm to establish the standard curve (Coombs et al., 1985).

*Extraction and quantification of starch:*

After performing the total sugar extraction experiment described above, the residue of the sample was dried at 70°C and then mixed with 2 ml of distilled water. After boiling in the water bath for 15 minutes, the mixture was supplemented with 2 ml of 7N perchloric acid ($HClO_4$), vortexed, continued to be boiled in the water for 15 minutes, and then supplemented with distilled water to reach a volume of 10 ml. The mixture was centrifuged at 4,000 rpm for 5 minutes, and the supernatant was collected. The residue was then supplemented with 2 ml of 4.6 N perchloric acid ($HClO_4$) and the process was repeated three times. The combined

supernatants from the three centrifugation steps were evaporated to a volume of 5 ml, and distilled water was added to reach a volume of 50 ml. One milliliter of the extracted solution was mixed with 1 ml of 5% phenol, 5 ml of concentrated sulfuric acid, and its optical density was measured at a wavelength of 490 nm. The starch content in the sample was determined by comparing it to the glucose standard curve (Coombs et al., 1985).

*2.8 Extract and estimate total phenolic*

Quantification of total phenolic compounds using the Folin-Ciocalteu method: Based on the reduction of phosphomolybdic/phosphotungstic acid complexes in the Folin-Ciocalteu reagent by phenolic compounds in an alkaline environment to produce blue complexes which are quantified through spectroscopic analysis with maximum absorbance at 765 nm (Ainsworth and Gillespie, 2007).

*Preparation of gallic acid standard curve*

1 mg of gallic acid was diluted in 10 ml of 70% methanol to achieve a concentration of 100 µg/ml. Then, the solution was diluted to a range of concentrations from 0-50 µg/ml. Next step, 0.4 ml of the diluted solution was added to 1 ml of 10% Folin reagent, 1 ml of distilled water, and 1.6 ml of 7.5% $Na_2CO_3$, incubated in the dark for 30 minutes, and measured the optical density at a wavelength of 765 nm. A standard curve was constructed and the relationship between the phenolic content of the sample (µg/ml) and the $OD_{765}$ value was determined. The equation used is $y = 0.0099x - 0.0081$ with $R^2=0.9994$.

*Extraction and determination of total phenolic content in the sample*

One gram of different plant organs (roots, stems, leaves) was isolated ground in 70% methanol, boiled in the water bath at 70°C for 10 minutes, and then centrifuged at 4,000 rpm for 5 minutes to collect the supernatant. The residue was retained, and 70% methanol was added to it, repeating the centrifugation steps 3 times. The total extract after centrifugation steps was

diluted to 50 ml with 70% methanol (Chen et al., 2011). Take 0.4 ml of the diluted extract, add 1 ml of 10% Folin reagent, 1 ml of distilled water, and 1.6 ml of 7.5% sodium carbonate ($Na_2CO_3$), incubate in the dark for 30 minutes, and measure the optical density at a wavelength of 765 nm (Baba and Malik, 2015).

The content of total phenolic compounds (mg/g $_{FW}$) in the leaf extract through $\Delta OD_{765}$ nm was calculated using the formula:

Total phenolic content = $\frac{(Y+0.0081)*V*a}{0.9994*m*1000}$. (mg/g $_{FW}$)

*Y: $\Delta OD_{765}$ nm; a: dilution factor; V: initial volume of the extract (ml); m: sample weight (g).*

### *2.9 Statistical analysis*

Each Wild Mint plant was used as a replicate. Data for plant height, the number of leaves, and the number of auxiliary buds were collected from 30 plants per LED treatment. Data for fresh weight, dry weight, sucrose content, starch content, and total phenolic content were determined using 8 plants per LED treatment. All data analysis was performed using R software (Version 4.3.1, the R Foundation for Statistical Computing, Vienna, Austria). The datasets were checked for normality using the Shapiro-Wilk test (Shapiro and Wilk, 1965).

The datasets for plant height, the number of leaves, and the number of auxiliary buds did not meet the criteria for normality. Therefore, non-parametric data analysis was conducted using the Kruskal-Wallis's test, followed by the Dunn test with Benjamini-Hochberg correction.

In contrast, the datasets for fresh weight, dry weight, sucrose content, starch content, and total phenolic content exhibited a normal distribution. For these datasets, parametric analysis was conducted using the One-way ANOVA test, followed by the Fisher's least significant difference (LSD) post hoc test to compare measurements between different LED light

treatments. Line plots and bar plots were generated using the 'ggpubr' and 'ggplot2' packages in R 4.3.1.

## 3. Result

To investigate the effects of LED light qualities on the growth and development of Wild Mint plants during the early vegetative phase, plants was illuminated with four different LED light conditions: 100% blue (B), 30% blue and 70% red (B3R7), 100% red (R), and cool white LEDs (W) closely resembling the terrestrial sunlight spectrum between 380 and 780 nm, all at the same photosynthetic photon flux density (PPFD) of 150 μmol photons $m^{-2}$ $s^{-1}$, within a hydroponic vertical cultivation system. The results revealed significant differences in plant morphological responses, including plant height, the number of leaves, and the number of auxiliary buds in Wild Mint plants (Figure 2.3).

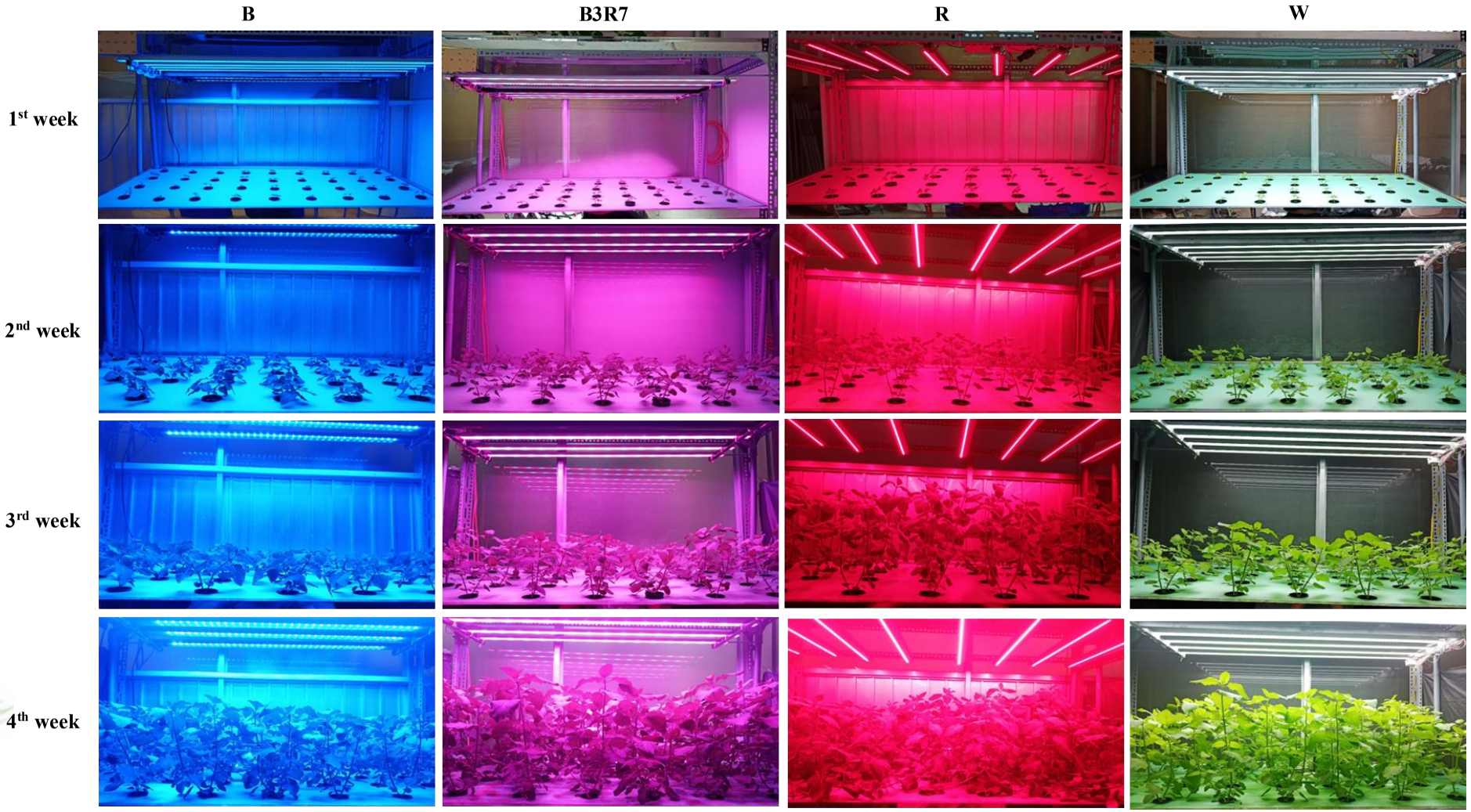


**Figure 2.3** Growth of *Mentha arvensis* L. plants in the hydroponic system under different LED lights over time, all with the same PPFD 150 μmol $m^{-2}$ $s^{-1}$. *B: Blue LED, B3R7: Combination of 30% blue and 70% red LED, R: Red LED, W: White LED.*

The number of fully developed leaf pairs along the stem increased in all plants over the course of the experiment, indicating the plants' growth under various light conditions. Wild Mint plants started with one leaf pair at the beginning of the experiment and reached nine fully developed leaf pairs along the main stem after four weeks. During the second week of the experiment, Wild Mint plants illuminated with colored LEDs exhibited a slightly higher number of leaf pairs compared to those under white LED lighting. This difference became significant in the last week of the experiment (Table 2.2 and Figure 2.4).

**Table 2.2** The statistical analysis number of leaves (pair of leaves) on *Mentha arvensis* L. plants grown under different LED light treatments.

| Time | Light | Rep. | Min | Max | Median | Mean | sd | Range | cv |
|---|---|---|---|---|---|---|---|---|---|
| 1st | B | 30 | 2.00 | 4.00 | 3.00 | 3.20 | 0.61 | 2.00 | 0.19 |
| | B3R7 | 30 | 2.00 | 5.00 | 3.00 | 3.17 | 0.70 | 3.00 | 0.22 |
| | R | 30 | 2.00 | 5.00 | 3.00 | 3.17 | 0.70 | 3.00 | 0.22 |
| | W | 30 | 2.00 | 4.00 | 3.00 | 3.13 | 0.51 | 2.00 | 0.16 |
| 2nd | B | 30 | 3.00 | 6.00 | 5.00 | 5.03 | 0.85 | 3.00 | 0.17 |
| | B3R7 | 30 | 4.00 | 7.00 | 5.50 | 5.43 | 0.73 | 3.00 | 0.13 |
| | R | 30 | 4.00 | 7.00 | 5.00 | 5.20 | 0.76 | 3.00 | 0.15 |
| | W | 30 | 4.00 | 6.00 | 5.00 | 4.90 | 0.55 | 2.00 | 0.11 |
| 3rd | B | 30 | 5.00 | 9.00 | 7.00 | 7.13 | 0.90 | 4.00 | 0.13 |
| | B3R7 | 30 | 6.00 | 9.00 | 8.00 | 7.70 | 0.92 | 3.00 | 0.12 |
| | R | 30 | 3.00 | 9.00 | 7.50 | 7.43 | 1.17 | 6.00 | 0.16 |
| | W | 30 | 6.00 | 9.00 | 8.00 | 7.57 | 0.77 | 3.00 | 0.10 |
| 4th | B | 30 | 6.00 | 10.00 | 8.00 | 8.37 | 1.00 | 4.00 | 0.12 |
| | B3R7 | 30 | 6.00 | 10.00 | 8.00 | 7.87 | 0.82 | 4.00 | 0.10 |
| | R | 30 | 7.00 | 11.00 | 9.50 | 9.40 | 1.10 | 4.00 | 0.12 |
| | W | 30 | 6.00 | 11.00 | 9.00 | 8.83 | 1.05 | 5.00 | 0.12 |

*All LED light treatments at the same PPFD 150 μmol $m^{-2}$ $s^{-1}$.*

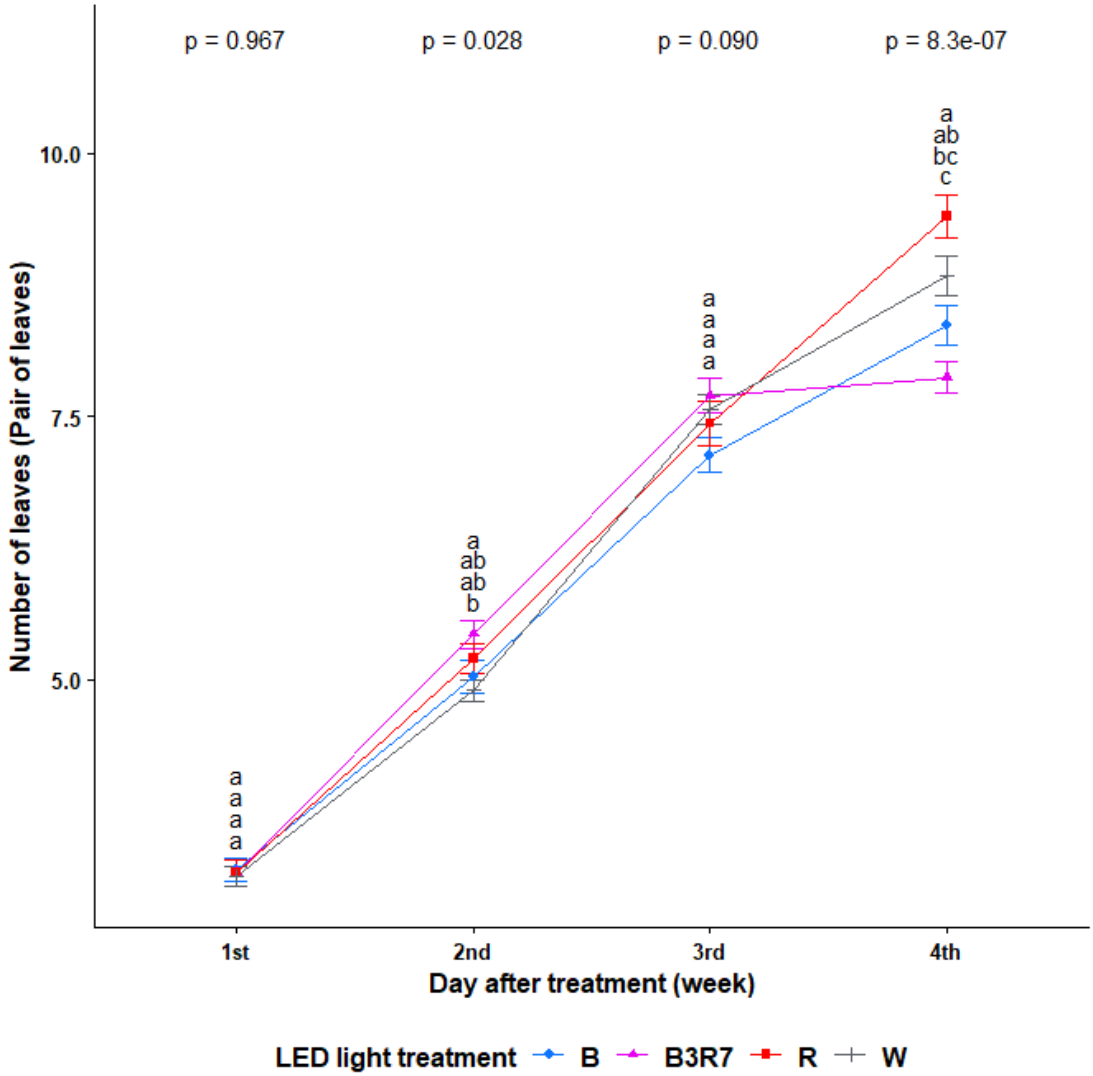


**Figure 2.4** Number of leaves on Mentha arvensis L. plants grown under different LED light treatments, all at the same PPFD 150 μmol $m^{-2}$ $s^{-1}$. *Statistical analysis was performed using a Kruskal–Wallis test (p-value ≤ 0.05) followed by a Dunn–Benjamini–Hochberg post hoc test for multiple comparisons. Different letters indicate a significant difference between the two medians.*

Wild Mint plants began to develop auxiliary buds in the 2nd week of the experiment, and they consistently exhibited greater bud formation in treatments with a high proportion of red light, such as 70% and 100% red LED. Conversely, blue light resulted in a reduction in the number of auxiliary buds in Wild Mint plants when compared to the other light conditions. By the last week of the experiment, there was no significant difference in the number of auxiliary buds between these LED treatments (Table 2.3 and Figure 2.5).

**Table 2.3** The statistical analysis number of auxiliary buds on *Mentha arvensis* L. plants grown under different LED light treatments.

| Time | Light | Rep. | Min | Max | Median | Mean | sd | Range | cv |
|---|---|---|---|---|---|---|---|---|---|
| 1st | B | 30 | - | - | - | - | - | - | - |
| | B3R7 | 30 | - | - | - | - | - | - | - |
| | R | 30 | - | - | - | - | - | - | - |
| | W | 30 | - | - | - | - | - | - | - |
| 2nd | B | 30 | 0 | 4 | 2.00 | 1.83 | 1.15 | 4.00 | 0.63 |
| | B3R7 | 30 | 0 | 5 | 3.00 | 2.83 | 0.99 | 5.00 | 0.35 |
| | R | 30 | 0 | 4 | 3.00 | 2.30 | 1.09 | 4.00 | 0.47 |
| | W | 30 | 0 | 4 | 2.00 | 1.73 | 1.17 | 4.00 | 0.68 |
| 3rd | B | 30 | 1 | 7 | 5.00 | 4.57 | 1.41 | 6.00 | 0.31 |
| | B3R7 | 30 | 2 | 7 | 6.00 | 5.83 | 1.02 | 5.00 | 0.17 |
| | R | 30 | 2 | 7 | 5.50 | 5.43 | 1.14 | 5.00 | 0.21 |
| | W | 30 | 0 | 7 | 5.00 | 4.97 | 1.47 | 7.00 | 0.30 |
| 4th | B | 30 | 3 | 10 | 8.00 | 7.37 | 1.63 | 7.00 | 0.22 |
| | B3R7 | 30 | 4 | 10 | 8.00 | 8.20 | 1.13 | 6.00 | 0.14 |
| | R | 30 | 2 | 11 | 8.00 | 7.77 | 1.89 | 9.00 | 0.24 |
| | W | 30 | 0 | 10 | 8.00 | 7.50 | 1.93 | 10.00 | 0.26 |

*All LED light treatments at the same PPFD 150 μmol $m^{-2}$ $s^{-1}$.*

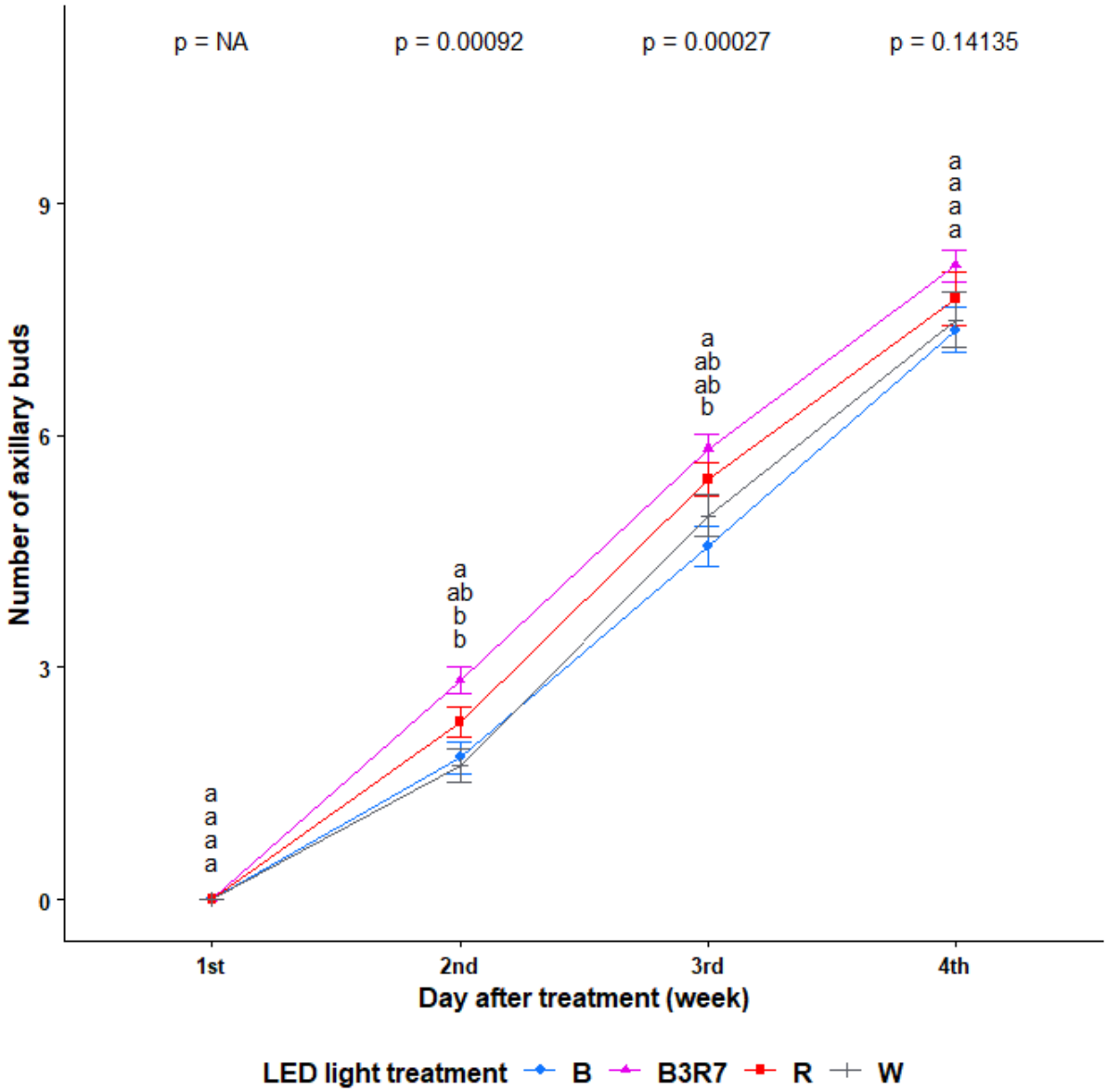


**Figure 2.5** Number of auxiliary buds on *Mentha arvensis* L. plants grown under different LED light treatments, all at the same PPFD 150 µmol $m^{-2}$ $s^{-1}$. *Statistical analysis was performed using a Kruskal–Wallis test (p-value ≤ 0.05) followed by a Dunn–Benjamini–Hochberg post hoc test for multiple comparisons. Different letters indicate a significant difference between the two medians.*

After four weeks since the experiment, the height of Wild Mint plants was divided into two groups. Plants grown under red LED lighting significantly exceeded the heights of plants in other treatments (B, B3R7, and W) starting from the first week, with an average height of

21.56 ± 8.5 mm. The difference in plant height continued to increase between these two LED groups over the four weeks of the experiment. Wild Mint plants grown under red LED lighting were 1.5 times taller than those grown under B, B3R7, and W LED treatments, reaching average heights of 51.43 ± 13.84 mm, 201.67 ± 45.57 mm, or 346.17 ± 63.76 mm, respectively, after 2, 3, or 4 weeks (Table 2.4 and Figure 2.6).

In the second group, Wild Mint plants exposed to blue LED lighting did not exhibit significant changes in plant height compared to the control group under white LED treatment. The height of plants under the combination of blue and red LEDs was slightly higher during the first three weeks but became significantly lower than that of control plants in the last week of the experiment (Table 2.4 and Figure 2.6). Furthermore, red light increased the variation in plant height among individual plants within the same experimental group, with a large range between the min and max value; conversely, plants grown under combined lighting exhibited greater uniformity among the plants within the same LED light treatment, with small of range, standard deviation (sd) and coefficient of variation (cv) value (Table 2.4).

**Table 2.4** The statistical analysis of plant height (mm) of *Mentha arvensis* L. grown under different LED light treatments.

| Time | Light | Rep. | Min | Max | Median | Mean | sd | Range | cv |
|---|---|---|---|---|---|---|---|---|---|
| 1st | B | 30 | 3.22 | 30.30 | 15.26 | 14.80 | 4.87 | 27.08 | 0.33 |
| | B3R7 | 30 | 9.97 | 28.84 | 15.77 | 16.96 | 4.42 | 18.87 | 0.26 |
| | R | 30 | 2.42 | 45.94 | 20.66 | 21.56 | 8.50 | 43.52 | 0.39 |
| | W | 30 | 3.25 | 24.46 | 14.33 | 14.51 | 4.14 | 21.21 | 0.29 |
| 2nd | B | 30 | 12.62 | 49.75 | 29.78 | 29.38 | 7.20 | 37.13 | 0.24 |
| | B3R7 | 30 | 23.70 | 45.11 | 36.08 | 35.61 | 6.24 | 21.41 | 0.18 |
| | R | 30 | 27.25 | 86.33 | 49.40 | 51.43 | 13.84 | 59.08 | 0.27 |
| | W | 30 | 11.48 | 45.73 | 31.41 | 31.56 | 6.34 | 34.25 | 0.20 |
| 3rd | B | 30 | 45.61 | 115.57 | 80.79 | 82.69 | 16.79 | 69.96 | 0.20 |
| | B3R7 | 30 | 66.58 | 110.28 | 97.58 | 95.86 | 10.20 | 43.70 | 0.11 |
| | R | 30 | 70.00 | 280.00 | 205.00 | 201.67 | 45.57 | 210.00 | 0.23 |
| | W | 30 | 49.00 | 114.89 | 85.63 | 84.36 | 16.62 | 65.89 | 0.20 |
| 4th | B | 30 | 170.00 | 310.00 | 267.50 | 248.83 | 38.52 | 140.00 | 0.15 |
| | B3R7 | 30 | 195.00 | 270.00 | 235.00 | 236.50 | 16.51 | 75.00 | 0.07 |
| | R | 30 | 150.00 | 450.00 | 340.00 | 346.17 | 63.76 | 300.00 | 0.18 |
| | W | 30 | 160.00 | 330.00 | 265.00 | 263.83 | 34.03 | 170.00 | 0.13 |

*All LED light treatments at the same PPFD 150 μmol $m^{-2}$ $s^{-1}$.*

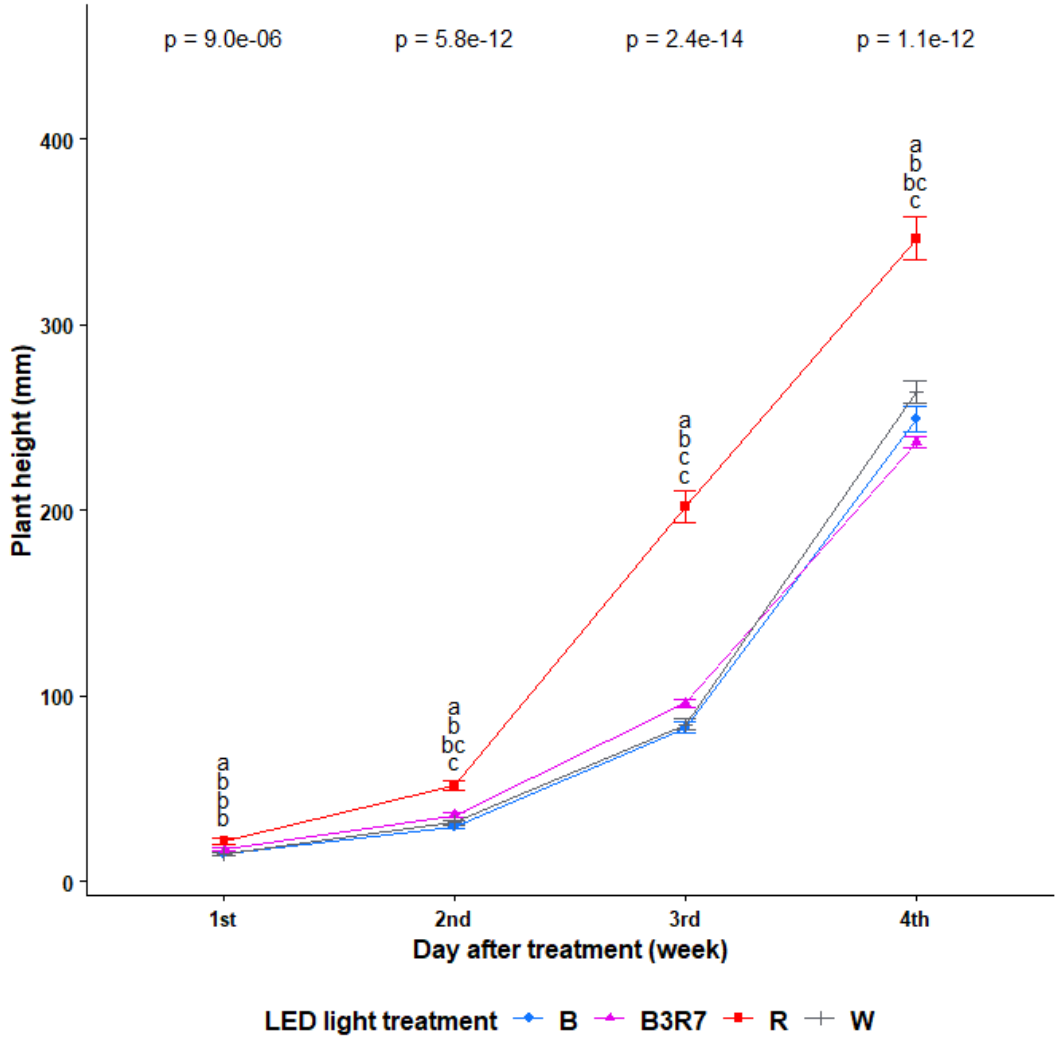


**Figure 2.6** Plant height of *Mentha arvensis* L. grown under different LED light treatments, all at the same PPFD 150 μmol $m^{-2}$ $s^{-1}$. *Statistical analysis was performed using a Kruskal–Wallis test (p-value ≤ 0.05) followed by a Dunn–Benjamini–Hochberg post hoc test for multiple comparisons. Different letters indicate a significant difference between the two medians.*

The results of fresh weight measurements highlight the impact of different LED colors on biomass properties and allocation in *Mentha arvensis* L. during hydroponic cultivation. Our analysis encompasses fresh-weight ratios of leaves, stem weight percentages, and biomass distribution to the roots, with the data presented in Table 2.5, Figures 2.7 and 2.8.

The total fresh weight of the entire plant ranged from 15.39 to 21.21 g. It was notably higher under B3R7 or red LED lighting but lower under blue LED lighting compared to the

control with white LED lighting. Furthermore, the combined light spectrum resulted in a significant increase in fresh weight for both roots and stems compared to the other treatments (Table 2.5). When considering the aerial parts of the plant, enhanced growth was observed in the presence of B3R7 or red LED lighting, while only the root portion displayed improvement under B3R7 LED lighting after four weeks of cultivation (Figure 2.7). Further analysis revealed that all color LEDs caused a decrease in the fresh-weight ratio of leaves, accompanied by an increase in the percentage of stem weight, indicating a shift in biomass allocation from leaves to stems across all treatments. Notably, both blue and B3R7 LED treatments exhibited a significant increase in biomass allocation to the roots, suggesting enhanced root development under these light conditions (Figure 2.8).

**Table 2.5** Fresh weight of different plant organs (roots, stems, leaves) of *Mentha arvensis* L. after 4 weeks grown under different LED light treatments, at the same PPFD 150 μmol $m^{-2}$ $s^{-1}$.

| Light | Fresh weight (g) | | | |
|---|---|---|---|---|
| | Root | Stem | Leaves | Total plant |
| B | 1.20 ± 0.04 $^{b}$ | 6.92 ± 0.13 $^{c}$ | 7.28 ± 0.14 $^{b}$ | 15.39 ± 0.38 $^{c}$ |
| B3R7 | 1.71 ± 0.05 $^{a}$ | 9.98 ± 0.12 $^{a}$ | 9.52 ± 0.26 $^{a}$ | 21.21 ± 0.21 $^{a}$ |
| R | 1.38 ± 0.16 $^{b}$ | 8.35 ± 0.72 $^{b}$ | 8.99 ± 0.95 $^{a}$ | 18.72 ± 1.74 $^{ab}$ |
| W | 1.23 ± 0.02 $^{b}$ | 7.33 ± 0.38 $^{bc}$ | 8.58 ± 0.21 $^{ab}$ | 17.15 ± 0.59 $^{bc}$ |
| ANOVA's test | 0.0048 ** | 0.0010 ** | 0.0481 * | 0.0062 ** |

*Means of ± standard errors followed by different letters within columns are significantly different by Fisher's least significant difference (LSD) test with one-way ANOVA; n = 8.*

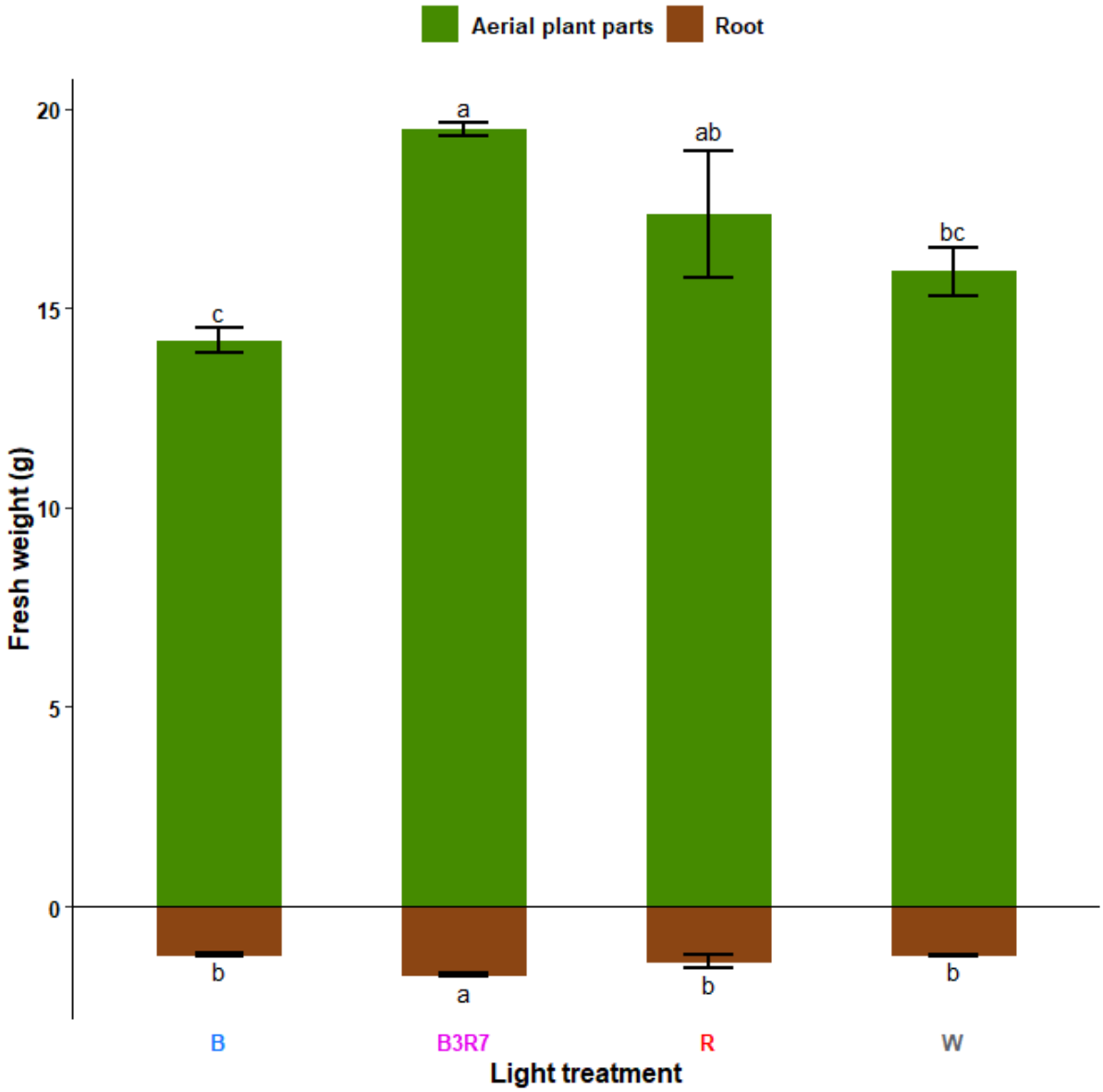


**Figure 2.7** Influence of LED light treatments on shoots and roots fresh weight in of *Mentha arvensis* L. after 4 weeks grown under the same PPFD 150 µmol $m^{-2}$ $s^{-1}$. *Statistical analysis was performed using a ANOVA test (p-value ≤ 0.05) followed by a Fisher's least significant difference (LSD) post hoc test for multiple comparisons. Bars represent means of eight biological replicates ± standard errors, different letters indicate a significant difference between the two means.*

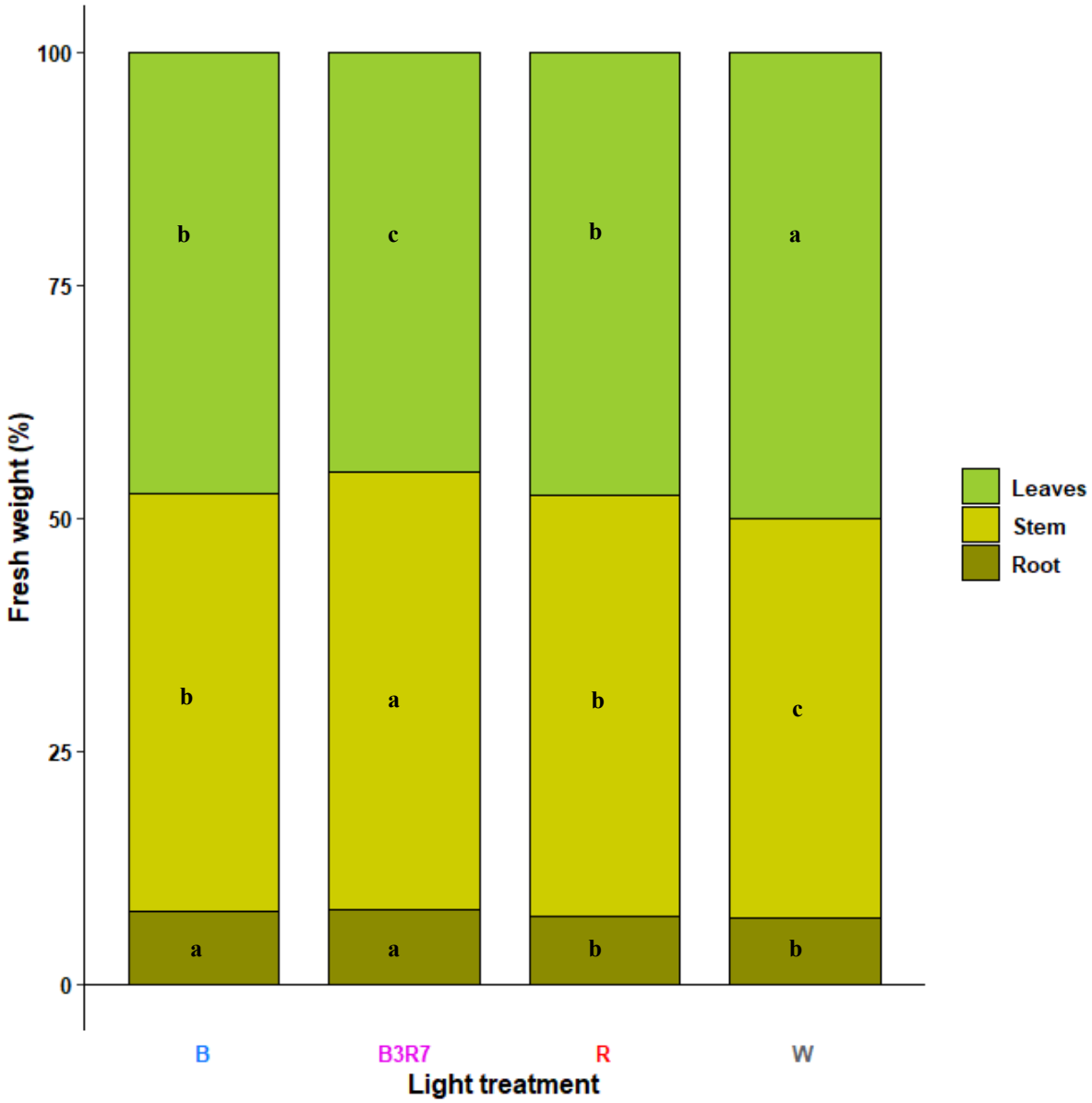


**Figure 2.8** Percentage of the total fresh weight per plant partitioned to different organs of *Mentha arvensis* L. after 4 weeks grown under different LED light treatments, at the same PPFD 150 µmol $m^{-2}$ $s^{-1}$. *Statistical analysis was performed using a ANOVA test (p-value ≤ 0.05) followed by a Fisher's least significant difference (LSD) post hoc test for multiple comparisons. Different letters indicate a significant difference between the two means.*

The same pattern of the LED light effect was observed in the total dry matter of *Mentha arvensis* L. plants grown under red LED lighting tended to have a greater total plant dry weight, while blue LED lighting decreased the dry biomass in both leaves and stem organs, consequently reducing the overall plant dry matter of Wild Mint. And no significant difference in plant dry weight was observed between the combination LED treatment and the control using white LED lighting (Table 2.6). An increase in plant dry weight under B3R7 and red LED lighting was recorded in both the aerial and root parts of the plant. Meanwhile, Wild Mint plants grown under blue LED treatment showed no significant differentiation compared to those under white LED lighting (Figure 2.9). The investigation into the partitioning of dry matter to individual organs exposed that different LED light treatments led to changes in the dry weight distribution among storage organs. Blue light increased leaf dry mass, red LED tended to accumulate dry weight in the stems, while plants grown under a combination of B3R7 LED lighting exhibited an enhanced dry biomass ratio in the roots (Figure 2.10)

**Table 2.6** Dry weight of different plant organs (roots, stems, leaves) of *Mentha arvensis* L. after 4 weeks grown under different LED light treatments, at the same PPFD 150 μmol $m^{-2}$ $s^{-1}$.

| Light | Dry weight (mg) | | | |
|---|---|---|---|---|
| | Root | Stem | Leaves | Total plant |
| B | 111.25 ± 3.94 $^{b}$ | 375.88 ± 10.82 $^{c}$ | 629.38 ± 27.65 $^{c}$ | 1116.50 ± 40.93 $^{c}$ |
| B3R7 | 153.13 ± 3.79 $^{a}$ | 508.50 ± 9.16 $^{b}$ | 747.75 ± 22.71 $^{b}$ | 1409.38 ± 42.89 $^{ab}$ |
| R | 136.88 ± 10.88 $^{a}$ | 607.88 ± 51.75 $^{a}$ | 845.00 ± 45.36 $^{a}$ | 1589.75 ± 111.31 $^{a}$ |
| W | 112.88 ± 3.36 $^{b}$ | 452.88 ± 26.94 $^{bc}$ | 688.75 ± 23.73 $^{bc}$ | 1254.50 ± 16.92 $^{bc}$ |
| ANOVA's test | 0.0013 ** | 0.0011 ** | 0.0025 ** | 0.0013 ** |

*Means of ± standard errors followed by different letters within columns are significantly different by Fisher's least significant difference (LSD) test with one-way ANOVA; n = 8.*

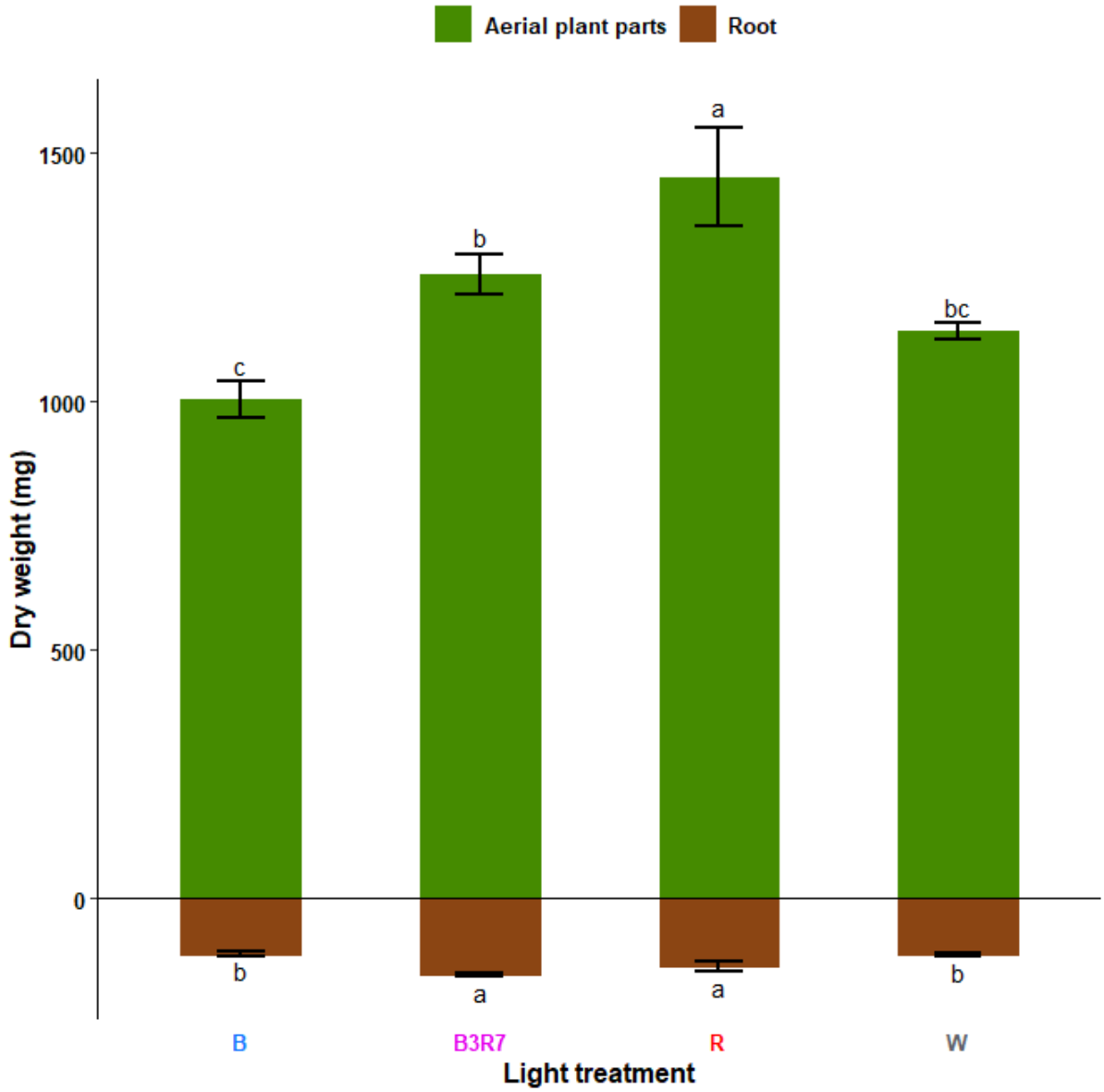


**Figure 2.9** Influence of LED light treatments on shoots and roots dry weight in of *Mentha arvensis* L. after 4 weeks grown under the same PPFD 150 µmol $m^{-2}$ $s^{-1}$. *Statistical analysis was performed using a ANOVA test (p-value ≤ 0.05) followed by a Fisher's least significant difference (LSD) post hoc test for multiple comparisons. Bars represent means of eight biological replicates ± standard errors, different letters indicate a significant difference between the two means.*

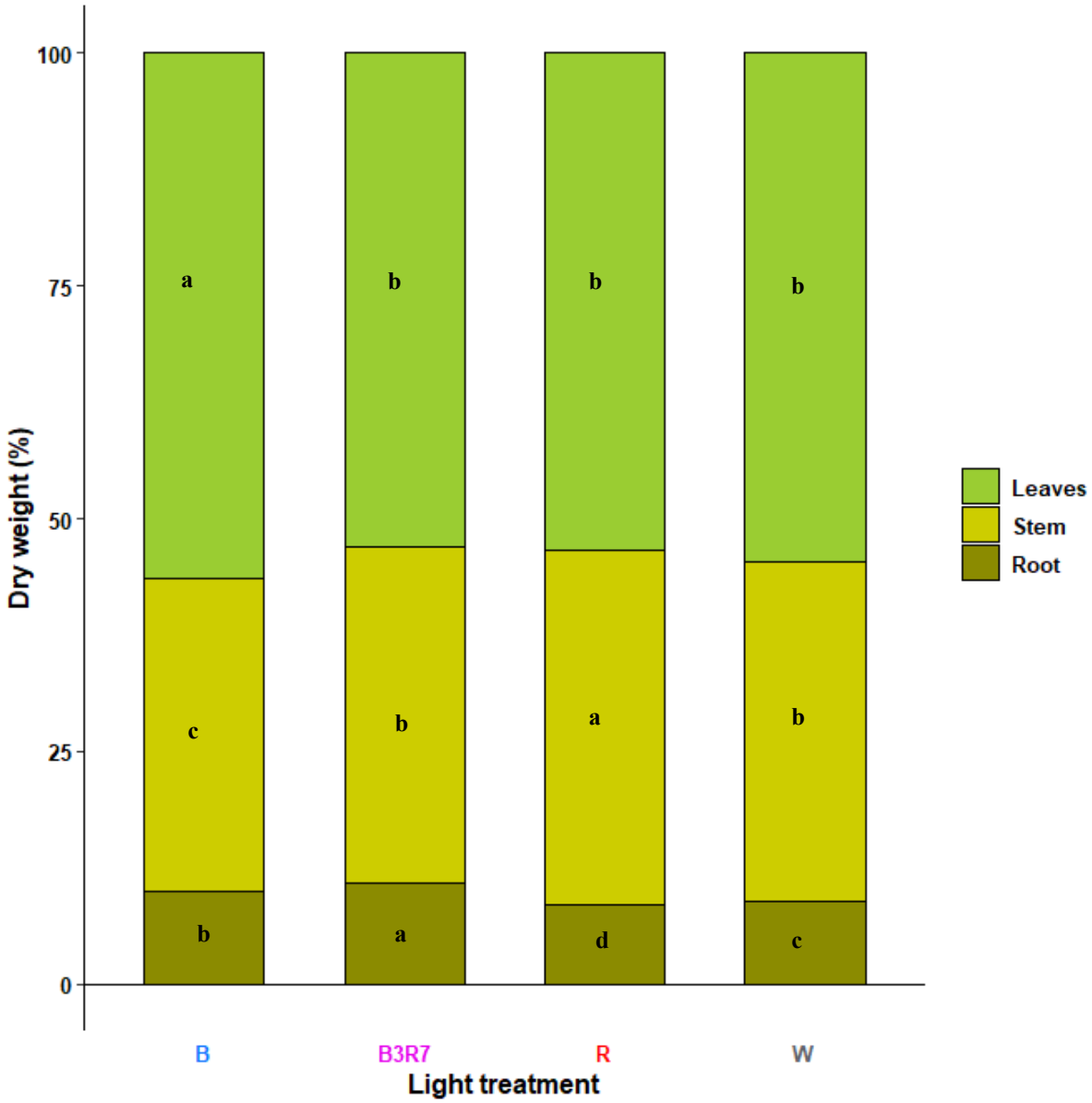


**Figure 2.10** Percentage of the total dry weight per plant partitioned to different organs of *Mentha arvensis* L. after 4 weeks grown under different LED light treatments, at the same PPFD 150 µmol $m^{-2}$ $s^{-1}$. *Statistical analysis was performed using a ANOVA test (p-value ≤ 0.05) followed by a Fisher's least significant difference (LSD) post hoc test for multiple comparisons. Different letters indicate a significant difference between the two means.*

The light spectrum not only influences plant morphogenesis and biomass but also affects plant metabolic compounds. Table 2.7 presents the sucrose content of Wild Mint plants after four weeks of exposure to different LED light sources, with the highlight being the higher sucrose yield in the combined B3R7 LED treatment compared to the other light treatments. When considering the results for each plant organ, lower sucrose content in the roots of plants grown under a high red LED ratio was observed. Conversely, plants under blue LED lighting showed no significant change compared to those under white LED lighting. All LED color treatments enhanced the sucrose content in the stems. However, only the leaves of plants grown under red LED lighting had significantly higher sucrose content than the other treatments (Table 2.7). Upon closer investigation, all LED color treatments significantly reduced the percentage of sucrose content in leaves while increasing sucrose content in stems compared to the control. Clear differences were noted in the combined blue and red LED light treatments. In the root part, both blue and combined B3R7 LEDs had a higher ratio of sucrose content, whereas no significant difference was observed between red and white LEDs (Figure 2.11).

**Table 2.7** Sucrose content in different plant organs (roots, stems, leaves) of *Mentha arvensis* L. after 4 weeks grown under different LED light treatments, at the same PPFD 150 μmol $m^{-2}$ $s^{-1}$.

| Light | Sucrose content (mg/g FW) | | | Total plant (mg/plant) |
|---|---|---|---|---|
| | Root | Stem | Leaves | |
| B | 2.59 ± 0.05 $^{a}$ | 4.84 ± 0.03 $^{b}$ | 8.30 ± 0.13 $^{b}$ | 100.56 ± 1.71 $^{b}$ |
| B3R7 | 2.44 ± 0.05 $^{b}$ | 5.10 ± 0.09 $^{a}$ | 7.86 ± 0.08 $^{b}$ | 166.65 ± 10.37 $^{a}$ |
| R | 2.13 ± 0.04 $^{c}$ | 4.83 ± 0.09 $^{b}$ | 9.27 ± 0.27 $^{a}$ | 102.85 ± 5.23 $^{b}$ |
| W | 2.58 ± 0.03 $^{a}$ | 4.45 ± 0.01 $^{c}$ | 7.93 ± 0.14 $^{b}$ | 99.65 ± 1.89 $^{b}$ |
| ANOVA's test | 2.36e-05 *** | 0.0002 *** | 0.0002 *** | 6.71e-06 *** |

*Means of ± standard errors followed by different letters within columns are significantly different by Fisher's least significant difference (LSD) test with one-way ANOVA; n = 8.*

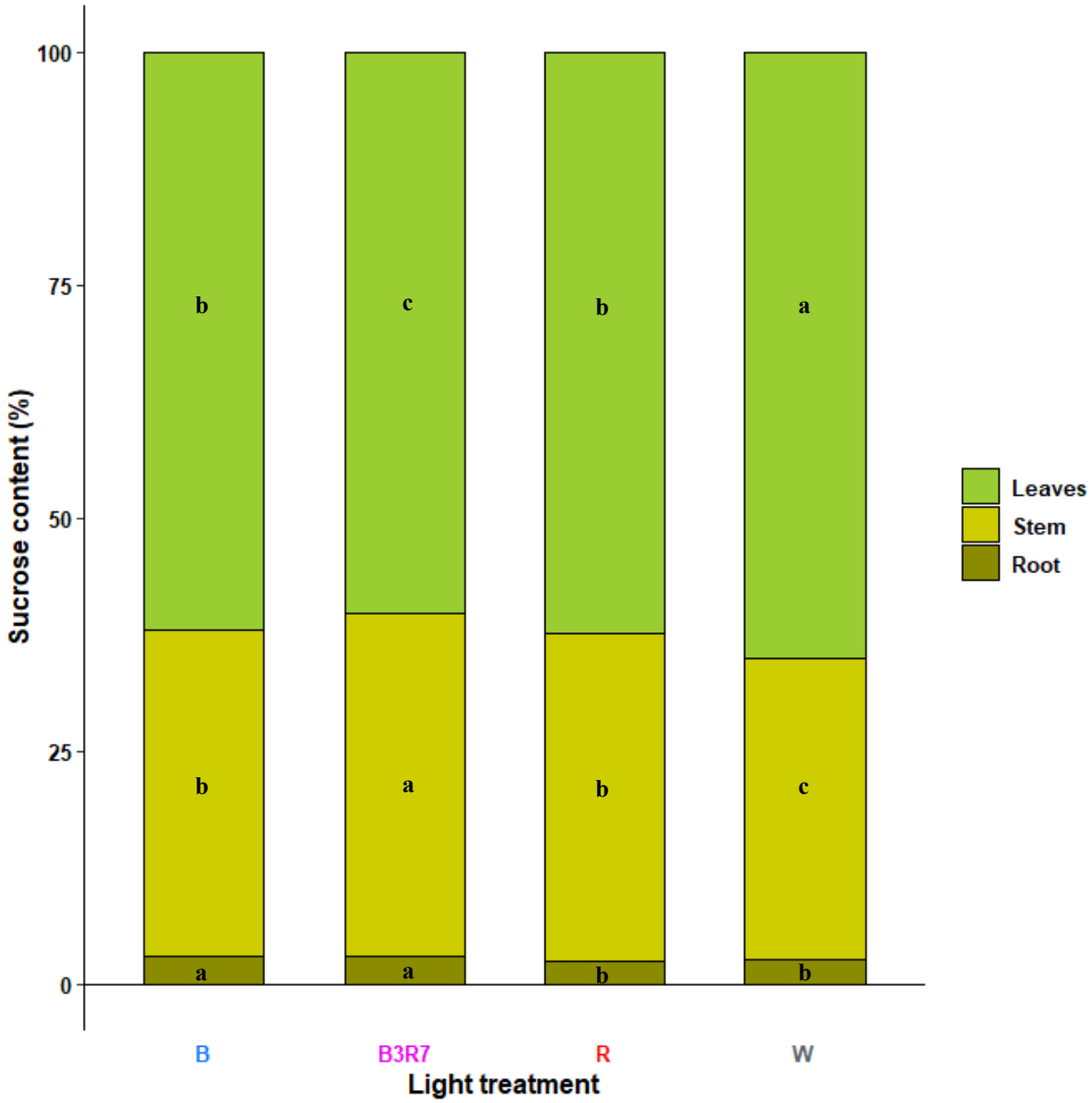


**Figure 2.11** Percentage of sucrose content per plant partitioned to different organs of *Mentha arvensis* L. after 4 weeks grown under different LED light treatments, at the same PPFD 150 µmol $m^{-2}$ $s^{-1}$. *Statistical analysis was performed using a ANOVA test (p-value ≤ 0.05) followed by a Fisher's least significant difference (LSD) post hoc test for multiple comparisons. Different letters indicate a significant difference between the two means.*

The starch content of Wild Mint plants cultivated under the combined B3R7 LED treatment exhibited significantly greater yields compared to other light treatments (Table 2.8). Furthermore, all LED treatments led to a notable shift in starch storage, with a transition from leaves to stem or root organs observed (Figure 2.12). Specifically, the highest starch content was recorded in the roots of plants exposed to the combined B3R7 LED light, while plants grown under blue LED lighting accumulated this compound primarily in the stems (Table 2.8, Figure 2.12).

**Table 2.8** Starch content in different plant organs (roots, stems, leaves) of *Mentha arvensis* L. after 4 weeks grown under different LED light treatments, at the same PPFD 150 μmol $m^{-2}$ $s^{-1}$.

| Light | Starch content (mg/g FW) | | | Total plant (mg/plant) |
|---|---|---|---|---|
| | Root | Stem | Leaves | |
| B | 12.42 ± 0.54 $^{b}$ | 12.65 ± 0.50 $^{a}$ | 12.06 ± 0.17 $^{ab}$ | 203.42 ± 5.11 $^{b}$ |
| B3R7 | 17.27 ± 0.39 $^{a}$ | 9.88 ± 0.12 $^{c}$ | 11.11 ± 0.03 $^{c}$ | 250.37 ± 18.54 $^{a}$ |
| R | 12.28 ± 0.10 $^{b}$ | 10.65 ± 0.23 $^{bc}$ | 11.31 ± 0.48 $^{bc}$ | 183.38 ± 9.64 $^{c}$ |
| W | 13.31 ± 0.25 $^{b}$ | 11.41 ± 0.15 $^{b}$ | 12.48 ± 0.17 $^{a}$ | 197.26 ± 3.08 $^{bc}$ |
| ANOVA's test | 1.19e-06 *** | 0.000155 *** | 0.0117 * | 0.0052 ** |

*Means of ± standard errors followed by different letters within columns are significantly different by Fisher's least significant difference (LSD) test with one-way ANOVA; n = 8.*

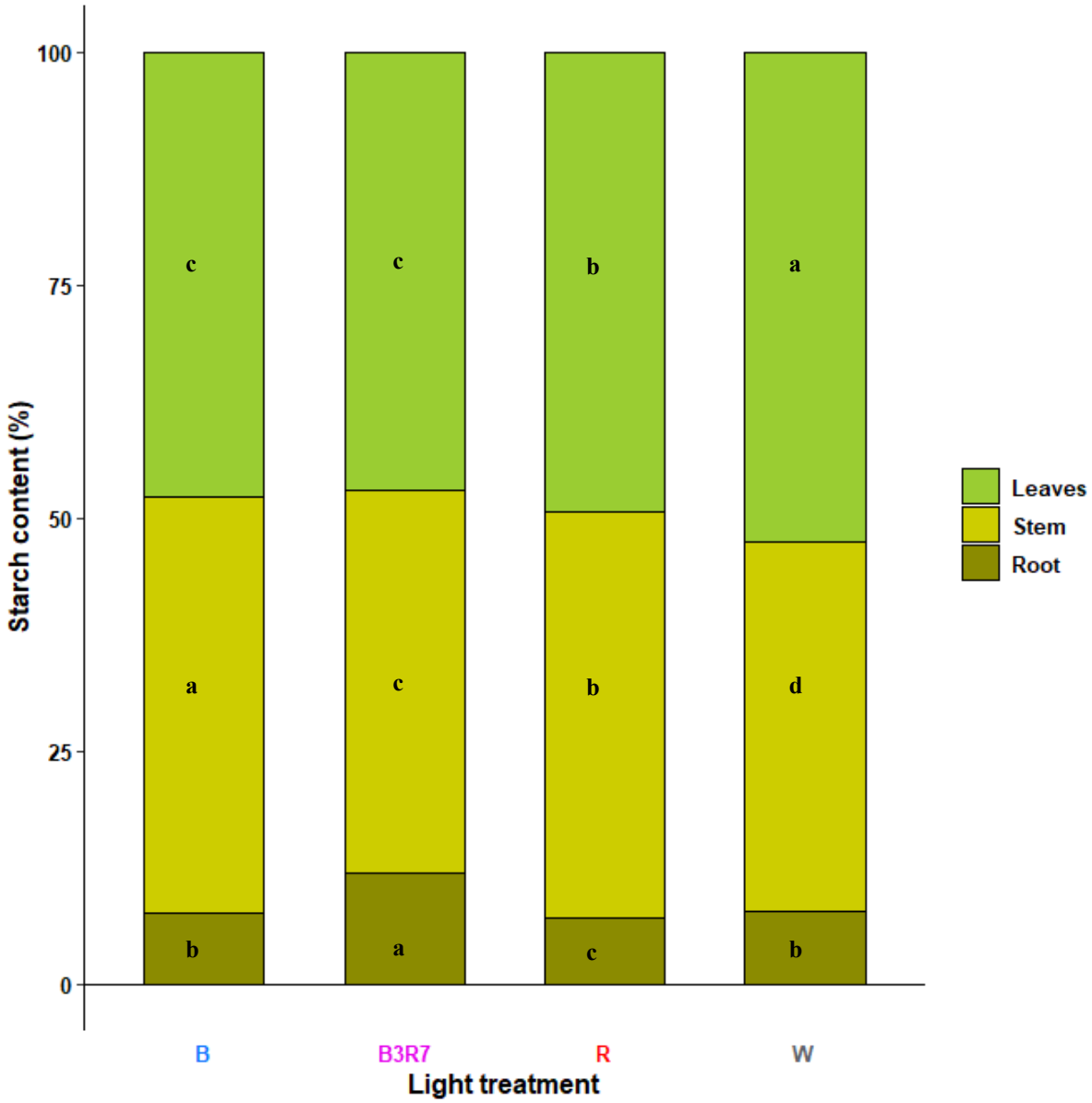


**Figure 2.12** Percentage of starch content per plant partitioned to different organs of *Mentha arvensis* L. after 4 weeks grown under different LED light treatments, at the same PPFD 150 µmol $m^{-2}$ $s^{-1}$. *Statistical analysis was performed using a ANOVA test (p-value ≤ 0.05) followed by a Fisher's least significant difference (LSD) post hoc test for multiple comparisons. Different letters indicate a significant difference between the two means.*

Lastly, the results illustrate the total phenolic content extracted from Wild Mint plants after four weeks of growth under different LED light sources, as detailed in Table 2.9. Significantly higher total phenolic concentrations were observed in plants subjected to all color LED treatments compared to the control group exposed to white LED lights. Notably, phenolic compounds were highest in the B3R7 combined LED treatment. They tended to accumulate in the stems of plants exposed to blue LED light, whereas, in plants subjected to red light, accumulation primarily occurred in the roots. (Table 2.9, Figure 2.13).

**Table 2.9** Total phenolic content in different plant organs (roots, stems, leaves) of *Mentha arvensis* L. after 4 weeks grown under different LED light treatments, at the same PPFD 150 μmol $m^{-2}$ $s^{-1}$.

| Light | Total phenolic content (mg GAE/g FW) | | | Total plant (mg GAE/plant) |
|---|---|---|---|---|
| | Root | Stem | Leaves | |
| B | 7.08 ± 0.19 [a] | 4.28 ± 0.20 [a] | 17.85 ± 0.67 [a] | 198.22 ± 1.76 [b] |
| B3R7 | 5.12 ± 0.10 [b] | 2.63 ± 0.03 [bc] | 15.95 ± 0.41 [a] | 252.07 ± 12.22 [a] |
| R | 7.28 ± 0.23 [a] | 2.93 ± 0.06 [b] | 17.50 ± 0.84 [a] | 193.36 ± 10.37 [b] |
| W | 3.23 ± 0.16 [c] | 2.31 ± 0.09 [c] | 12.18 ± 0.15 [b] | 134.60 ± 2.69 [c] |
| ANOVA's test | 4.38e-09 *** | 2.26e-07 *** | 0.0002 *** | 3.51e-06 *** |

*Means of ± standard errors followed by different letters within columns are significantly different by Fisher's least significant difference (LSD) test with one-way ANOVA; n = 8.*

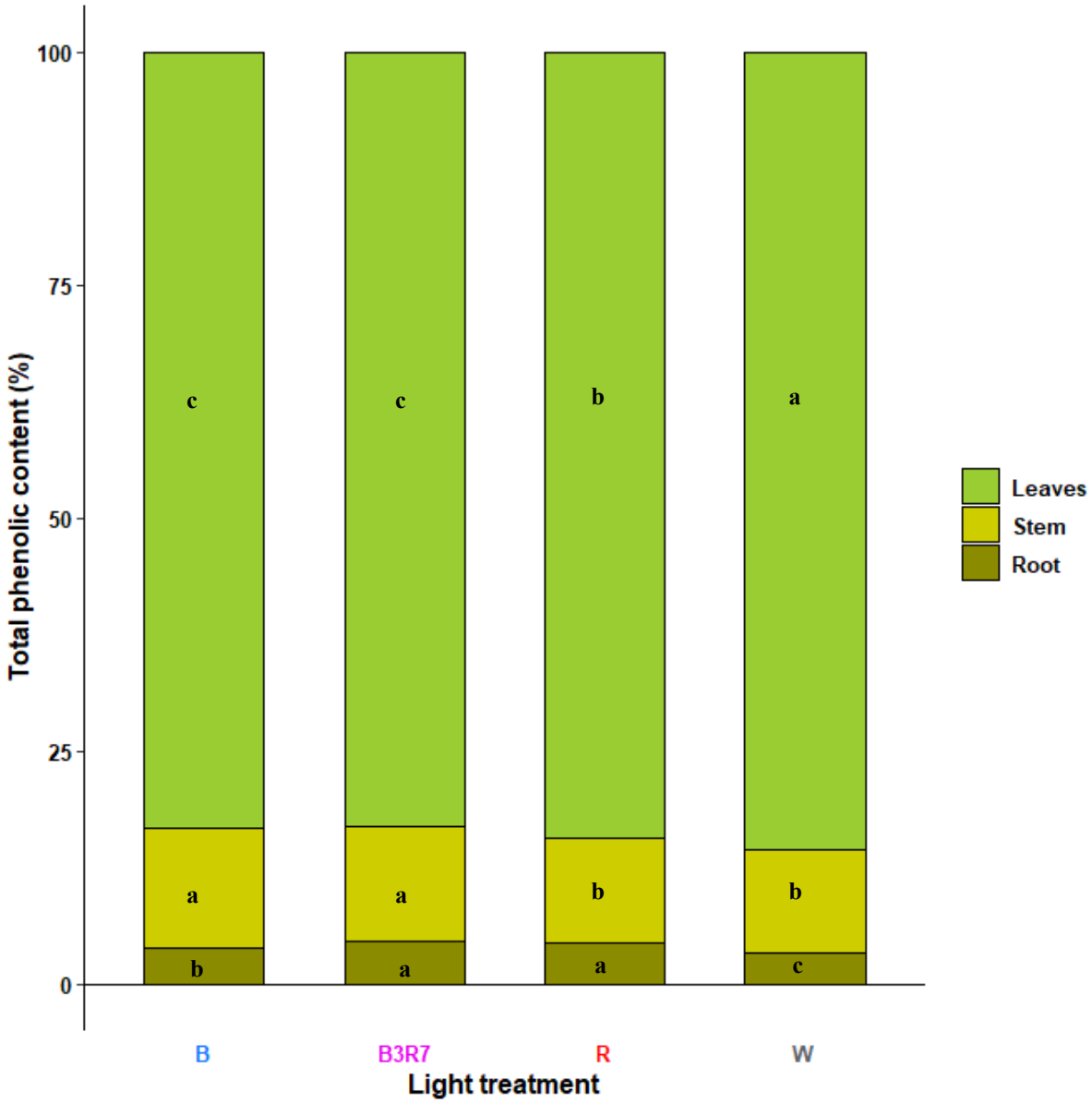


**Figure 2.13** Percentage of total phenolic content per plant partitioned to different organs of *Mentha arvensis* L. after 4 weeks grown under different LED light treatments, at the same PPFD 150 µmol $m^{-2}$ $s^{-1}$. *Statistical analysis was performed using a ANOVA test (p-value ≤ 0.05) followed by a Fisher's least significant difference (LSD) post hoc test for multiple comparisons. Different letters indicate a significant difference between the two means.*

## 4. Discussion

Several studies have reported that differences in light quality are a significant factor affecting plant growth in indoor farming (Kozai et al., 2016; Rahman et al., 2021; Sheibani et al., 2023). In this study, four LED light conditions, all providing the same PPFD of 150 μmol $m^{-2}$ $s^{-1}$, were applied to investigate the overall plant growth traits and yield of Wild Mint in a plant factory. The results showed that red and blue light played opposing roles in determining the height of Wild Mint plants, the number of leaves, and axillary buds (Figure 2.9-2.11). A high ratio of red LEDs promoted the number of leaves and axillary buds in the cultivation system of Wild Mint. Meanwhile, these traits did not significantly differ between plants grown under blue and white LEDs.

Axillary buds, originating from axillary meristems within the leaf axils, can remain dormant or extend to form branches of varying sizes (Holalu and Finlayson, 2017; Leduc et al., 2014). According to Kong et al. (2018), the effect of different LED light spectra on leaf and axillary bud growth is related to phytochrome activity (Kong et al., 2018). Plants grown under red light enhanced phytochrome B (PHYB) receptor activity, leading to bud outgrowth in Arabidopsis and Sorghum (Childs et al., 1997; Finlayson et al., 2010; Kebrom et al., 2006). The development of axillary buds and branches can improve light absorption for photosynthesis in plants, consequently increasing the red LED ratio in supplementary lighting will have a positive effect on the overall growth of Wild Mint plants.

Furthermore, red LED light significantly increased the height of Wild Mint in the cultivation system. Red light, acting through phytochrome receptors, induces the synthesis of $GA_3$ and auxins, augmenting the synthesis of cell wall extensions, leading to the elongation of internodes in *Arabidopsis* plants (Schneider et al., 2019). Conversely, blue light acts as a signal for the inhibition of cell division and cell expansion, thereby reducing the elongation of stem

internodes in spinach plants (Spaninks et al., 2020).

The combination of blue and red light at specific ratios has a positive impact on plant growth compared to white light, as reported in *Morus alba*, *Vaccinium corymbosum* L., *Latuca sativa* L. (Hu et al., 2016; Hung et al., 2016; Li and Kubota, 2009; Stutte et al., 2009). The same trend was observed in Wild Mint exposed to B3R7 combination LEDs, with a limitation on plant height, similar to the effect of blue light but with enhanced branch and leaf development. Our results determined that changing light quality can be used to manipulate plant performance and development.

Modifications in branching and plant structure have a direct impact on the final crop yield and overall plant productivity (Murchie and Burgess, 2022; Yang and Hwa, 2008). In the case of Wild Mint plants, those cultivated under B3R7, or red LED lighting exhibited favorable plant architecture that efficiently supported photosynthesis, resulting in high plant biomass. The absence of a red-light spectrum (in blue-led treatment) was unfavorable for plant biomass accumulation when compared to plants under white LED lighting. (Tables 2.5 and 2.6). The majority of the increase in Wild Mint plant weight can be attributed to the biomass of the above-ground portions (Figures 2.12 and 2.14), which hold particular economic significance due to their crucial role in the production of valuable commercial products within the Mint species (Ellis, 1960; Fatih et al., 2017). Interestingly, the fresh biomass produced by plants under red LED light was lower than that of plants under B3R7 combination LEDs. However, the dry biomass showed the opposite results, indicating a difference in the water content consumed by Wild Mint plants under these light conditions.

A similar growth pattern was observed in the root biomass produced by plants under red or B3R7 LED treatments, surpassing the growth observed in plants under blue and white LEDs. This indicates accelerated root development in plants under these treatments. Roots play a vital

role in plant growth, serving as the primary structures responsible for water and nutrient absorption from the soil (Palacio et al., 2007; Tajima, 2021). Numerous studies have shown that deeper roots, characterized by higher deep root ratios and greater rooting depth, tend to absorb more water from the soil. Additionally, higher root length densities are associated with increased nutrient absorption (Groff and Kaplan, 1988; Li et al., 2021). The parallel growth of both roots and shoots highlights the adaptability of Wild Mint to changing of these light conditions.

Photosynthesis, influenced by various LED light spectra, also affects the production of primary metabolite in Wild Mint plants. In most plants, sucrose is the primary organic compound found in the cytosol of photosynthetic (source) cells. It serves as an immediately available form for transport to heterotrophic (sink) organs, where it can be used for metabolism and respiration to generate the energy source ATP, or it can be stored as starch, playing a crucial role in biomass (W. Patrick et al., 2013). Therefore, the content of substances such as sucrose and starch are essential for evaluating the photosynthetic performance and growth of Wild Mint plants under different light conditions. The increase in photosynthetic product accumulation, such as sugar or starch (Table 2.7 and 2.8), leads to an increase in water uptake, consequently resulting in increased fresh weight in Wild Mint plants grown under B3R7 combined light compared to those in other LED light treatments (Figures 2.12 and 2.14). Similarly, the transport, distribution, and storage of sucrose and starch in different plant organs are closely correlated with the percentage of organ biomass in Wild Mint plants under various light conditions (Figures 2.13, 2.15, 2.16, and 2.17).

Moreover, the sugars produced by the photosynthetic fixation of $CO_2$ provide raw material for the biosynthesis of all the organic molecules found in plant, the photosynthetic primary compound metabolism serves as a source of raw materials and energy, either directly or

indirectly through respiration, for the biosynthesis of secondary compounds such as phenolics in plants (Darko et al., 2014). In this study, all colored LED light treatments demonstrated an increase in the total phenolic content in Wild Mint leaves compared to the control. Particularly, the decrease in sugar content in the blue or red monochromatic light treatments was correlated with an increase in the total phenolic content in Wild Mint plants. A similar trend was observed in other plant species, such as *Brassica napus* L., *Lactuca sativa*, *Ocimum basilicum*, and *Rhodiola imbricata*, when exposed to red or blue LEDs with light intensities ranging from 50 to 200 μmol $m^{-2}$ $s^{-1}$ (Bantis et al., 2016; Johkan et al., 2010; Kapoor et al., 2018; Park et al., 2019). The total phenolic compound increased with additional color LED lights, even when blue or red LEDs were applied only as supplemental light or in combination light source (Hasan et al., 2017; Jung et al., 2021). Results in lettuce also indicated an increase in the total phenolic compound after short- or long-term exposure to red or blue LED light when compared to white light (Son et al., 2012). Several studies have reported the relationship between red or blue LED light and phenylalanine ammonia-lyase (PAL), a key gene encoding the enzyme responsible for phenolic metabolites (Heo et al., 2012; Park et al., 2020; Son et al., 2012).

## 5. Conclusion

The results revealed that monochromatic blue light suppressed Wild Mint plant growth, while monochromatic red light stimulated it. Plants grown under a combined light spectrum (30% blue: 70% red) exhibited significantly enhanced productivity and biomass compared to other treatments. The distribution and accumulation of photosynthesis products and biomass in different plant organs were notably influenced by these distinct light treatments, impacting source-sink relationships in plants, including factors such as assimilate demand.

All colored LED light treatments increased the phenolic content of Wild Mint leaves. Additionally, combination B3R7 LED light proved to be a more effective source to produce total phenolic compounds in Wild Mint plants. These findings underscore the potential of LED technology in manipulating the growth and accumulation of desirable bioactive compounds during Wild Mint plant cultivation, contributing to the refinement of indoor herb cultivation protocols to meet production demands.

## Chapter II: Growth traits and photosynthetic characteristics in *Mentha arvensis* L. under varied LED lighting conditions based on high throughput phenotyping

### 1. Introduction

Photosynthesis is the process of converting light energy into chemical energy in the form of reducing power, such as NADPH or NADH, and ATP. These chemical compounds are subsequently utilized to facilitate the fixation of carbon dioxide and its reduction into sugars, with the by-product of $O_2$ release (Bowyer and Leegood, 1997; Johnson, 2016). The outputs of photosynthesis serve as the primary organic for plant biomass construction, thus, crucial in determining crop yield and food production (Chen et al., 2018; Hu et al., 2021). With the world's population growing at an increasingly rapid rate, there is a heightened demand for pharmaceuticals, agricultural products, and food safety, necessitating a doubling of yields by 2050 (Valin et al., 2014). Consequently, there is an ongoing and pressing need to comprehensively understand the mechanisms of photosynthesis and to develop strategies for enhancing crop yield and quality through improvements in photosynthetic processes.

A comprehensive understanding of the light mechanisms that regulate photosynthesis represents a complex study. Furthermore, achieving accurate measurements of photosynthetic efficiency remains a challenge (Yahia et al., 2019). Currently, the most widely used method for assessing photosynthesis is the gas-exchange method, which provides instantaneous measurements and allows for the quantification of $CO_2$ assimilation, ranging from individual leaves to canopy-level photosynthetic rates (Haworth et al., 2018). However, it is important to note that these techniques are significantly influenced by environmental variables, particularly temperature, which can compromise their precision. Furthermore, conventional measurement techniques tend to be time-consuming, costly, destructive in certain phenological stages and not suitable for large-scale phenotyping trials, even when incorporating methods designed to

expedite data collection (Fu et al., 2022).

In response to "phenotyping bottlenecks" posed by limitations in traditional methods, the emergence of high-throughput phenotyping techniques for measuring plant photosynthesis represents a significant advancement (Furbank and Tester, 2011; Stirbet et al., 2020). This development has given rise to the concept of “phenomics” which can essentially be described as “high-throughput plant physiology”. Various high-throughput phenotyping (HTP) platforms, combining novel technologies such as non-invasive imaging, spectroscopy, image analysis, robotics, and high-performance computing, have been emerging to address the challenges of traditional low-throughput methods (Fu et al., 2022; Stirbet et al., 2020).

Huichun Zhang et al. demonstrated the potential of optical sensing in assessing a wide range of plant leaf characteristics, including morphology, physiology, and biochemical traits (Zhang et al., 2023). High-throughput phenotyping has proven its power in large-scale evaluations of plant yield, biomass, and phenotype using RGB images (Du et al., 2020; Han et al., 2021). Non-destructive optical techniques, performed in situ, have become popular for providing relative indications of photosynthetic pigment concentration by measuring the percentage of light transmitted through and reflected off the leaf surface (Cerovic et al., 2015, 2012; Kuleshova et al., 2018; Parry et al., 2014). Additionally, researchers have used chlorophyll fluorescence as a dynamic measurement to delve into the maintenance of photosynthetic function under specific environmental conditions. This measurement can now be carried out using affordable commercial instruments, particularly those utilizing pulse amplitude-modulated (PAM) fluorometry (Baker, 2008, 2004; Fu et al., 2022; Kalaji et al., 2017; Stirbet et al., 2020).

As a result, the evaluation of plant performance in the field has become significantly faster, allowing for a more comprehensive measurement throughout the plant's lifecycle and reducing

the reliance on periodic destructive assays (Fu et al., 2022; Furbank and Tester, 2011; Stirbet et al., 2020; Zhang et al., 2023). Moreover, these platforms are flexible and can be implemented on different scales from in vitro, trials to field environments (Araus and Cairns, 2014; Awlia et al., 2016; Bethge et al., 2023; Cho and Yang, 2023; Yang et al., 2020, 2020). The availability of commercial sensors has made it possible to integrate various sensing technologies on a single platform, offering a non-invasive, cost-effective, and efficient means of characterizing plant growth and photosynthesis over time (Cho and Yang, 2023; Qiu et al., 2018). The application of these tools in dedicated high-throughput, controlled-environment facilities have the potential to enhance precision and reduce the need for replication in field studies. So far, these techniques have had a substantial impact on our understanding of photosynthesis and photosynthetic physiology, ranging from individual leaves to entire canopy scales (Araus and Cairns, 2014; Fu et al., 2022; Valin et al., 2014).

In the present study, various high-throughput phenotyping methods were employed to assess the effect of varying blue-to-red LED light ratio influences on the overall growth, chlorophyll fluorescence parameters, and photosynthetic traits of Wild Mint plants. These findings enhance the comprehension of how Wild Mint plants react to alterations in environmental light conditions and assist in establishing consistent procedures for cultivating and tending to these plants on a commercial scale.

## 2. Materials and methods

### *2.1 Plant material and experiment design*

10-day-old *Mentha arvensis* L. (Wild Mint) plants were used as plant material. Plant material was grown under four different LED lights: 100% blue (B), 30% blue and 70% red (B3R7), 100% red (R), and cool white (W), 12/12 photoperiod, at the same PPFD 150 μmol photon.$m^{-2}$ $s^{-1}$. The growth conditions were controlled by using an indoor hydroponics system with temperature at 27 ± 2°C, relative humidity of 65 ± 5%, 6.8 ± 0.2 pH.

### *2.2 Images acquisition*

For the photograph of the Wild Mint plants, an indoor studio (600*600*600 mm) was set up to reduce the influence of ambient light. An 18W class white (5600K) LED (CN-T96, Plastic, Korea) was added to adjust the required illumination to prevent distortion and damage to the data caused by shadows, and the background plate was made in-house in white considering the green color of the plant. A 12.1-megapixel CMOS sensor digital camera (IXUS 220 HS, Canon, Japan) was used as the camera. The camera settings had an ISO value of 400 and an exposure time of 1/10.

For the examination of the leaf area, all leaves, including those on the lateral stem, were isolated and placed on A4 paper as a background. Top-view leaf imaging was conducted within the studio, maintaining a 90-degree angle and a 400 mm distance between the camera and the leaf surface.

For the assessment of plant area or plant convex hull, side-view images of entire Wild Mint plants, including stems and leaves were captured. The plants were positioned within the same studio at a 400 mm distance from the camera, with the camera angle adjusted to 90 degrees relative to the plant surface.

*2.3 Leaves area based on RGB images*

The leaf area was measured using ImageJ (National Institutes of Health, NIH, USA) (Schindelin et al., 2012), following these steps:

The leaf image (Figure 3.1A) was imported into ImageJ2 (Fiji) and its contrast was enhanced by 30% to eliminate shadows (Figure 3.1B). Subsequently, the color threshold levels (hue, saturation, and brightness) were adjusted to segment the leaves from the background and convert the image into a binary format, with leaves represented as white pixels and the background as black pixels. Any noise or small artifacts in the binary image were removed using the "Fill Holes" tool (Figure 3.1C). Finally, the leaf area was measured from the binary image using the "Analyze Particles" function (Figure 3.1D).

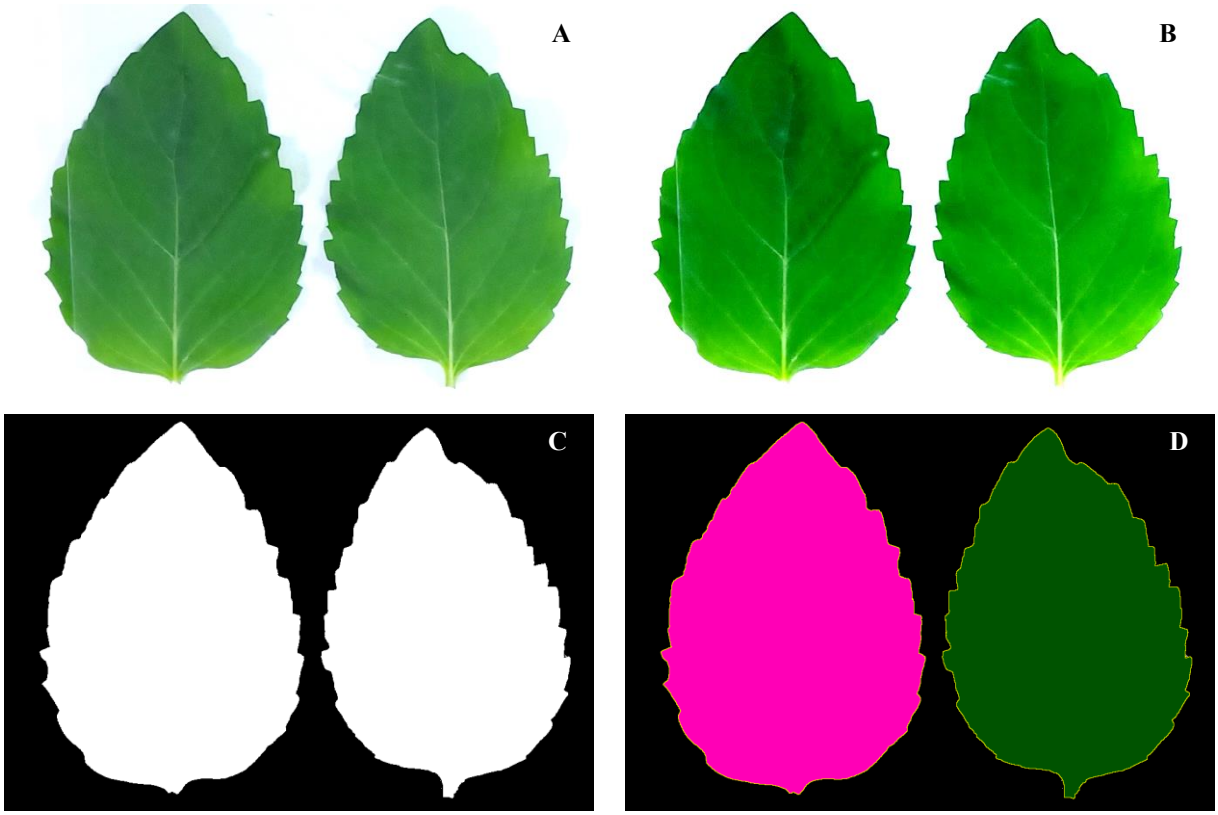


**Figure 3.1** Representative picture showing the extraction of leaves area using ImageJ2 (Fiji) software. *Original image (A), enhancing contrast image (B), binary image (C), and extract leaves area (D).*

*2.4 Plant area and plant convex hull based on RGB images*

The plant area and plant convex hull were measured using ImageJ (National Institutes of Health, NIH, USA) (Schindelin et al., 2012), following these steps:

Side-view images of entire Wild Mint plants (Figure 3.2A) were imported into ImageJ2 (Fiji) and their contrast was enhanced by 30% to eliminate shadows (Figure 3.2B). Subsequently, the color threshold levels (hue, saturation, and brightness) were adjusted to segment the plant from the background and convert the image into a binary format, with the plant area represented as white pixels and the background as black pixels (Figure 3.2C). The plant area was measured from the binary image using the “Wand Tool” and the “Measure" function (Figure 3.2D). The plant convex hull was measured from the binary image using the “Convex hull” and “Measure" function (Figure 3.2E), and the original convex hull image is shown in Figure 3.2F.

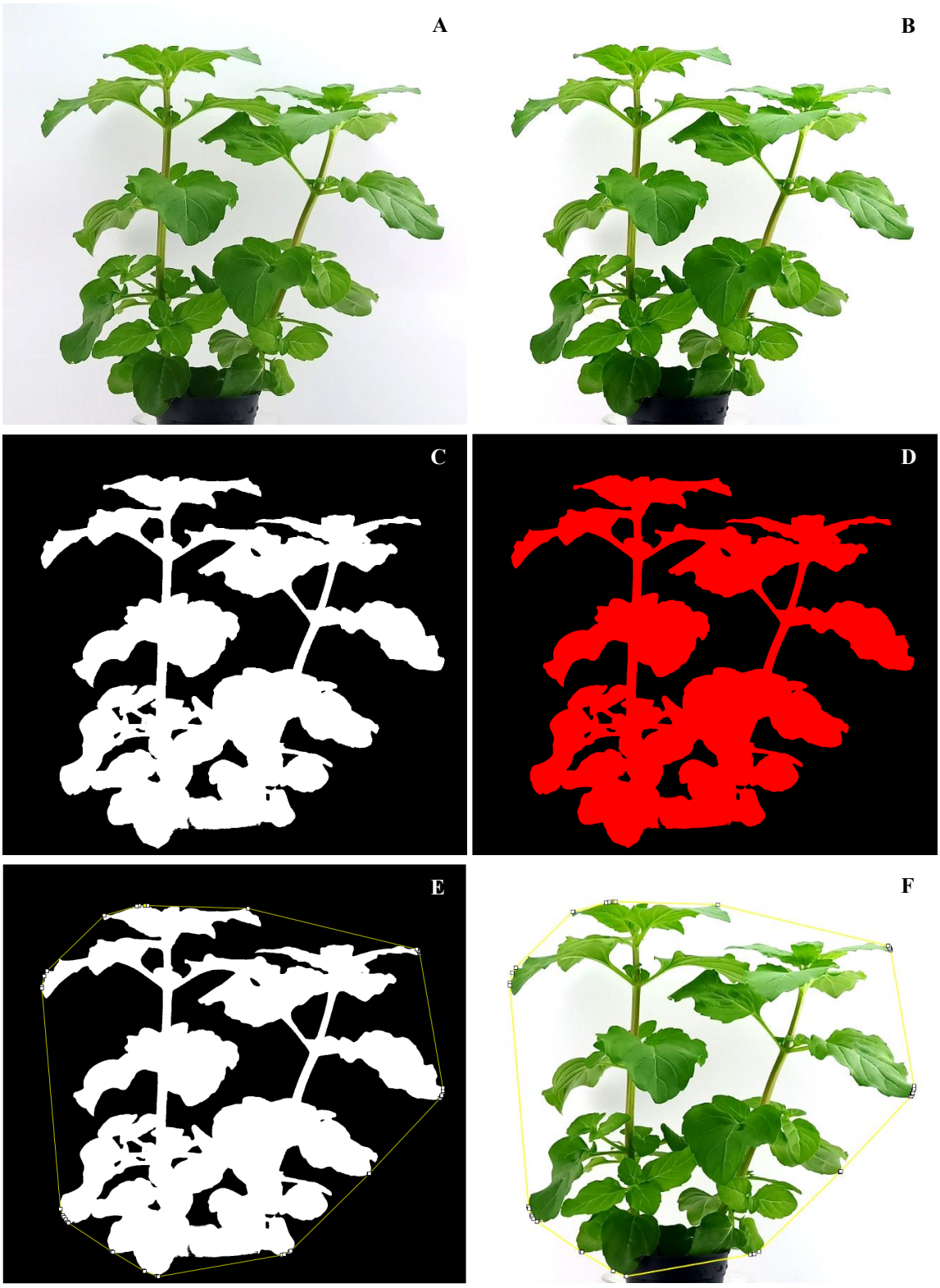


**Figure 3.2** Representative picture showing the extraction of plant area and plant convex hull value using ImageJ2 (Fiji) software. *Original image (A), enhancing contrast image (B), binary image (C), extract plant area (D), plant convex hull (E, F).*

*2.5 Determination of stomatal characteristics based on leaf micrograph images*

The fifth leaves from the tip of the plant's canopy, at harvest time, were isolated and swept onto the underside with a cyanoacrylate glue (mixed in toluene and ethyl acetate solvents) and fixed on microscope slides. The stomatal micrographs of leaf on cyanoacrylate film were captured by a CKX41 inverted microscope (Olympus, Tokyo, Japan) with a DFC450 camera (Leica, Wetzlar, Germany), and the original images were stored in JPEG format with a resolution of 3360 x 4480 pixels (Figure 3.3A). The stomatal characteristics in leaves of *Mentha arvensis* L. were measured using ImageJ (National Institutes of Health, NIH, USA), following as illustration below:

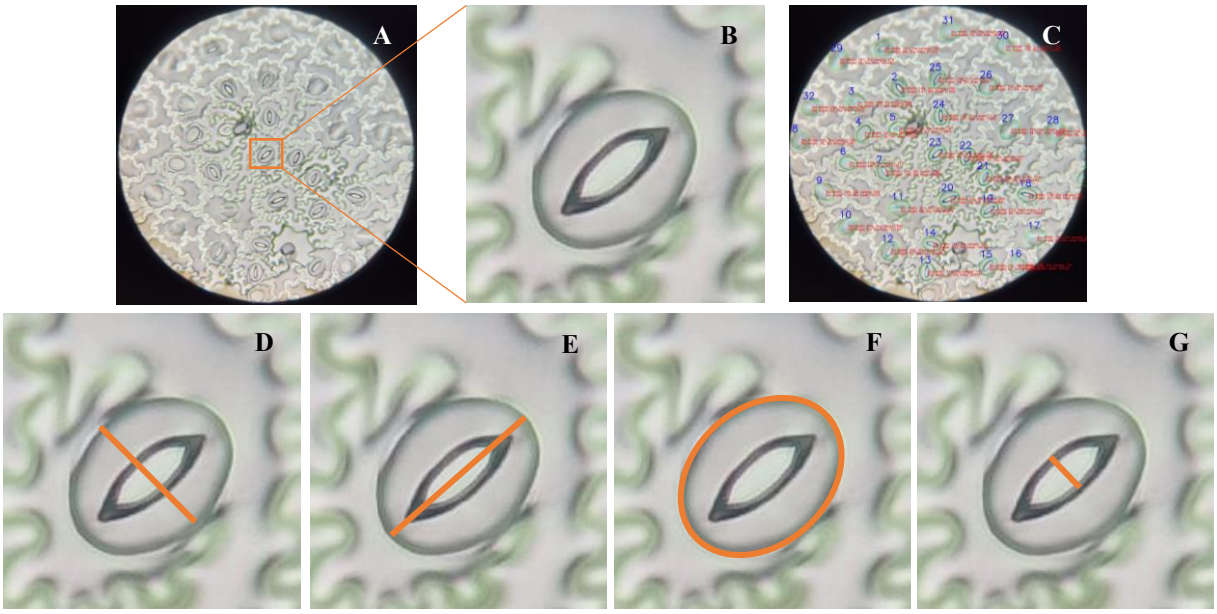


**Figure 3.3** The stomatal characteristics measurement process in the leaves of *Mentha arvensis* L. *Original image (A), SD: stomatal density (C), separated individual stomata (B), GCW: guard cell width (D), GCL: guard cell length (E) GCA: guard cell area (F), and SPA: stomatal pore apertures (G).*

*2.6 Chlorophyll concentration index*

The Chlorophyll Concentration Index (CCI) value of the 5$^{th}$ leaf position from the plant tip was measured using a handheld CCM-200 plus (Apogee, USA). The leaves were clamped

randomly at 4 positions on the leaf blade and averaged as a measurement value. The measurement results are based on the light transmission ratio at two wavelengths: red and infrared bands, through the leaf of the plant. The red wavelength spectrum falls within the chlorophyll absorbance range while the other serves to compensate for mechanical differences such as tissue thickness. Assuming an even distribution of chlorophyll in the leaf, the chlorophyll index depends on the molecular chlorophyll content in the leaf and can be determined using the formula:

$$CCI = \frac{Amount\ of\ light\ transmitted\ at\ 931\ nm}{Amount\ of\ light\ transmitted\ at\ 653nm}$$

Chlorophyll Concentration Index (CCI) value that is proportional to the amount of chlorophyll in the sample.

*2.7 Polyphenols measurement*

The flavonol index (Flav) value of the 5$^{th}$ leaf position from the plant tip was measured using a handheld Dualex Scientific$^{+TM}$ device (Force-A, France). The leaves were randomly clamped at four positions on the leaf blade and then averaged to obtain a measurement value. The measurement results are based on the fluorescence light ratio at two wavelengths: red and UV-A, through the plant's leaf (Figure 3.4).

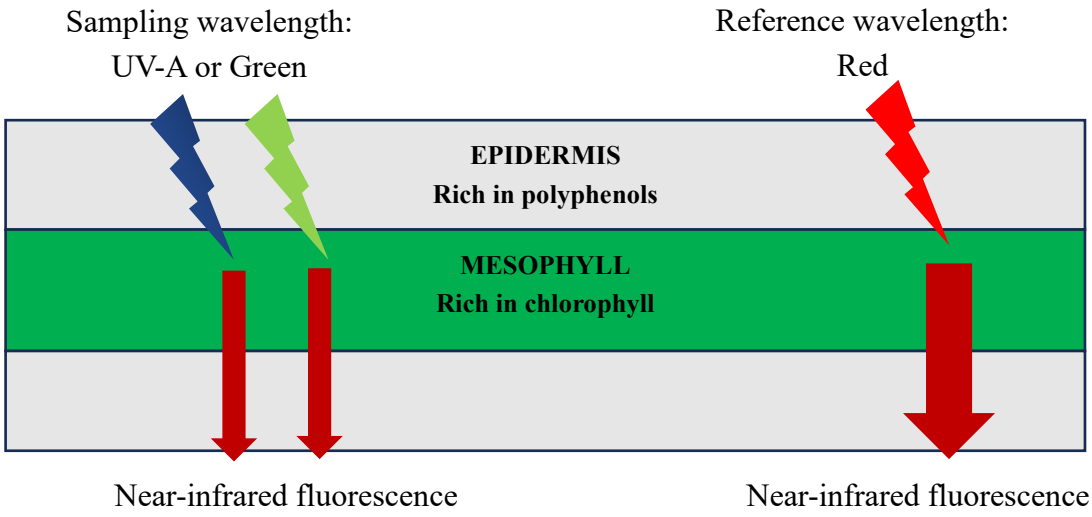


**Figure 3.4** Operating principle of the handheld Dualex Scientific$^{+TM}$ meter.

First, near-infrared chlorophyll fluorescence is measured under red excitation light as a reference, which is not absorbed by polyphenols. Second, the fluorescence excitation under the UV-A light wavelength spectrum, falling within the absorbance range of flavonols, was measured. Only a fraction of this light reaches the chlorophyll in the mesophyll and can generate near-infrared fluorescence. The flavonol index can be determined using the following formula:

$$Flavonol\ index = Log\ \frac{Near-infrared\ fluorescence\ excited\ red}{Near-infrared\ fluorescence\ excited\ UV-A}$$

Similarly, the anthocyanin index was measured under red and green light, followed by the formula:

$$Anthocyanin\ index = Log\ \frac{Near-infrared\ fluorescence\ excited\ red}{Near-infrared\ fluorescence\ excited\ green}$$

*2.8 Measurements of the chlorophyll fluorescence parameters*

The fluorescence yield of chlorophyll in Wild Mint plant leaves under varying LED light ratios was investigated by PAM-2500 Portable Chlorophyll Fluorometer (Walz, Germany) with DLC-8 (Dark Leaf Clip DLC-8) and Leaf-Clip Holder 2030B.

The 5$^{th}$ leaf position was isolated and dark-adapted for 15 minutes. The minimum

fluorescence value ($F_o$) was measured after a 1-minute in the dark and the maximum fluorescence value ($F_m$) during a 1-second saturating light pulse 5700 μmol $m^{-2}$ $s^{-1}$. Then, the leaf samples were exposed to experimental light conditions for 10 minutes, and fluorescence values (F), maximum fluorescence values (Fm') during a 1-second saturating light pulse 5700 μmol $m^{-2}$ $s^{-1}$, and minimum fluorescence values (Fo') within 5 seconds under far-red light were sequentially recorded over time. Fluorescence parameters were calculated using the following formulas (Baker, 2008):

Maximal quantum yield of photosystem II:

$$\mathrm{Y(II)}_{max} = \mathrm{Fv/Fm} \text{ (ranging from 0 to 1)}$$

Non-photochemical fluorescence quenching coefficient:

$$qN = 1 - \frac{\mathrm{Fm' - Fo'}}{\mathrm{Fm - Fo}}$$

Photochemical fluorescence quenching coefficient:

$$qP = \frac{\mathrm{Fm' - F}}{\mathrm{Fm' - Fo'}}$$

Maximum electron transport rate:

$$ETR = PAR \times ETR - Factor \times P_{PS2}/P_{PPS} \times Y(II)$$

Where:

PAR is the photosynthetically active radiation intensity.

ETR-Factor: Absorptance of photons by photosynthetic pigments (default value is 0.84).

PPS2/PPPS Photons absorbed by PS II relative to photons absorbed by photosynthetic pigments (default value is 0.5).

Y(II): Effective photochemical quantum yield of PSII

*2.9 Statistical analysis*

Each Wild Mint plant was used as a replicate. All experiments were conducted with 8 plants/LED treatment. Data analysis was performed using R software (Version 4.3.1, the R Foundation for Statistical Computing, Vienna, Austria). The datasets were checked for normality using the Shapiro-Wilk test (Shapiro and Wilk, 1965).

For datasets that did not meet the criteria for normality distribution, non-parametric data analysis was conducted using the Kruskal-Wallis test, followed by the Dunn test with Benjamini-Hochberg correction.

In contrast, the datasets exhibited a normal distribution. For these datasets, parametric analysis was conducted using the One-way ANOVA test, followed by Fisher's least significant difference (LSD) post hoc test to compare measurements between different LED light treatments. Bar plots and box plots were generated using the 'ggpubr' package in R 4.3.1.

## 3. Result

Recent developments in portable devices for photosynthetic measurement enable the assessment of photosynthetic rates in individual leaves and provide the means to project these leaf measurements to estimate the overall photosynthetic rates of the entire plant or canopy throughout the growth cycle (Araus and Cairns, 2014; Fu et al., 2022; Haworth et al., 2018; Zhang et al., 2023). However, the effect of light conditions on individual leaves varies depending on their position and the heterogeneity within the plant canopy (Bauerle et al., 2020; Constable and Rawson, 1980; Dwyer and Stewart, 1986; P. Zhang et al., 2020). To improve the precision of experimental measurements, a leaf growth curve was constructed to assess the photosynthetic rate of Wild Mint plant leaves, typically up to the stage of full leaf expansion. The leaf area of Wild Mint plants, after 4 weeks of cultivation under white LED light, gradually increases with leaf position. The maximum leaf area is observed at the $5^{th}$ position from the plant tip, measuring 4.87 $cm^2$. In the $4^{th}$ and $5^{th}$ leaf groups, both biomass and chlorophyll content exhibit significant increases, with measurements of 458 mg and 21.8 CCI, respectively (Table 3.1, Figure 3.5). The increase in both the number of leaves and the total leaf area is directly relative to the expansion of the overall plant area and canopy size as time progresses (Figure 3.6 and 3.7).

**Table 3.1** Fresh weight, dry weight, leaf area and chlorophyll content index of leaves at different positions in *Mentha arvensis* L. 4-week-old plants exposed to a white LED with a PPFD of 150 µmol $m^{-2}$ $s^{-1}$.

| Leaves position | Leaves area ($cm^2$) | Fresh weight (mg) | Dry weight (mg) | Chlorophyll content index (CCI) |
|---|---|---|---|---|
| 2 | 0.74 ± 1.29$^{d}$ | 76.5 ± 9.25$^{d}$ | 10.1 ± 1.14 $^{e}$ | - |
| 3 | 2.60 ± 3.51$^{c}$ | 296.8 ± 22.64 $^{c}$ | 32.9 ± 2.63 $^{d}$ | 17.1 ± 0.73 $^{b}$ |
| 4 | 4.18 ± 3.55 $^{ab}$ | 484.9 ± 15.76 $^{a}$ | 56.2 ± 2.18 $^{ab}$ | 20.9 ± 0.60 $^{a}$ |
| 5 | 4.87 ± 3.27$^{a}$ | 548.7 ± 22.87 $^{a}$ | 61.9 ± 3.30 $^{a}$ | 21.8 ± 0.71 $^{a}$ |
| 6 | 4.58 ± 3.04$^{ab}$ | 478.4 ±25.39 $^{a}$ | 49.0 ±3.84 $^{b}$ | 19.8 ± 0.68 $^{b}$ |
| 7 | 4.02 ± 3.77 $^{b}$ | 371.6 ±35.29 $^{b}$ | 46.2 ±4.67 $^{c}$ | 15.2 ± 0.60 $^{c}$ |
| 8 | 2.96 ± 2.80 $^{c}$ | 291.9 ±28.56 $^{c}$ | 28.2 ±2.84 $^{d}$ | 14.8 ± 0.57 $^{c}$ |
| 9 | 2.42 ± 2.16 $^{c}$ | 255.3 ±19.38 $^{c}$ | 29.0 ±2.11 $^{d}$ | 14.6 ±0.32 $^{c}$ |

*Statistical analysis was performed using a Kruskal Wallis test (p-value ≤ 0.05) followed by a Dunn Benjamini Hochberg post hoc test for multiple comparisons. Different letters indicate a significant difference between two medians.*

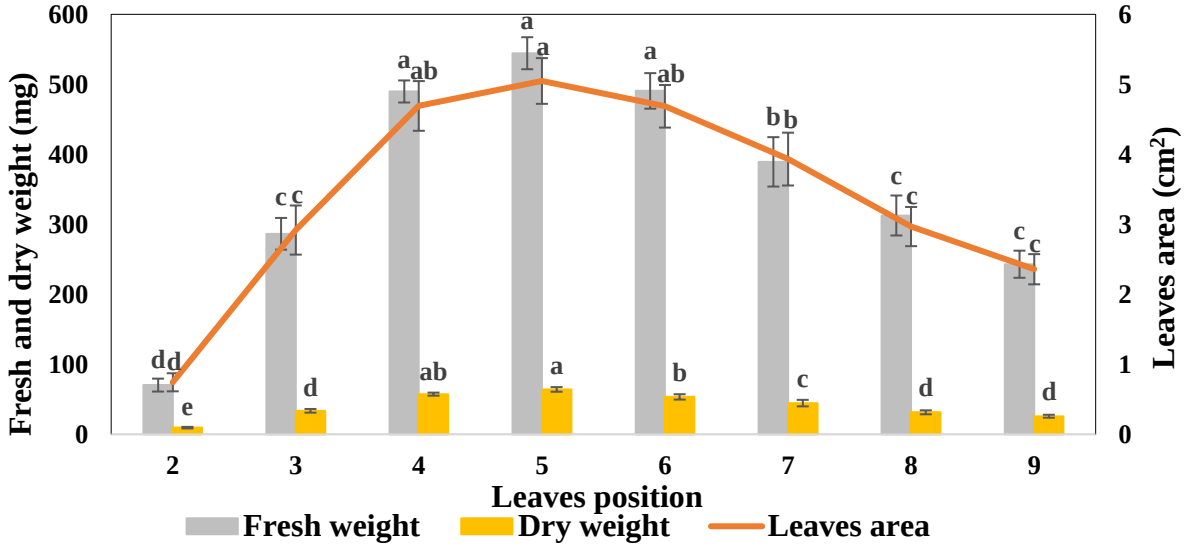


**Figure 3.5** Fresh weight, dry weight, leaf area and chlorophyll content index of leaves at different positions in Mentha arvensis L. 4-week-old plants exposed to a white LED with a PPFD of 150 µmol $m^{-2}$ $s^{-1}$. *Statistical analysis was performed using a Kruskal Wallis test (p-value ≤ 0.05) followed by a Dunn Benjamini Hochberg post hoc test for multiple comparisons. Different letters indicate a significant difference between two medians.*

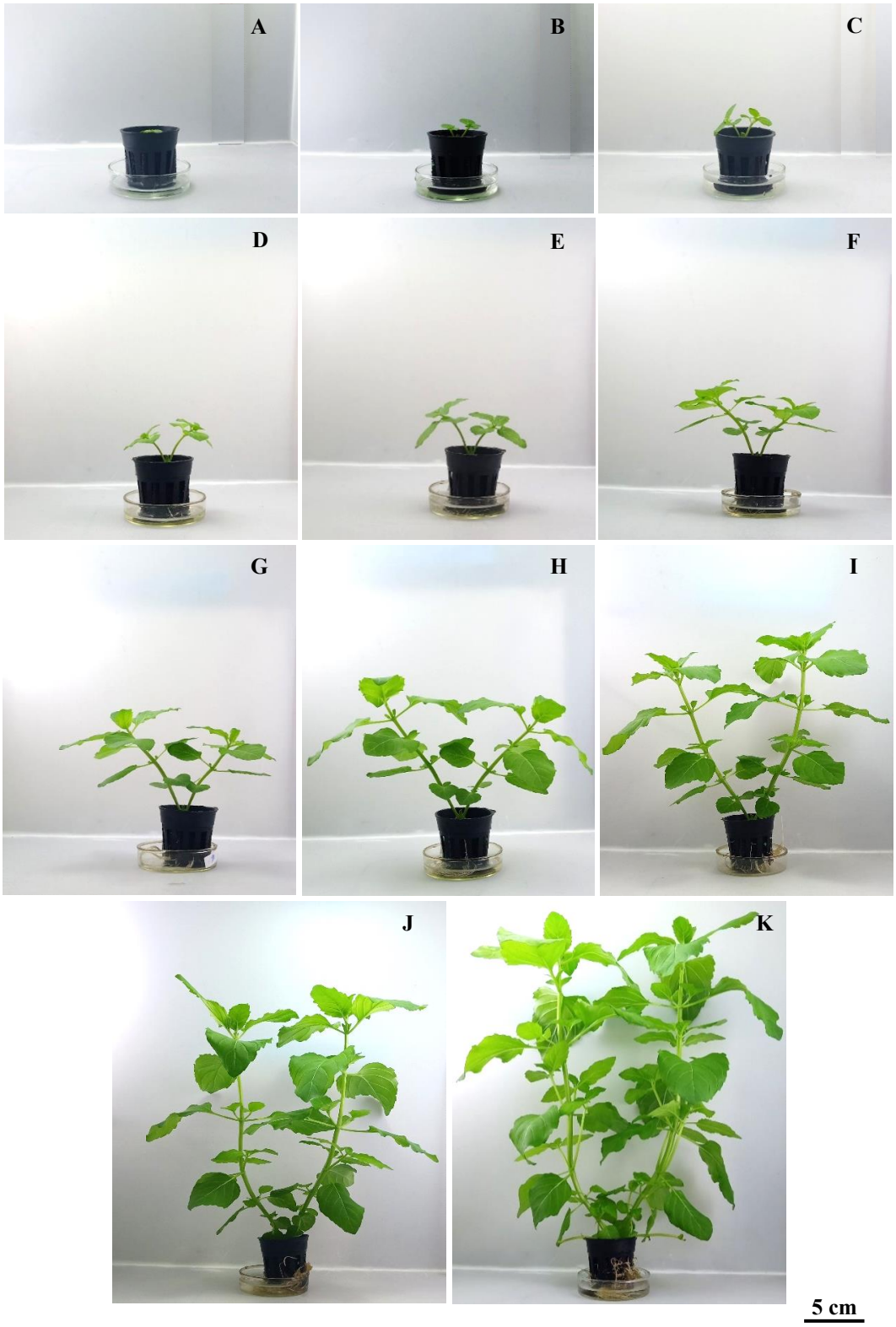


**Figure 3.6** Side view images of *Mentha arvensis* L. taken at 0 (A), 3 (B), 6 (C), 9 (D), 12 (E), 15 (F), 18 (G), 21 (H), 24 (I). 27 (J), 30 (K) days after transfer to white LED with a PPFD of 150 μmol $m^{-2}$ $s^{-1}$.

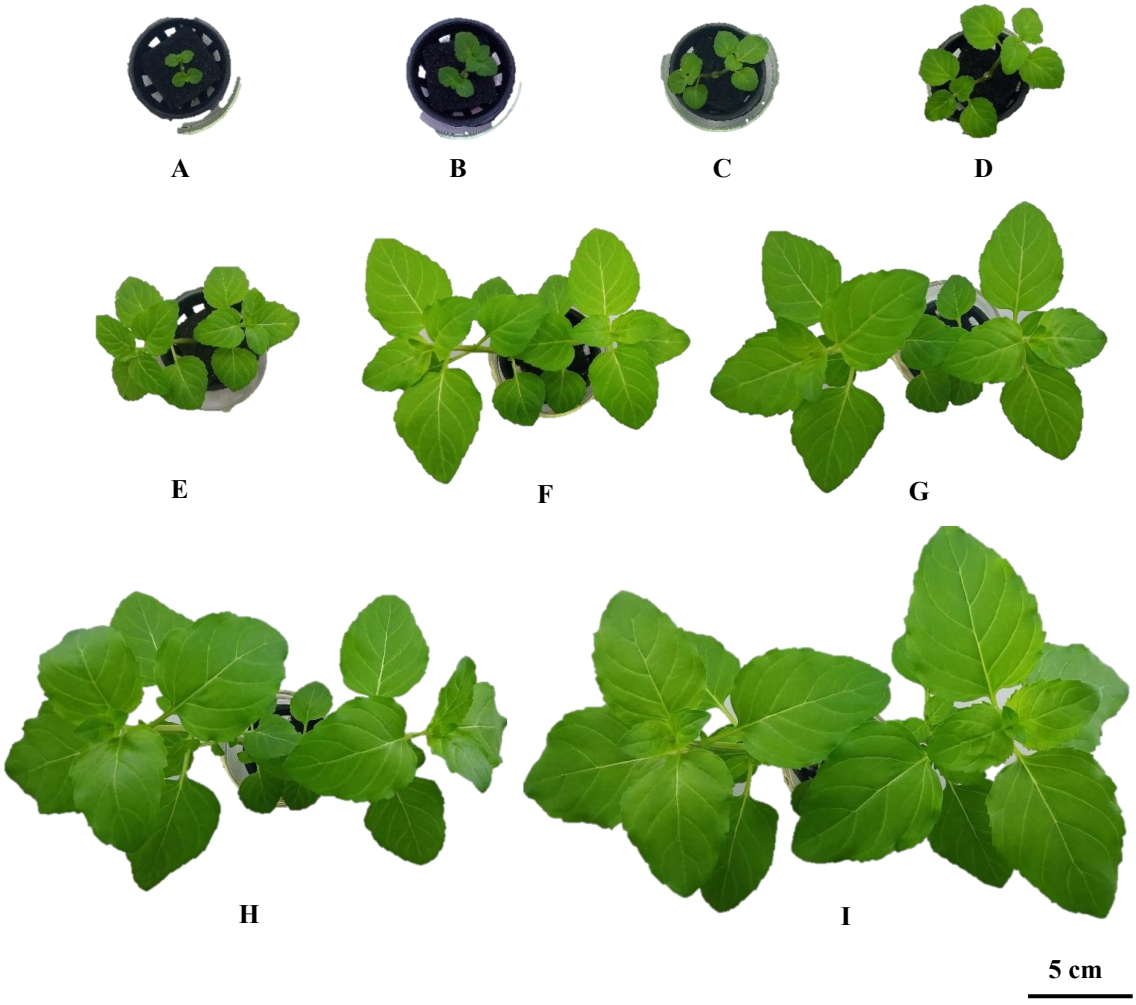


**Figure 3.7** Top view images of *Mentha arvensis* L. taken at 0 (A), 3 (B), 6 (C), 9 (D), 12 (E), 15 (F), 18 (G), 21 (H), 24 (I) days after transfer to white LED with a PPFD of 150 μmol $m^{-2}$ $s^{-1}$.

The experiments with Wild Mint plants were conducted under three different light conditions: monochromatic red LED (660 nm - R), blue LED (450 nm - B), and a combination of B3R7 LEDs. These conditions were compared to white LED light, which served as the control. Table 3.2 shows that supplementation with monochromatic blue or red LED light resulted in a decreased maximum leaf area of *Mentha arvensis* L. compared to white or combined B3R7 LED light. Red LED light had the most significant effect on the total leaf area and plant area, but no significant differences were observed between blue LED light and the control, whether used alone or in combination with red LED lights. A high ratio of red LED light increased the plant's convex hull in both the 100% red and combined B3R7 treatments compared to the control under white LED light (Table 3.2, Figure 3.8).

**Table 3.2** Leaves area and total leaves area/plant, plant area and plant convex hull of *Mentha arvensis* L. plant after 4 weeks grown under different LED light treatments, at the same PPFD 150 $\mu mol.m^{-2}.s^{-1}$.

| Light | $5^{th}$ leaves area ($cm^2$) | Total leaves area ($cm^2$) | Plant area ($cm^2$) | Plant convex hull ($cm^2$) |
|---|---|---|---|---|
| B | 25.86 ± 0.38 $^{b}$ | 632.11 ± 11.62 $^{b}$ | 327.80 ± 14.89 $^{b}$ | 550.75 ± 20.83 $^{b}$ |
| B3R7 | 28.10 ± 1.18 $^{a}$ | 669.53 ± 29.89 $^{b}$ | 412.44 ± 55.32 $^{b}$ | 843.21 ± 146.04 $^{a}$ |
| R | 25.52 ± 0.80 $^{b}$ | 913.62 ± 74.42 $^{a}$ | 585.97 ± 24.00 $^{a}$ | 859.90 ± 21.12 $^{a}$ |
| W | 28.05 ± 0.42 $^{a}$ | 678.30 ± 43.36 $^{b}$ | 349.65 ± 38.37 $^{b}$ | 617.93 ± 74.57 $^{ab}$ |
| ANOVA's test | 0.0433 * | 0.00197 ** | 0.0012 ** | 0.0481 * |

*Means of ± standard errors followed by different letters within columns are significantly different by Fisher's least significant difference (LSD) test with one-way ANOVA; n = 8.*


**Figure 3.8** Side view images of *Mentha arvensis* L. after 4 weeks grown under blue (A), combined BR (B), red (C) and white LED (D) treatments, at the same PPFD 150 μmol $m^{-2}$ $s^{-1}$.

Based on the micrograph image and using the Fiji platform, we investigated the stomatal characteristics on the abaxial side of Wild Mint plant leaves under various light sources (Table 3.3). The results showed that the stomatal density was not affected by supplemental LEDs. All color LED treatments significantly decreased the width and length of the stomata guard cells, resulting in a reduced stomatal guard cell area. However, the stomatal pore apertures in these treatments were larger than those under white LED light.

**Table 3.3** Stomatal characteristics in leaves of *Mentha arvensis* L. after 4 weeks grown under different LED light treatments, at the same PPFD 150 μmol $m^{-2}$ $s^{-1}$.

| Light | SD (SD $mm^{-2}$) | GCW (μm) | GCL (μm) | GCA ($\mu m^2$) | SPA (μm) |
|---|---|---|---|---|---|
| B | 165 ± 5 | 20.54 ± 0.09 $^{c}$ | 30.56 ± 0.12 $^{c}$ | 483.88 ± 3.83 $^{c}$ | 5.50 ± 0.05 $^{a}$ |
| B3R7 | 160 ± 5 | 20.60 ± 0.08 $^{c}$ | 30.71 ± 0.12 $^{bc}$ | 489.56 ± 3.55 $^{bc}$ | 4.86 ± 0.05 $^{b}$ |
| R | 173 ± 6 | 20.90 ± 0.09 $^{b}$ | 31.00 ± 0.12 $^{b}$ | 498.78 ± 3.75 $^{b}$ | 4.66 ± 0.06 $^{b}$ |
| W | 157 ± 4 | 21.66 ± 0.11 $^{a}$ | 31.77 ± 0.13 $^{a}$ | 525.19 ± 4.62 $^{a}$ | 4.90 ± 0.08 $^{c}$ |
| ANOVA's test | 0.101 | 2e-16 *** | 3.78e-12 *** | 2.05e-13 *** | 2e-16 *** |

*Means of ± standard errors followed by different letters within columns are significantly different by Fisher's least significant difference (LSD) test with one-way ANOVA; n = 8.*

*SD: stomatal density, GCW: guard cell width, GCL: guard cell length, GCA: guard cell area, and SPA: stomatal pore apertures.*

Using an innovative optical leaf-clip device, the contents of three pigment types (chlorophyll, flavonoids, anthocyanins) and the nitrogen balance index were measured to investigate how each pigment responds to various light sources (Table 3.4-3.7, Figure 3.9). The red LED light treatment decreased the chlorophyll content in *Mentha arvensis* L. leaves compared to other light treatments. Meanwhile, both monochromatic red and blue LEDs led to an increase in anthocyanin content. The irradiated plants exhibited significantly higher flavonoid content compared to the control plants, which correlated negatively with the nitrogen balance index in *Mentha arvensis* L. leaves under these LED treatments.

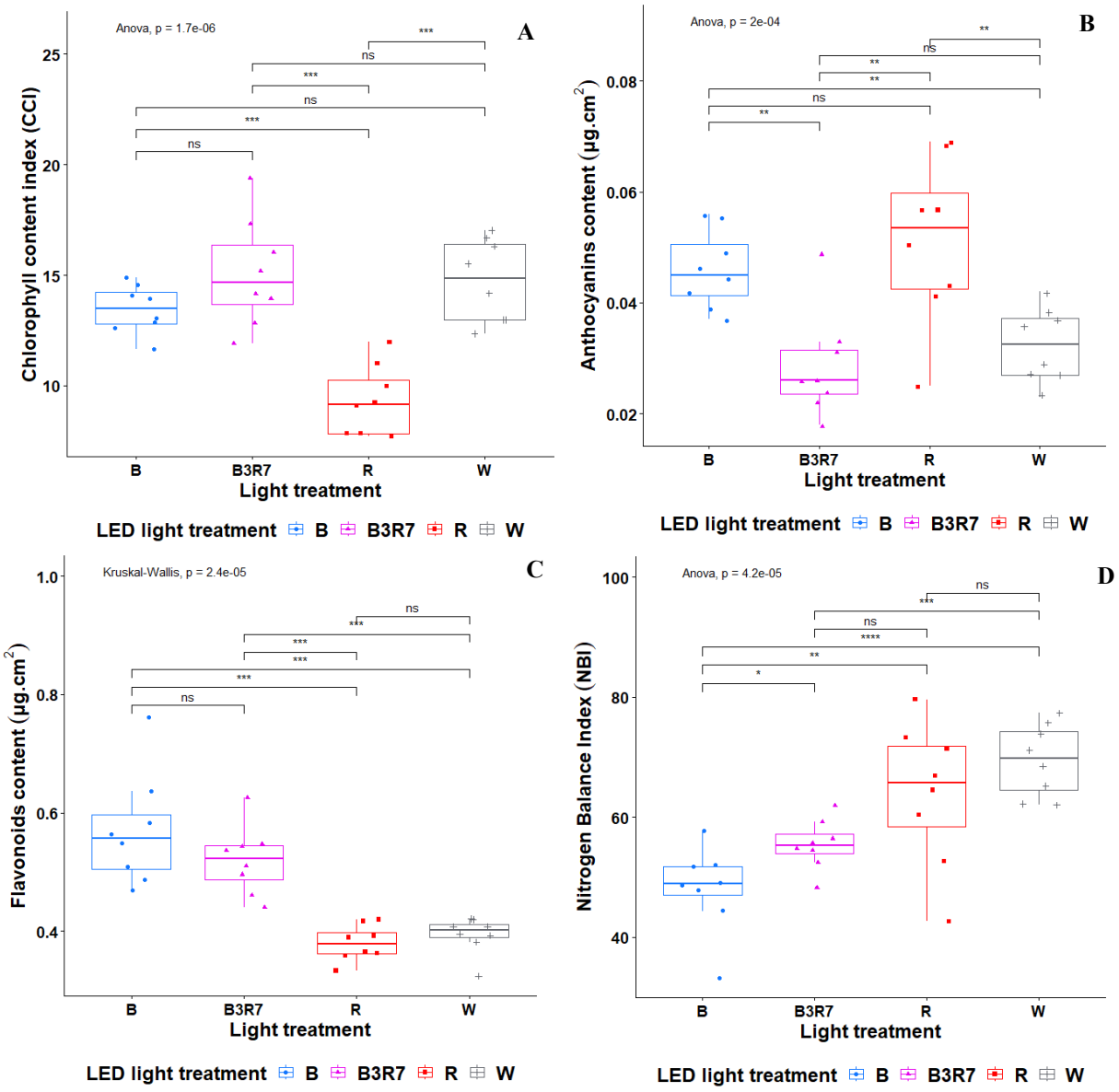


**Figure 3.9** Physiological parameters of the leaves, including chlorophyll content index (A), flavonoid content (B), anthocyanin content (C), and nitrogen balance index (D), were measured in the fifth leaves of *Mentha arvensis* L. plants after 4 weeks under different light treatments, at the same PPFD of 150 µmol $m^{-2}$ $s^{-1}$. *ns: non-significant at P < 0.05;*, **, *** and **** Significant at the 0.05, 0.01, 0.001 and 0.0001 probability level.*

**Table 3.4** The statistical analysis of chlorophyll content index (CCI) of *Mentha arvensis* L. leaves, after 4 weeks grown under different LED light treatments.

| Light | Rep. | Min | Max | Median | Mean | sd | Range | cv |
|---|---|---|---|---|---|---|---|---|
| B | 32 | 10.00 | 16.50 | 13.20 | 13.46 | 1.62 | 6.50 | 0.12 |
| B3R7 | 32 | 8.80 | 21.30 | 15.60 | 15.10 | 2.93 | 12.50 | 0.19 |
| R | 32 | 6.40 | 13.90 | 9.25 | 9.43 | 1.77 | 7.50 | 0.19 |
| W | 32 | 9.60 | 19.10 | 14.45 | 14.75 | 2.35 | 9.50 | 0.16 |

**Table 3.5** The statistical analysis of anthocyanins content of *Mentha arvensis* L. leaves, after 4 weeks grown under different LED light treatments.

| Light | Rep. | Min | Max | Median | Mean | sd | Range | cv |
|---|---|---|---|---|---|---|---|---|
| B | 8 | 0.04 | 0.06 | 0.05 | 0.05 | 0.01 | 0.02 | 0.15 |
| B3R7 | 8 | 0.02 | 0.05 | 0.03 | 0.03 | 0.01 | 0.03 | 0.33 |
| R | 8 | 0.03 | 0.07 | 0.05 | 0.05 | 0.01 | 0.04 | 0.29 |
| W | 8 | 0.02 | 0.04 | 0.03 | 0.03 | 0.01 | 0.02 | 0.21 |

**Table 3.6** The statistical analysis of flavonoids content of *Mentha arvensis* L. leaves, after 4 weeks grown under different LED light treatments.

| Light | Rep. | Min | Max | Median | Mean | sd | Range | cv |
|---|---|---|---|---|---|---|---|---|
| B | 8 | 0.47 | 0.76 | 0.56 | 0.57 | 0.09 | 0.29 | 0.17 |
| B3R7 | 8 | 0.44 | 0.63 | 0.52 | 0.52 | 0.06 | 0.19 | 0.11 |
| R | 8 | 0.33 | 0.42 | 0.38 | 0.38 | 0.03 | 0.09 | 0.08 |
| W | 8 | 0.32 | 0.42 | 0.40 | 0.39 | 0.03 | 0.10 | 0.08 |

**Table 3.7** The statistical analysis of nitrogen balance index (NBI) of *Mentha arvensis* L. leaves, after 4 weeks grown under different LED light treatments.

| Light | Rep. | Min | Max | Median | Mean | sd | Range | cv |
|---|---|---|---|---|---|---|---|---|
| B | 8 | 33.20 | 57.79 | 48.88 | 48.09 | 7.17 | 24.59 | 0.15 |
| B3R7 | 8 | 48.22 | 61.94 | 55.25 | 55.40 | 4.14 | 13.72 | 0.07 |
| R | 8 | 42.67 | 79.58 | 65.69 | 63.89 | 11.87 | 36.91 | 0.19 |
| W | 8 | 62.05 | 77.33 | 69.80 | 69.48 | 5.97 | 15.28 | 0.09 |

The photosynthetic rate prediction models were also assessed via chlorophyll-a fluorescence investigation (Table 3.8-3.11, Figure 3.10). The $F_v/F_m$ values in the leaves under 100% red LED were significantly lower than in the other treatments, while the presence of a blue light spectrum maintained this value. Additionally, plants grown under a high proportion of blue LEDs exhibited a higher $F_v/F_m$ value, surpassing 0.8, while the treatment with high red LED ratios had values lower than 0.8. No significant differences were observed between all the LED treatments for the non-photochemical fluorescence quenching coefficient rate (qN). Both qP and ETR value of plants under the blue LED lights was higher than that under the red LED light and control. Several studies have demonstrated that long-term red LED treatment can reduce the quantum yield of PSII photochemistry, but blue or B3R7-combined LEDs could alleviate these symptoms (Miao et al., 2019, 2016; Ouzounis et al., 2015; Zheng and Van Labeke, 2017), which aligns with our results. This suggests that a high proportion of blue LEDs is more effective in enhancing the photosynthetic properties of the *Mentha arvensis* L. leaves.

**Table 3.8** The statistical analysis of maximal quantum yield of PSII ($F_v/F_m$) values of *Mentha arvensis* L. leaves, after 4 weeks grown under different LED light treatments.

| Light | Rep. | Min | Max | Median | Mean | sd | Range | cv |
|---|---|---|---|---|---|---|---|---|
| B | 8 | 0.77 | 0.81 | 0.80 | 0.79 | 0.01 | 0.04 | 0.02 |
| B3R7 | 8 | 0.78 | 0.81 | 0.80 | 0.80 | 0.01 | 0.03 | 0.01 |
| R | 8 | 0.71 | 0.78 | 0.75 | 0.75 | 0.03 | 0.07 | 0.04 |
| W | 8 | 0.75 | 0.81 | 0.80 | 0.79 | 0.02 | 0.06 | 0.02 |

**Table 3.9** The statistical analysis of non-photochemical fluorescence quenching coefficient (qN) values of *Mentha arvensis* L. leaves, after 4 weeks grown under different LED light treatments.

| Light | Rep. | Min | Max | Median | Mean | sd | Range | cv |
|---|---|---|---|---|---|---|---|---|
| B | 8 | 0.48 | 0.66 | 0.58 | 0.56 | 0.06 | 0.18 | 0.11 |
| B3R7 | 8 | 0.45 | 0.57 | 0.53 | 0.53 | 0.04 | 0.12 | 0.08 |
| R | 8 | 0.47 | 0.60 | 0.54 | 0.54 | 0.05 | 0.13 | 0.08 |
| W | 8 | 0.52 | 0.63 | 0.55 | 0.56 | 0.04 | 0.11 | 0.07 |

**Table 3.10** The statistical analysis of photochemical fluorescence quenching coefficient (qP) values of *Mentha arvensis* L. leaves, after 4 weeks grown under different LED light treatments.

| Light | Rep. | Min | Max | Median | Mean | sd | Range | cv |
|---|---|---|---|---|---|---|---|---|
| B | 8 | 0.73 | 0.82 | 0.78 | 0.77 | 0.04 | 0.09 | 0.05 |
| B3R7 | 8 | 0.73 | 0.84 | 0.79 | 0.79 | 0.04 | 0.11 | 0.05 |
| R | 8 | 0.61 | 0.78 | 0.72 | 0.71 | 0.06 | 0.17 | 0.09 |
| W | 8 | 0.63 | 0.79 | 0.69 | 0.70 | 0.06 | 0.16 | 0.08 |

**Table 3.11** The statistical analysis of maximal electron transfer rate (ETR) of *Mentha arvensis* L. leaves, after 4 weeks grown under different LED light treatments.

| Light | Rep. | Min | Max | Median | Mean | sd | Range | cv |
|---|---|---|---|---|---|---|---|---|
| B | 8 | 28.57 | 34.97 | 30.61 | 31.21 | 2.33 | 6.40 | 0.07 |
| B3R7 | 8 | 30.22 | 35.94 | 32.91 | 32.81 | 1.98 | 5.72 | 0.06 |
| R | 8 | 23.03 | 30.53 | 26.55 | 26.77 | 2.69 | 7.50 | 0.10 |
| W | 8 | 25.15 | 32.09 | 28.23 | 28.25 | 2.69 | 6.94 | 0.10 |

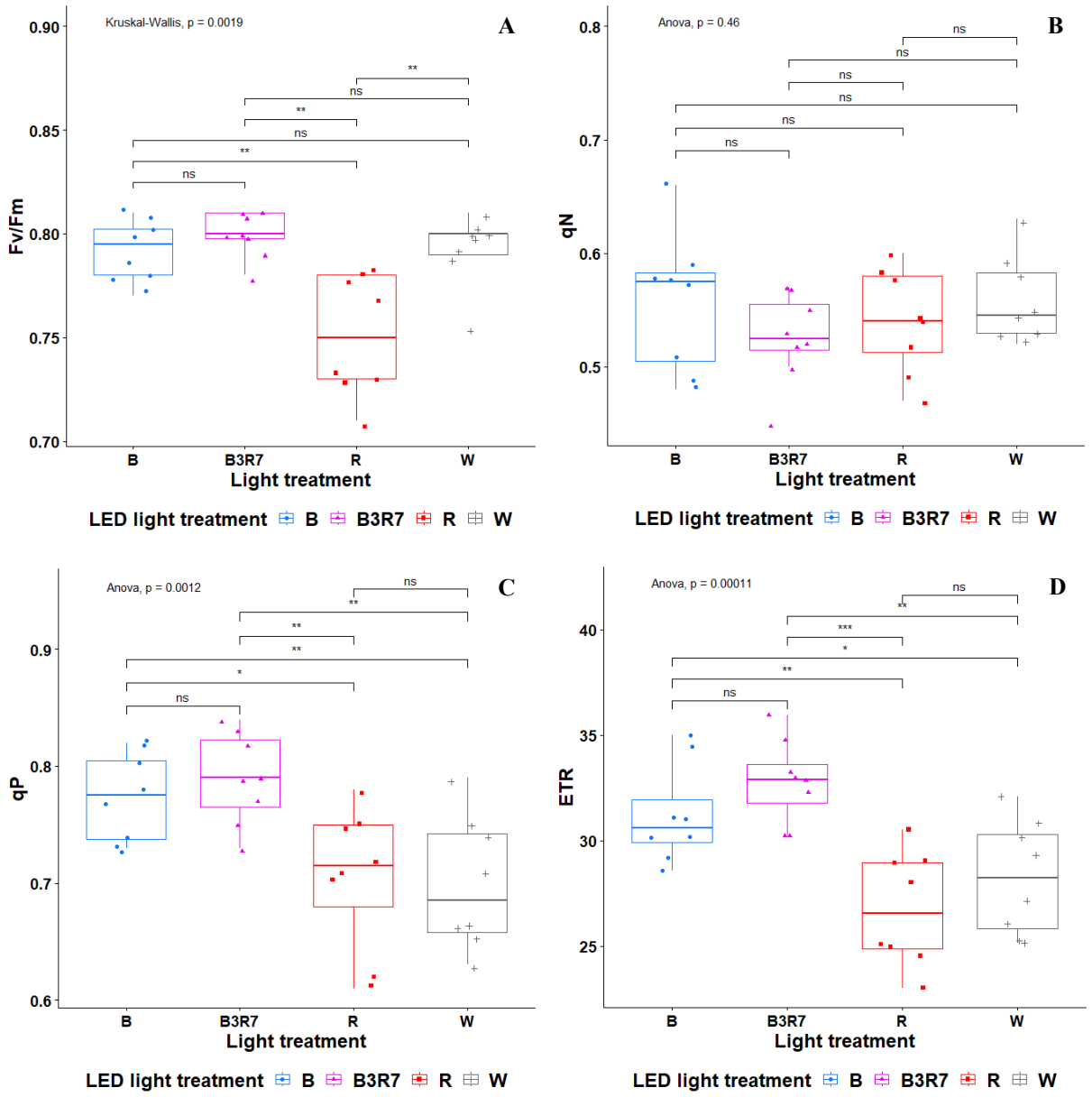


**Figure 3.10** The maximal quantum yield of PSII (A), non-photochemical fluorescence quenching coefficient (B), photochemical fluorescence quenching coefficient (C), and electron transport rate (D), were measured in the fifth leaves of *Mentha arvensis* L. plants after 4 weeks grown under different LED light treatments, at the same PPFD 150 μmol.m$^{-2}$.s$^{-1}$. *ns: non-significant at P < 0.05;*, ** and *** Significant at the 0.05, 0.01 and 0.001 probability level.*

## 4. Discussion

Research on photosynthesis is crucial for gaining insights into the physiological responses of crops and for accurately predicting the degree of dry matter accumulation in crop plants (Hind, 1985, 1985; Rabinowitch and Livingston, 1946; Stirbet et al., 2020). In indoor cultivation, the process of leaf photosynthesis is influenced not only by environmental factors like light, temperature, nutrition, and water availability but also by plant-related factors such as leaf age, leaf position, sink effects, and mutual shading (Dwyer and Stewart, 1986; Hardwick et al., 1968; Jewiss and Woledge, 1967; Peat, 1970; Wang et al., 2023). This raises an essential question in agricultural research: How can we precisely control the photosynthetic traits of crops based on their physiological characteristics?

In higher plant species, it is well-known that photosynthetic rates change with leaf age and leaf position on the main stem. A distinct “old and new alternation” behavior pattern is observed in the photosynthetic rates of individual leaves within a crop canopy (Zhang et al., 2020a). As new leaves in a plant canopy grow and develop into functional leaves, there is an increase in the photosynthetic rate in the growing leaf, typically reaching its peak at the time of full leaf expansion. Subsequently, there is a descent in photosynthetic rate that accompanies leaf senescence (Dwyer and Stewart, 1986; Peat, 1970). The leaf growth curve of Wild Mint plants, after being exposed to white LEDs for four weeks, followed a similar pattern. Leaf area, chlorophyll content index, and leaf biomass increased with leaf position, reaching their maximum in the $4^{th}$ and $5^{th}$ leaf groups, and decreased in the following leaves. Therefore, $5^{th}$ leaves were chosen for further experiments to establish which LED light was more effective in photosynthesis and the growth of the Wild Mint plants.

Red (600–700 nm) and blue (400–500 nm) LED lights are widely employed as light sources in plant factories (Fang et al., 2021; Kozai et al., 2016; Mickens et al., 2018). Light

energy is mainly absorbed by plant leaves, making leaf area and the plant canopy key traits that correlate with photosynthesis, respiration, and transpiration in plants (Morisette et al., 2006; Zhao et al., 2012). Both monochromatic red and blue LEDs led to a reduction in the maximum leaf area of *Mentha arvensis* L when compared to B3R7 and white LEDs in controlled cultivation. Furthermore, in the blue-light treatment, the reduction in leaf size led to a significant decrease in total leaf area (Table 3.3). Excessive exposure to blue light caused reduced leaf expansion, stem elongation, and plant growth (Craver et al., 2020; Fan et al., 2013; Hernández and Kubota, 2016; Kusuma et al., 2020). In contrast, under red light, there was no reduction in the total leaf area, likely due to an increase in the total number of leaves and branches. Consequently, plants grown without blue light exposure showed a tendency towards bolting (Karimi et al., 2022; Rehman et al., 2020). The absence of blue light in the combined spectrum led to a substantial increase in total leaf and plant area. Increasing the red ratio in supplementary light had a significant impact on the plant area and the plant's convex hull, highlighting the influence of the LED light spectrum on these plant traits. This has particular significance for assessing matter and energy exchange between crops and the environment and for designing plant density to manipulate crop production in plant factories.

In mature leaves, stomata typically cover only 0.5% to 5% of the leaf's surface. Nevertheless, stomata have a significant impact on plant photosynthesis, as stomatal conductance is closely linked to $CO_2$ assimilation and helps regulate water loss in response to changing environmental conditions (Kim et al., 2010; Lawson, 2009; Mott et al., 2008; Shimazaki et al., 2007). Higher stomatal density facilitates more efficient and rapid gas exchange between plants and the atmosphere. Stomatal density changes are associated with phytochrome-based red light receptors, particularly phyB, which plays a dominant role in this process (Casson et al., 2009; Driesen et al., 2020; Matthews et al., 2020; Roni et al., 2017).

Research has shown that lettuce exposed to 100% red LED light displayed the highest stomatal frequency among various treatments involving different red-to-blue (R:B) light ratios, both on the abaxial and adaxial leaf surfaces (Wang et al., 2016). Furthermore, plants exposed to a combination of red and blue LEDs or fluorescent light exhibited a greater number of stomata (Heo et al., 2002; Kim et al., 2004). However, an increase in stomatal density is inversely related to stomatal size, as documented in previous studies (Camargo and Marenco, 2011; Kim et al., 2004; Seif et al., 2021). The influence of LED lighting on stomatal development in *Mentha arvensis* L leaves is consistent with the findings of these studies. Additionally, stomatal pore openings are regulated by the light spectrum. Both blue and red light stimulate stomata opening through distinct pathways (Driesen et al., 2020). Blue light serves as a signaling cue, while red light functions as both a signal and an energy source (Driesen et al., 2020; Shimazaki et al., 2007). Plants treated with colored LEDs exhibited increased stomatal openings and well-organized guard cells (Muneer et al., 2014). This suggests that supplementing blue or red LED light during plant cultivation will reduce stomatal size while enhancing stomatal opening in *Mentha arvensis* L.

Chlorophyll (a+b) plays an important role in light absorption and converts it into chemical energy during the photosynthetic process; hence, chlorophyll content is directly associated with the efficiency and capacity of the photosynthetic apparatus (Rabinowitch and Govindjee, 1965). The CCI (chlorophyll content index) value is measured based on the chlorophyll optical properties, which are correlated to the photosynthetic pigment concentration in the leaf (Parry et al., 2014). This value was significantly decreased in leaves of Wild Mint plants grown under red LEDs, meanwhile, both monochromatic blue and combination LEDs were similarly effective on leaves chlorophyll content compared to the white LEDs (Table 1). The pigment synthesis is regulated by various photoreceptors that absorb lighting for different wavelengths.

A positive correlation between the blue light intensity and the total chlorophyll content in lettuce, spinach, kale, basil, and sweet pepper was reported (Naznin et al., 2019). Besides that, red light decreased the chlorophyll content by 45% compared with blue light in Rice leaves, that consistent with our results (Hamdani et al., 2019). A combination of blue and red light significantly increased the expression of several genes encoding important enzymes in the chlorophyll cycle such as Glutamyl-tRNA reductase (HEMA), glutamate-1-semialdehyde aminomutase 1 (HEML), Chlorophyll oxygenase (CAO) (Wang et al., 2022). Thus, the R70B30 treatment increased the accumulation of chlorophyll a + b (Zhang et al., 2019). This suggests that blue light plays a more significant role in inducing the chlorophyll biosynthesis, absent blue spectrum in supplemental light will reduce chlorophyll content in leaves of *Mentha arvensis* L.

Light photons are absorbed by photosynthetic pigments within the light-harvesting complex (LHC) and subsequently transferred to chlorophyll-a in the photosynthetic system (PS) (Grouneva et al., 2013). In addition to chlorophylls, plant pigments encompass various categories, including carotenoids, betalains, and specific flavonoid subclasses like anthocyanins, anthocyanidins, and anthoxanthins (De Mello et al., 2023). These pigments broaden the spectrum of light absorption for photosynthesis in plants. On another hand, anthocyanins possess the capacity to protect photosynthetic tissues from photoinhibition by absorbing blue-green light, thereby reducing the amount of light reaching chloroplasts (Agati et al., 2021; Dou et al., 2019; Yang et al., 2016). In the case of Wild Mint leaves, exposure to monochromatic blue or red LED light significantly boosts anthocyanin content (Figure 3.9B), possibly due to the prolonged exposure to these LED treatments, resulting in an excess of energy in reaction centers and triggering the photoinhibition process. More recently, it was pointed out that anthocyanins act as light attenuators to compensate for inadequate photoprotection in young

leaves of *Acmena acuminatissima* (Zhu et al., 2018).

Furthermore, flavonoids, including anthocyanins, exhibit potent antioxidant properties, suggesting their potential role in scavenging reactive oxygen species (ROS) generated during photosynthesis, especially under photoinhibition conditions (Albert et al., 2009; Ferreyra et al., 2021). Blue light, characterized by a short wavelength and high energy, serves as a signal for inducing photoprotection under similar light intensities (Liu and Van Iersel, 2021; Stanford and Tanner, 1985). As expected, our findings demonstrated higher flavonoid content in the blue LED treatment, whether in monochromatic blue light or in combination with LED (Figure 3.9C). Gene structure analyses identified 73 genes involved in flavonoid biosynthesis in *Brassica rapa*. These analyses indicated that chalconeisomerase (*CHI*) serves as the first key enzyme in the flavonoid metabolic pathway, with chalcone synthase (*CHS*) being the initiating enzyme in this pathway (Guo et al., 2014). Notably, these genes exhibited significant up-regulation in all purple leaves of Brassica under light stress conditions (Zhu et al., 2017). Previous reports indicated that the expression of *CHS* and *CHI* genes in red-leaved lettuce depends on the red-to-blue light ratio, and the expression of *CHS* genes increased under monochromatic LED light compared to the control (Soufi et al., 2023). This implies that the combination of red and blue light synergistically enhances the production of anthocyanins and flavonoids in Wild Mint plants.

During plant growth, nitrogen (N) content ranks as the second most important element, following carbon. Nitrogen plays a crucial role in the formation of proteins, nucleic acids, enzymes, chlorophyll, and various other cellular metabolites (Y. Fan et al., 2022; Zhang et al., 2014). To assess the nitrogen status in plants and predict crop yields, the nitrogen balance index (NBI) is employed. NBI is defined as the ratio of chlorophyll to epidermal flavonoids (Chl/Flav) and can be rapidly and non-destructively measured using Dualex4 (Cerovic et al., 2015, 2012).

In our experiment, significantly lower nitrogen balance indexes along with higher flavonol indexes were observed in plants exposed to blue and B3R7 LED light compared to the control plants. This suggests reduced nitrogen availability in Wild Mint plant leaves under these LED conditions. Previous studies have demonstrated that the enzyme nitrate reductase, responsible for converting nitrate into nitrite, is activated by light and becomes inactive in darkness (Lillo, 1994; Sawhney and Naik, 1972). Activation of this enzyme after exposure to high photosynthetically active radiation leads to a reduction in nitrate concentration in plants like Brassica, Rose, and Lettuce (Matysiak, 2021; Matysiak et al., 2021; Trejo-Téllez et al., 2019). Conversely, inactivation of the enzyme results in nitrate accumulation in plant tissues. In our study, exposing plants to high light energy conditions (blue LED lights) caused the activation of the nitrate reductase enzyme, resulting in decreased nitrate concentrations in leaves, which in turn led to a decrease in the nitrogen balance index.

Various aspects of the photosynthetic apparatus and models for predicting photosynthetic rates can be explored through the analysis of chlorophyll-a fluorescence parameters (Baker, 2004; Kalaji et al., 2017). Notably, $F_v/F_m$, qP, and ETR values of *Mentha arvensis* L. under Blue LED light were significantly higher than those observed under Red LED light, while the qN value in all light treatments remained consistent (Figure 3.10). $F_v/F_m$, in particular, serves as a critical indicator, representing the maximal quantum yield and the maximum light-capturing capability of PSII. This observation aligns with the findings in Cucumber plants, which noticed that the $F_v/F_m$ ratio in leaves exposed to monochromatic red light consistently registered lower values than in plants exposed to blue LED light either alone or in combination with other light sources (Hogewoning et al., 2010). In addition, prolonged exposure to red LED light at 660 nm induced a phenomenon known as the "red light syndrome," characterized by a reduction in photosynthetic ability (Miao et al., 2019, 2016).

Light energy is transformed by chlorophyll molecules through both the photochemical quenching (qP) and non-photochemical quenching (qN) processes. There was no significant variation in the non-photochemical fluorescence quenching coefficient (qN) across different LED ratios (Figure 3.10B). This uniformity indicates that the protective mechanisms, mitigating light-induced inhibition of photosynthesis and facilitating the dissipation of excess energy through heat loss pathways (Baker, 2008), were consistent across all treatments.

The incorporation of additional blue LEDs into the cultivation system enhanced light-capturing capabilities in Wild Mint leaves, resulting in an increase in the photochemical fluorescence quenching coefficient (qP) and, consequently, a boost in the electron transfer rate (ETR) within these treatments (Figure 3.10 C, D). The quantum yield of PSII photochemistry is inherently linked to the electron transport rate through PSII (ETR) and has direct implications on photosynthetic products. The results clearly indicated that ETR values were higher when a substantial proportion of blue LEDs was used compared to those exposed to red LED light, underscoring the superior efficacy of blue LEDs in promoting photosynthesis in Wild Mint plant leaves.

## 5. Conclusion

This study aimed to investigate high-throughput phenotyping methods to evaluate traits of *Mentha arvensis* L. concerning growth and photosynthetic characteristics under various LED lighting conditions. RGB image-based analysis proved to be a powerful tool for assessing several significant plant morphology and biomass traits in Wild Mint, such as leaf area, plant area, plant convex hull, and stomatal characteristics. In addition to that, non-destructive optical techniques demonstrated efficiency and precision in determining photosynthetic traits in the leaves of Wild Mint plants.

Based on these measurements, Wild Mint plants grown under blue LED light exhibited greater effectiveness in the light-dependent stages of the photosynthesis process, including the maximal quantum yield of PSII, photochemical fluorescence quenching coefficient, and electron transport rate. Meanwhile, red LED light notably affected plant morphological and biomass indicators. These findings suggest that high-throughput phenotyping methods could be valuable tools for plant management and cultivation, significantly reducing the effort, time, and costs associated with larger-scale assessment of photosynthetic traits.

## Chapter III: Correlation between the conventional and high-throughput phenotyping analysis traits of *Mentha arvensis* L. under different combinations of LEDs lights

### 1. Introduction

Photosynthesis is the entry point of carbon into vegetation and therefore is a critical determinant of crop production, as well as food security. The photosynthetic process consists of two interconnected sets of phases: the light reactions, which produce energy-rich molecules like NADPH and ATP, and the carbon fixation reactions, known as the Calvin-Benson cycle, which utilize these products (Cardona et al., 2018; Kitao et al., 2021). Most of the plant's biomass consists of carbon, hydrogen, and oxygen percentage, which essentially depends on the photosynthetic synthesis activities of mature green leaves (Bowyer and Leegood, 1997; Johnson, 2016). Photosynthetically reduced carbon products are transported from sources (plant leaf), and sites of production, to sinks, sites of use, and storage. There, photoassimilates support the maintenance of tissue growth and development. Photoassimilates in excess of growth and maintenance requirements are accumulated in parenchyma storage tissues of organs (Van Bel et al., 2003; Yahia et al., 2019). Many studies have shown a close connection between photosynthetic activity and biomass accumulation, metabolism of primary and secondary substances, as well as growth and development in plants (Fang et al., 2021; Jung and Arar, 2023; Jung et al., 2021; Maddison et al., 2017).

Light wavelengths, perceived through plant photoreceptors, represent significant environmental factors influencing the regulation of photosynthesis and the photomorphogenesis of plants. These factors affect various aspects, including shoot elongation, antioxidant enzyme activities, leaf anatomy, chlorophyll content, and chlorophyll fluorescence (Dueck et al., 2016; Hu et al., 2016; Liu and Van Iersel, 2021). Red light initiates the photosynthetic process (Meng et al., 2019; Rahman et al., 2021), while blue light enhances photosynthetic activity

(Hogewoning et al., 2010; Miao et al., 2019, 2016). A consistent trend of increased biomass and secondary metabolite production has been demonstrated when a combination of red and blue LEDs is utilized (Li and Kubota, 2009; Ma et al., 2021; Park et al., 2019). The number of studies exploring the effects of different LED light spectra on plant photosynthesis is continuously growing, providing valuable insights into various impact mechanisms and measurement approaches. However, it is important to note that photosynthetic characteristics can vary significantly among different plant species, light intensities, treatment durations, and environmental conditions (Fan et al., 2013; Lejeune et al., 2022; Son et al., 2012; Zheng and Van Labeke, 2017).

So far, research has explored the connection between photosynthesis and plant growth traits. This study aimed to investigate the correlations between plant traits, particularly their relation to photosynthetic characteristics and production in Wild Mint, based on both conventional and high-throughput phenotyping methods. These findings could prove instrumental in developing screening methods and evaluating the impact of LED light on modeling the growth and development of Wild Mint in controlled environments.

## 2. Statistical analysis

Statistical analysis was conducted using R software (Version 4.3.1, the R Foundation for Statistical Computing, Vienna, Austria). The normality of the data sets was assessed using the Shapiro-Wilk test. Since some data sets did not exhibit a normal distribution, the nonparametric Kruskal-Wallis's rank sum test was used to compare measured Wild Mint plant traits under different LED lights. Similarly, the Spearman rank correlation test was conducted to compare the measurements of 22 traits of the Wild Mint plants under different light sources. Correlation plots were generated using the "ggcorrplot" R package.

For a more comprehensive description of the results, principal component analysis (PCA) was employed to summarize the relationship among the measure traits. PCA plots were generated by using the "factoextra" R package.

## 3. Result

The result indicates that there are no significant differences between replications, but the traits exhibit significant variations among different light treatments, with the exceptions being stomatal density (SD) and the non-photochemical fluorescence quenching coefficient (qN) (Table 4.1). When conventional and phenomics-based evaluations were combined to assess the growth and photosynthetic traits in *Mentha arvensis* L. under various LED lighting conditions, a high degree of variance was observed, and the distribution pattern also varied, as depicted in the box plot (Fig. 4.1).

Spearman's rank correlations among CCI, Flav, Anth, NBI, SD, GCW, GCL, GCA, SPA, $F_v/F_m$, qN, qP, ETR, LA, TLA, PA, PCH, FW, DW, Suc, and Sta in *Mentha arvensis* L. plants grown under supplementary LED light are detailed in Table 4.2. The correlation visualization plot is available in Figure 4.2. The correlation analysis revealed distinct clusters of relationships among the observed traits.

In the first group, chlorophyll content index (CCI) exhibited a strong positive correlation with the maximal quantum yield of PSII ($F_v/F_m$) (rho: 0.85), and a low positive correlation with electron transport rate (ETR) and the flavonol index (Flav). These three traits also showed moderate positive correlations with each other.

The second group displayed a robust positive correlation among stomatal guard cell characteristics, including guard cell width (GCW), guard cell length (GCL), and guard cell area (GCL) (rho>0.7). Among these, guard cell width displayed a low positive relationship with stomatal pore apertures (SPA). However, no significant relationship was found between these traits and stomatal density or the traits in the first group.

In the third group, a strong positive correlation between plant biomass and plant metabolites, including fresh weight (FW), dry weight (DW), sucrose content (Suc), starch

content (Sta), and total phenolics content (TPC) were observed. These traits also demonstrated moderate positive correlations with the maximum leaf area (LA) and total leaf area (TLA), and low positive relationships with plant area (PA) and plant convex hull (PCH). However, no significant relationships were observed between the traits in the third group and the stomatal traits.

Conversely, the first group displayed a moderate negative correlation with the third group. Notably, there was a strong negative correlation between the flavonol index and the nitrogen balance index (NBI). The NBI also exhibited a moderate negative relationship with the maximal quantum yield of PSII, photochemical fluorescence quenching coefficient (qP), and electron transport rate.

**Table 4.1** Kruskal-Wallis rank sum test of *Mentha arvensis* L. plant at four LED light treatments.

| Source | Df | CCI | Flav | Anth | NBI | SD | GCW | GCL | GCA | SPA | $F_v/F_m$ | qN |
|---|---|---|---|---|---|---|---|---|---|---|---|---|
| Rep. | 7 | NS | NS | NS | NS | NS | NS | NS | NS | NS | NS | NS |
| Light | 3 | *** | *** | *** | *** | NS | *** | *** | *** | *** | ** | NS |
| Source | Df | qP | ETR | LA | TLA | PA | PCH | FW | DW | Suc | Sta | TPC |
| Rep. | 7 | NS | NS | NS | NS | NS | NS | NS | NS | NS | NS | NS |
| Light | 3 | ** | *** | * | ** | ** | * | ** | ** | *** | ** | *** |

*Rep.: Replication, Df: Degrees of Freedom, CCI: Chlorophyll content index, Flav: Flavonol index, Anth: Anthocyanin index, NBI: Nitrogen balance index, SD: Stomatal density, GCW: Guard cell width, GCL: Guard cell length, GCA: Guard cell area, SPA: Stomatal pore apertures, $F_v/F_m$: Maximal quantum yield of PSII, qN: Non-photochemical fluorescence quenching coefficient, qP: Photochemical fluorescence quenching coefficient, ETR: Electron transport rate, LA: Maximum leaf area, TLA: Total leaves area, PA: Plant area, PCH: Plant convex hull, FW: Fresh weight, DW: Dry weight, Suc: Sucrose content, Sta: Starch content, TPC: Total phenolics content.*

*NS, nonsignificant at $p \leq 0.05$*
** significant at the 0.05*
*** significant at the 0.01*
**** significant at 0.001.*

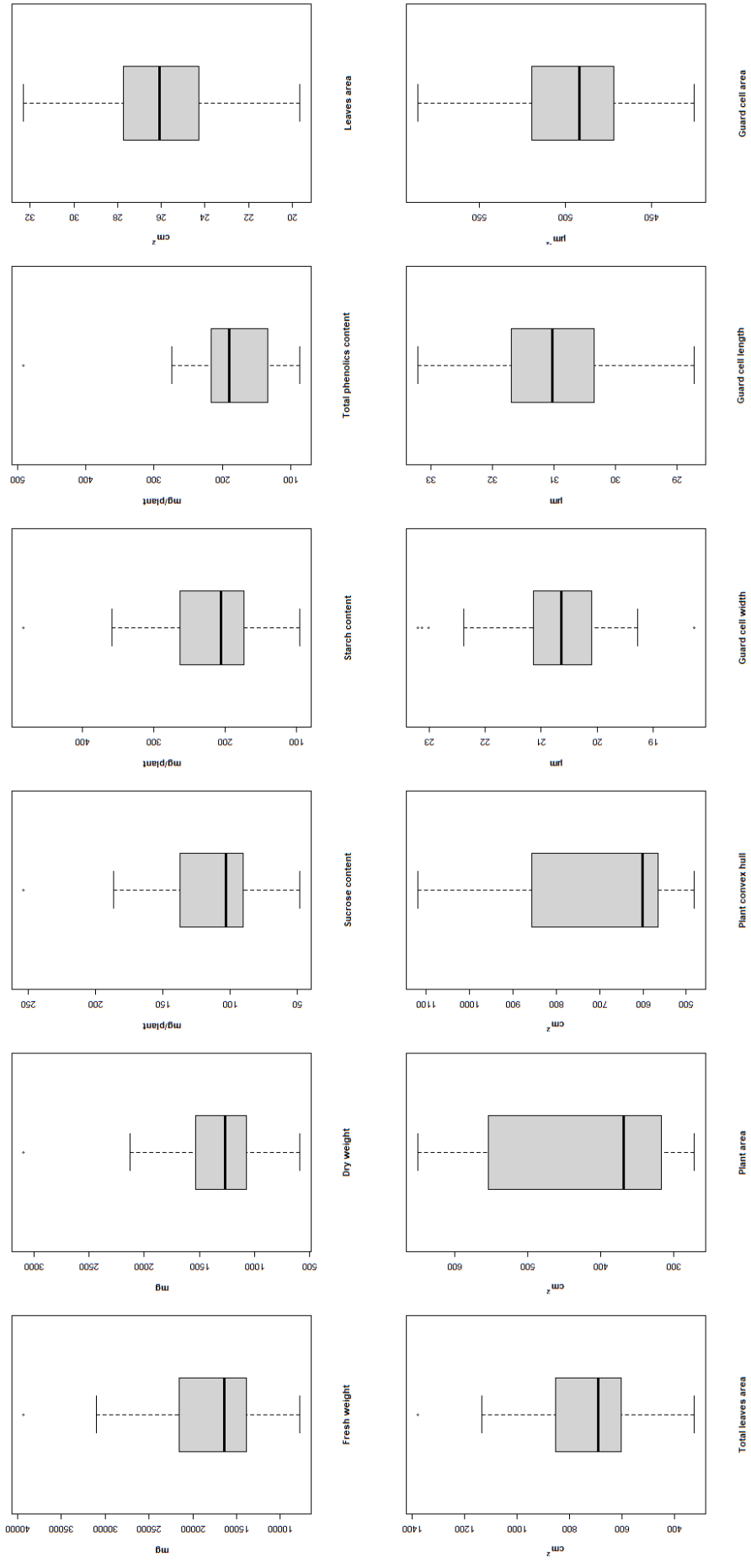

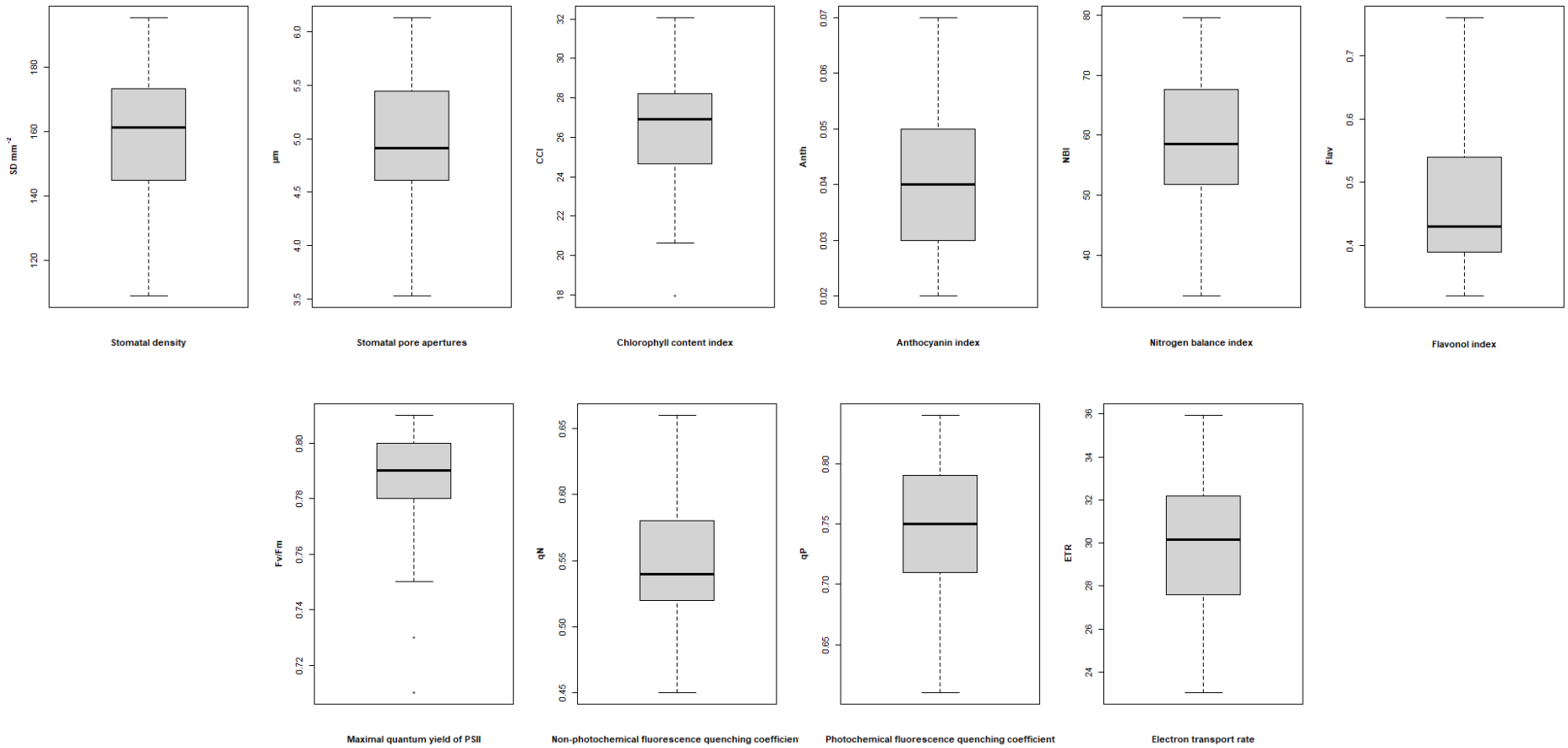


**Figure 4.1** Box plot showing the average (mean) of 22 traits of *Mentha arvensis* L. plant under all LED treatments.

**Table 4.2** Spearman's rank correlation among CCI, Flav, Anth, NBI, SD, GCW, GCL, GCA, SPA, $F_v/F_m$, qN, qP, ETR, LA, TLA, PA, PCH, FW, DW, Suc and Sta in *Mentha arvensis* L. plant grown under supplementary LED light.

| | CCI | Flav | Anth | NBI | SD | GCW | GCL | GCA | SPA | $F_v/F_m$ | qN | qP | ETR | LA | TLA | PA | PCH | FW | DW | Suc | Sta |
|---|---|---|---|---|---|---|---|---|---|---|---|---|---|---|---|---|---|---|---|---|---|
| Flav | 0.560*** | | | | | | | | | | | | | | | | | | | | |
| Anth | -0.315 | -0.121 | | | | | | | | | | | | | | | | | | | |
| NBI | -0.449** | -0.810*** | -0.364* | | | | | | | | | | | | | | | | | | |
| SD | -0.509** | -0.162 | 0.172 | 0.252 | | | | | | | | | | | | | | | | | |
| GCW | -0.080 | -0.271 | -0.028 | 0.306 | -0.026 | | | | | | | | | | | | | | | | |
| GCL | 0.314 | -0.036 | -0.103 | 0.122 | -0.352* | 0.733*** | | | | | | | | | | | | | | | |
| GCA | 0.084 | -0.171 | -0.089 | 0.246 | -0.162 | 0.954*** | 0.887*** | | | | | | | | | | | | | | |
| SPA | -0.221 | 0.155 | 0.240 | -0.180 | 0.242 | 0.354* | 0.105 | 0.245 | | | | | | | | | | | | | |
| $F_v/F_m$ | 0.851*** | 0.648*** | -0.347 | -0.516** | -0.518** | -0.049 | 0.238 | 0.068 | -0.036 | | | | | | | | | | | | |
| qN | -0.173 | -0.133 | -0.084 | 0.200 | 0.182 | 0.019 | -0.187 | -0.062 | 0.091 | -0.063 | | | | | | | | | | | |
| qP | 0.146 | 0.502** | -0.070 | -0.458** | -0.015 | 0.001 | -0.008 | 0.016 | 0.161 | 0.269 | -0.384* | | | | | | | | | | |
| ETR | 0.475** | 0.653*** | -0.185 | -0.571*** | -0.250 | -0.022 | 0.123 | 0.051 | 0.093 | 0.587*** | -0.522** | 0.910*** | | | | | | | | | |
| LA | -0.629*** | -0.573*** | -0.147 | 0.544** | 0.133 | 0.109 | -0.297 | -0.071 | 0.156 | -0.416* | 0.170 | -0.083 | -0.252 | | | | | | | | |
| TLA | -0.561*** | -0.537** | -0.185 | 0.544** | 0.080 | 0.134 | -0.213 | -0.025 | 0.026 | -0.497** | 0.083 | 0.008 | -0.197 | 0.757*** | | | | | | | |
| PA | -0.347 | -0.383* | 0.361* | 0.197 | 0.212 | 0.074 | 0.019 | 0.067 | -0.135 | -0.606*** | -0.264 | -0.204 | -0.323 | -0.063 | 0.062 | | | | | | |
| PCH | -0.085 | -0.228 | -0.018 | 0.130 | -0.090 | 0.023 | 0.012 | 0.034 | -0.216 | -0.307 | -0.187 | -0.068 | -0.113 | 0.096 | 0.157 | 0.697*** | | | | | |
| FW | -0.551** | -0.390* | -0.142 | 0.362* | 0.128 | 0.064 | -0.293 | -0.091 | 0.024 | -0.489** | -0.024 | 0.210 | -0.018 | 0.730*** | 0.895*** | 0.183 | 0.334 | | | | |
| DW | -0.634*** | -0.506** | 0.001 | 0.433* | 0.226 | 0.056 | -0.259 | -0.082 | -0.020 | -0.656*** | -0.033 | 0.064 | -0.195 | 0.638*** | 0.846*** | 0.357* | 0.356* | 0.938*** | | | |
| Suc | -0.579*** | -0.384* | -0.104 | 0.349 | 0.152 | 0.051 | -0.300 | -0.103 | 0.045 | -0.513** | -0.017 | 0.204 | -0.035 | 0.718*** | 0.893*** | 0.200 | 0.325 | 0.998*** | 0.948*** | | |
| Sta | -0.591*** | -0.391* | -0.091 | 0.356* | 0.163 | 0.058 | -0.296 | -0.099 | 0.063 | -0.523** | 0.002 | 0.202 | -0.044 | 0.725*** | 0.899*** | 0.174 | 0.292 | 0.995*** | 0.945*** | 0.997*** | |
| TPC | -0.682*** | -0.271 | 0.133 | 0.182 | 0.292 | -0.063 | -0.350* | -0.194 | 0.125 | -0.630*** | 0.019 | 0.216 | -0.083 | 0.541** | 0.752*** | 0.296 | 0.279 | 0.891*** | 0.909*** | 0.916*** | 0.919*** |

*CCI: Chlorophyll content index, Flav: Flavonol index, Anth: Anthocyanin index, NBI: Nitrogen balance index, SD: Stomatal density, GCW: Guard cell width, GCL: Guard cell length, GCA: Guard cell area, SPA: Stomatal pore apertures, $F_v/F_m$: Maximal quantum yield of PSII, qN: Non-photochemical fluorescence quenching coefficient, qP: Photochemical fluorescence quenching coefficient, ETR: Electron transport rate, LA: Maximum leaf area, TLA: Total leaves area, PA: Plant area, PCH: Plant convex hull, FW: Fresh weight, DW: Dry weight, Suc: Sucrose content, Sta: Starch content, TPC: Total phenolics content.*

** significant at the 0.05; ** significant at the 0.01; *** significant at 0.001.*

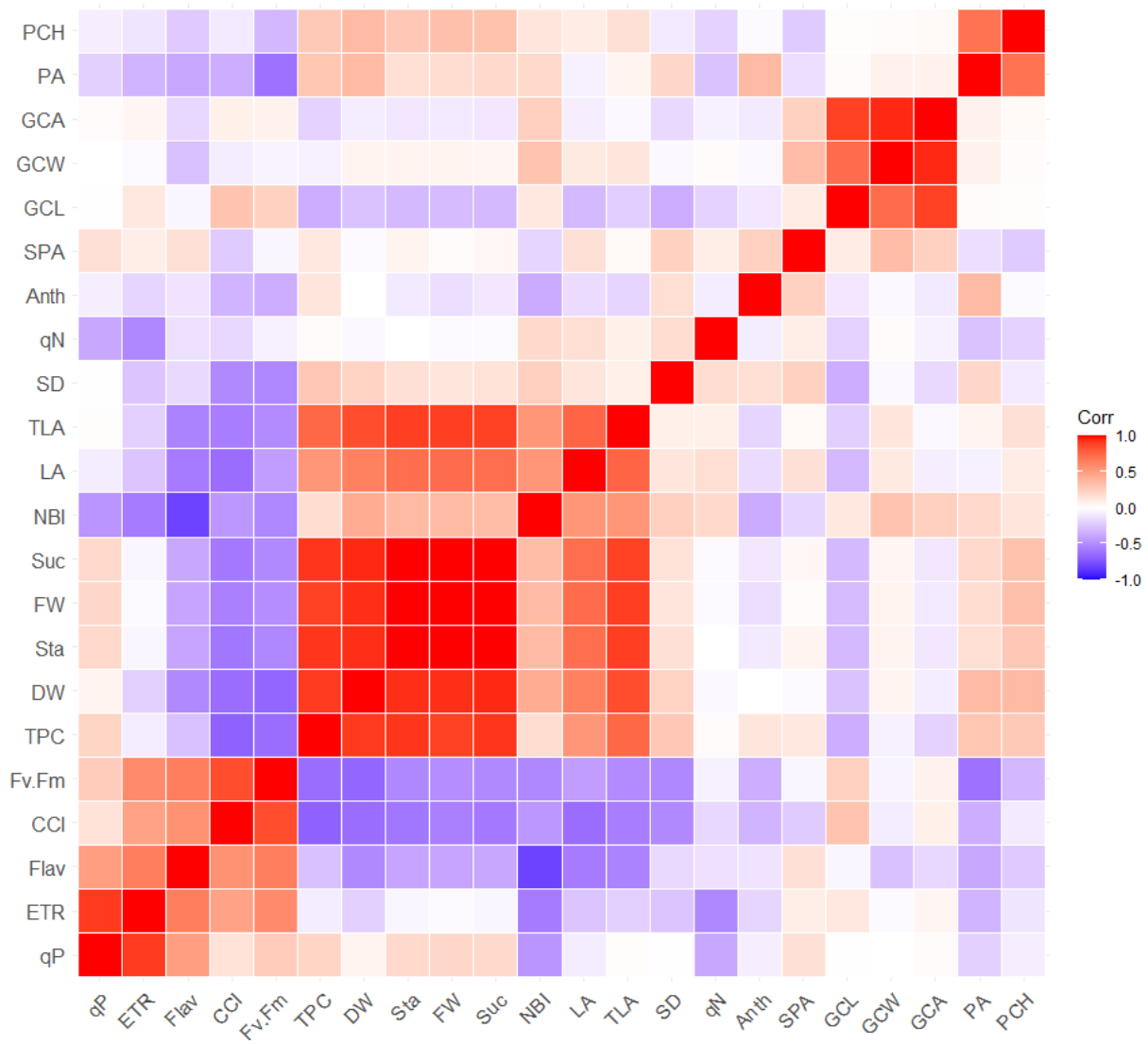


**Figure 4.2** Visualization plot showing the correlation between various traits of *Mentha arvensis* L. plants grown under supplementary LED light. *CCI: Chlorophyll content index, Flav: Flavonol index, Anth: Anthocyanin index, NBI: Nitrogen balance index, SD: Stomatal density, GCW: Guard cell width, GCL: Guard cell length, GCA: Guard cell area, SPA: Stomatal pore apertures, Fv/Fm: Maximal quantum yield of PSII, qN: Non-photochemical fluorescence quenching coefficient, qP: Photochemical fluorescence quenching coefficient, ETR: Electron transport rate, LA: Maximum leaf area, TLA: Total leaves area, PA: Plant area, PCH: Plant convex hull, FW: Fresh weight, DW: Dry weight, Suc: Sucrose content, Sta: Starch content, TPC: Total phenolics content.*

Principal component analysis (PCA), a statistical method, helps identify the contribution of each variable to the overall variance along the principal axes. Eigenvalues obtained from PCA are typically employed to select the most influential factors among the variables. In this study, PCA revealed that the first two components explained 52.4% of the variance in all *Mentha arvensis* L. plant traits grown under LED light (Table 4.3, Figure 4.3).

The first component was primarily characterized by plant biomass and plant metabolites, including fresh weight (FW), dry weight (DW), sucrose content (Suc), starch content (Sta), total phenolics content (TPC), chlorophyll content index (CCI), and maximal quantum yield of PSII ($F_v/F_m$). This component accounted for 36.9% of the variation (Table 4.3, 4.4, Figure 4.3, 4.4).

The second component was largely influenced by the flavonol index (Flav), photochemical fluorescence quenching coefficient (qP), electron transport rate (ETR), and nitrogen balance index (NBI), contributing to 15.4% of the total variation (Table 4.3, 4.4, Figure 4.3, 4.4).

The PCA biplot illustrated the positioning of *Mentha arvensis* L. plants grown under blue LED in the upper right quadrant of the PCA score plot, exhibiting higher values of CCI, Flav, $F_v/F_m$, qP, and ETR. Conversely, those cultivated under red LED located in the lower left quadrant and characterized by higher NBI, stomatal density (SD), guard cell width (GCW), plant area (PA), plant convex hull (PCH), non-photochemical fluorescence quenching coefficient (qN), and anthocyanin content (Anth). This indicated the distinct effects of monochromatic LED lights on the growth and development of *Mentha arvensis* L. Red LED had a similar effect to white LED, while mono-blue LED show a more contribution in combined B3R7 LED.

**Table 4.3** Eigenvalues and percentage of variances explained by each principal component.

| Variables | eigenvalue | percentage of variance | cumulative percentage of variance |
|---|---|---|---|
| Com 1 | 8.1290 | 36.9502 | 36.9502 |
| Com 2 | 3.3893 | 15.4058 | 52.3560 |
| Com 3 | 2.9263 | 13.3014 | 65.6575 |
| Com 4 | 2.1294 | 9.6790 | 75.3364 |
| Com 5 | 1.9155 | 8.7068 | 84.0432 |
| Com 6 | 0.9010 | 4.0956 | 88.1388 |
| Com 7 | 0.7963 | 3.6194 | 91.7582 |
| Com 8 | 0.5629 | 2.5585 | 94.3167 |
| Com 9 | 0.3783 | 1.7197 | 96.0364 |
| Com 10 | 0.2652 | 1.2056 | 97.2420 |
| Com 11 | 0.1761 | 0.8004 | 98.0424 |
| Com 12 | 0.1385 | 0.6296 | 98.6720 |
| Com 13 | 0.1092 | 0.4963 | 99.1683 |
| Com 14 | 0.0700 | 0.3183 | 99.4866 |
| Com 15 | 0.0438 | 0.1990 | 99.6856 |
| Com 16 | 0.0257 | 0.1170 | 99.8026 |
| Com 17 | 0.0242 | 0.1101 | 99.9127 |
| Com 18 | 0.0124 | 0.0565 | 99.9691 |
| Com 19 | 0.0045 | 0.0204 | 99.9896 |
| Com 20 | 0.0015 | 0.0069 | 99.9964 |
| Com 21 | 0.0006 | 0.0028 | 99.9993 |
| Com 22 | 0.0002 | 0.0007 | 100.0000 |

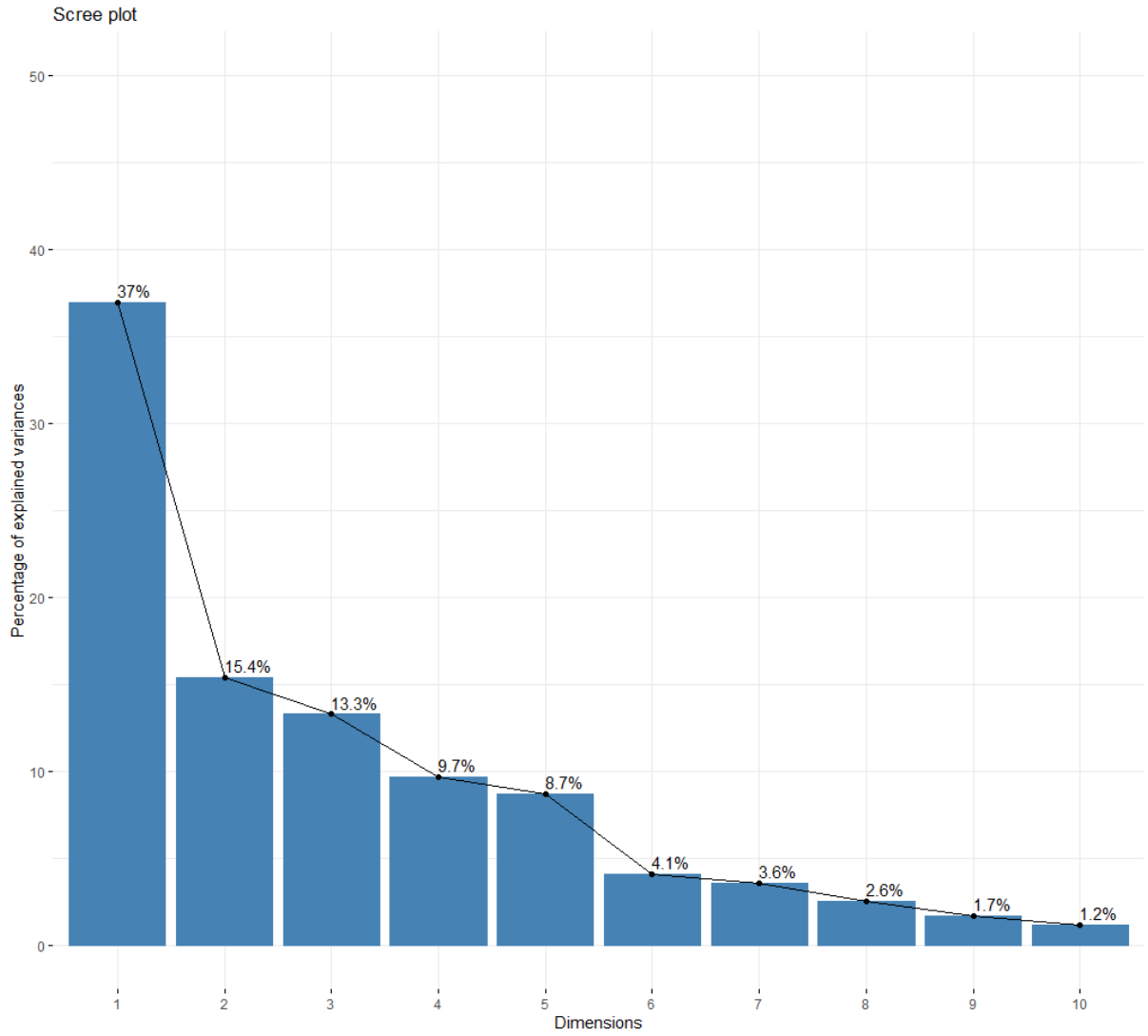


**Figure 4.3** Scree plot illustrates the percentage of variances explained by each principal component.

**Table 4.4** The contribution of a variable to a given principal component.

| Variables | Dim.1 | Dim.2 | Dim.3 | Dim.4 | Dim.5 |
|---|---|---|---|---|---|
| CCI | 7.843 | 0.988 | 1.179 | 0.510 | 7.178 |
| Flav | 5.295 | 10.466 | 0.017 | 0.145 | 1.263 |
| Anth | 0.013 | 0.591 | 3.340 | 17.410 | 10.354 |
| NBI | 4.157 | 9.438 | 0.733 | 5.199 | 2.498 |
| SD | 1.405 | 0.452 | 3.979 | 0.629 | 13.287 |
| GCW | 0.068 | 5.970 | 22.326 | 0.120 | 3.806 |
| GCL | 1.300 | 5.253 | 20.435 | 0.823 | 0.061 |
| GCA | 0.122 | 6.330 | 24.582 | 0.429 | 1.069 |
| SPA | 0.015 | 0.032 | 1.858 | 0.107 | 33.557 |
| $F_v/F_m$ | 7.496 | 3.154 | 1.876 | 4.907 | 0.984 |
| qN | 0.137 | 2.971 | 2.698 | 14.244 | 3.258 |
| qP | 0.107 | 18.136 | 4.620 | 1.783 | 1.981 |
| ETR | 1.817 | 17.499 | 6.102 | 0.842 | 0.045 |
| LA | 7.341 | 0.031 | 0.278 | 6.951 | 0.255 |
| TLA | 9.405 | 0.566 | 1.443 | 3.269 | 0.243 |
| PA | 1.689 | 2.935 | 0.322 | 28.160 | 3.187 |
| PCH | 1.424 | 0.096 | 0.205 | 12.663 | 15.223 |
| FW | 9.954 | 3.607 | 1.414 | 0.167 | 0.396 |
| DW | 10.800 | 0.941 | 0.383 | 0.298 | 0.357 |
| Suc | 10.164 | 3.551 | 1.113 | 0.059 | 0.159 |
| Sta | 10.225 | 3.390 | 1.096 | 0.138 | 0.029 |
| TPC | 9.224 | 3.604 | 0.000 | 1.148 | 0.813 |

*CCI: Chlorophyll content index, Flav: Flavonol index, Anth: Anthocyanin index, NBI: Nitrogen balance index, SD: Stomatal density, GCW: Guard cell width, GCL: Guard cell length, GCA: Guard cell area, SPA: Stomatal pore apertures, $F_v/F_m$: Maximal quantum yield of PSII, qN: Non-photochemical fluorescence quenching coefficient, qP: Photochemical fluorescence quenching coefficient, ETR: Electron transport rate, LA: Maximum leaf area, TLA: Total leaves area, PA: Plant area, PCH: Plant convex hull, FW: Fresh weight, DW: Dry weight, Suc: Sucrose content, Sta: Starch content, TPC: Total phenolics content.*

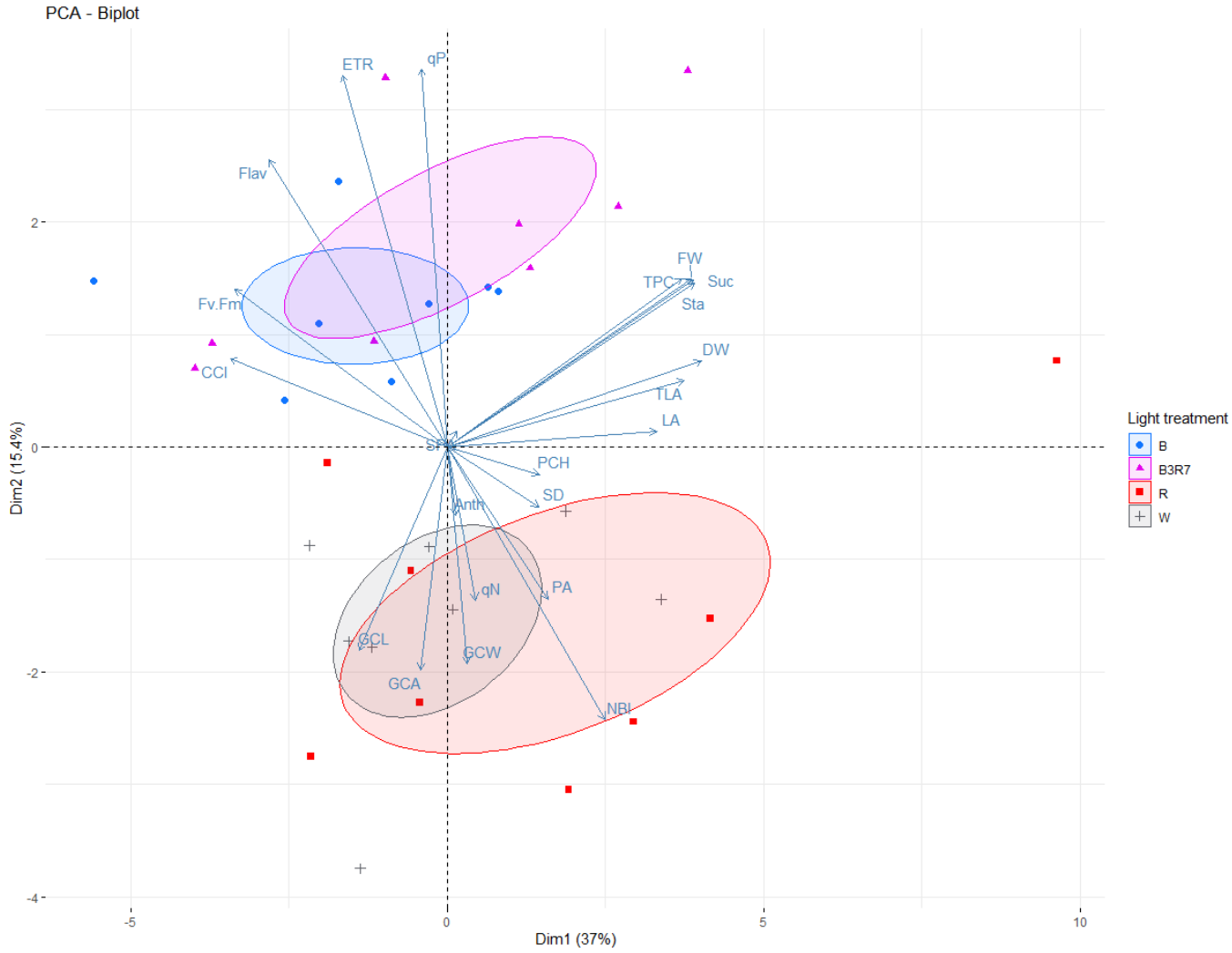


**Figure 4.4** Principal coordinate analysis displays the distribution of 22 traits in *Mentha arvensis* L. plants that were cultivated under supplementary LED light, presenting them as different coordinates. *CCI: Chlorophyll content index, Flav: Flavonol index, Anth: Anthocyanin index, NBI: Nitrogen balance index, SD: Stomatal density, GCW: Guard cell width, GCL: Guard cell length, GCA: Guard cell area, SPA: Stomatal pore apertures, Fv/Fm: Maximal quantum yield of PSII, qN: Non-photochemical fluorescence quenching coefficient, qP: Photochemical fluorescence quenching coefficient, ETR: Electron transport rate, LA: Maximum leaf area, TLA: Total leaves area, PA: Plant area, PCH: Plant convex hull, FW: Fresh weight, DW: Dry weight, Suc: Sucrose content, Sta: Starch content, TPC: Total phenolics content.*

## 4. Discussion

Artificial light sources are critical components in plant factory systems (Kozai et al., 2016; Rahman et al., 2021). The growth, morphogenesis, and differentiation of plant phenotypes are influenced by light quality, intensity, and duration (Burkholder, 1936). Light quality regulates photosynthetic activities and significantly impacts plant physiological processes, plant biomass as well as production of secondary metabolites (Hasan et al., 2017; Jung et al., 2021; Ma et al., 2021; Olle and Viršile, 2013; Paradiso and Proietti, 2022). In this study, different LED light spectra exhibited a significant effect on the degree of variance and the distribution of growth and photosynthetic traits in *Mentha arvensis* L. (Table 4.1, Figure 4.1). This suggests the potential for using blue and red LED light ratios to optimize Wild Mint cultivation in plant factories, targeting specific desired traits.

The rate of plant photosynthesis can vary depending on various factors, such as $CO_2$ concentration, water supplementation, or light quality (Jung and Arar, 2023; Xin et al., 2019). During the initial stage of the photosynthesis process, known as the “light reactions”, chlorophyll absorbs light energy, conversion, and generation of NADPH and high-energy ATP molecules. These molecules constitute vital outputs of the light reactions, the synthesis of ATP and NADPH in linear electron flow through the photosynthetic system (PS) is tightly coupled (Cardona et al., 2018; Kitao et al., 2021; Kramer and Evans, 2011). In Wild Mint plants, a significant positive correlation was observed between the chlorophyll content index and the maximum light absorption capacity of photosystem II ($F_v/F_m$) (Table 4.1, Figure 4.1). The enhancement of light absorption in photosystem II exhibited a positive correlation with an increase in the photochemical fluorescence quenching coefficient (qP), thus increasing the electron transfer rate (ETR). This finding suggests that an increase in the absorption of light photons can result in heightened photosynthetic activity in the cultivation of Wild Mint plants

in a controlled environment.

The high-energy molecules produced during the initial stage are used for $CO_2$ fixation in the Calvin–Benson cycle, resulting in the production of carbohydrates and other assimilatory processes (Cardona et al., 2018; Kitao et al., 2021). Sucrose is the major organic product of photosynthesis, which can be stored as starch, transported for metabolic use, or used for respiration to generate the energy source ATP (W. Patrick et al., 2013). The accumulation of sucrose and starch directly influences plant biomass (Coleman et al., 2010). Maddison et al. have shown a positive relationship between carbohydrate metabolism and biomass yield in Miscanthus (De Vega et al., 2021; Maddison et al., 2017). The same trend was confirmed in Wild Mint plants, where increased sucrose and starch content have a strong correlation with the increase in plant fresh weight and dry weight. In addition, sucrose, as a primary metabolite, serves as a precursor for secondary metabolites such as polyphenols (Feduraev et al., 2019). The transglycosylation from sucrose to phenolic and related compounds is associated with sucrose phosphorylase activity (Kitao and Sekine, 1994). This explains the strong positive correlation observed between sucrose content, starch content, plant biomass, and total phenolics content in Wild Mint plants.

In addition to carbon (C), plant nitrogen (N) stoichiometry reflects the relative strength of metabolism and can be used to predict plant growth and development (Elser et al., 2010; Luo et al., 2015). Carbon and nitrogen nutrient balance signaling drive the plant's physiological response to changes in the environment (Luo et al., 2017; Zheng, 2009). Therefore, the nitrogen balance index (NBI), which is highly correlated with the N content in leaves, has been widely employed in plant physiology research to determine nitrogen content (Camargo and Marenco, 2011; Cerovic et al., 2015; Deng et al., 2019; K. Fan et al., 2022; Matysiak et al., 2021). The NBI is positively correlated with the chlorophyll index in cabbage and barley leaves

(Kaniszewski et al., 2021; O'Neill et al., 1984). However, the opposite trend was observed in Wild Mint plants. In this study, a negative relationship was found between NBI and photosynthetic traits such as CCI, $F_v/F_m$, qP, ETR, and Flav in Wild Mint plant leaves. Meanwhile, the NBI has a positive correlation with plant biomass, as well as plant area and leaf area. Flavonoids, as nitrogen-free secondary metabolites, are considered indicators of nitrogen availability in the plant (Deng et al., 2019). The negative correlation between flavonoid concentration and NBI value has been reported in various plants (Deng et al., 2019; Liu et al., 2021; Matysiak et al., 2021). Our results suggest that plants with a high C/N ratio would exhibit better photosynthetic performance and enhance flavonoid accumulation. In contrast, the plant's preference for increasing plant biomass and leaf area leads to a reduction in the C content in leaves, subsequently reducing the C/N ratio. Therefore, changes in NBI values could be an indicator to indicate the changes in photosynthesis, growth, and canopy development in Wild Mint plants.

The negative correlation between photosynthetic variables and plant growth traits was once again confirmed in the PCA analysis. Combining all the trait variances in a PCA score plot revealed the differential responses of Wild Mint plants to different light spectra. The blue and red LED lights showed distinct effects on the growth and development of *Mentha arvensis* L. Blue LED light had a significant impact on CCI, Flav, $F_v/F_m$, qP, and ETR, consequently enhancing photosynthetic performance. Meanwhile, the red LED light had a greater effect on plant growth rate indicators such as NBI, LA, TLA, PA, PCH, and Anth. Both of them had a significant impact on plant biomass and metabolites, including FW, DW, Suc, Sta, and TPC.

## 5. Conclusion

This study established correlations between photosynthetic characteristics and plant production in Wild Mint, utilizing both conventional and high-throughput phenotyping techniques. The principal component analysis highlighted the unique responses of Wild Mint plants to mono-blue and red LED lights as supplementary lighting. A positive relationship was found between CCI, Flav, Fv/Fm, qP, and ETR traits. Additionally, image-based analysis results, such as LA, TLA, PA, and PCH, showed strong correlations with photosynthetic production and plant biomass traits, including NBI, FW, DW, Suc, Sta, and TPC.

The combination of conventional and high-throughput phenotyping techniques allows for a deeper understanding of the complex interactions between light spectra and photosynthesis in Wild Mint plants. This study enhances the understanding of how artificial light sources influence photosynthetic characteristics and plant growth traits, which could significantly impact crop cultivation and management. By utilizing specific light qualities, farmers can enhance plant photosynthetic performance, leading to improved plant biomass, metabolite production, and overall crop yield.

## References


Agati, G., Guidi, L., Landi, M., Tattini, M., 2021. Anthocyanins in photoprotection: knowing the actors in play to solve this complex ecophysiological issue. New Phytologist 232, 2228–2235. https://doi.org/10.1111/nph.17648

Ainsworth, E.A., Gillespie, K.M., 2007. Estimation of total phenolic content and other oxidation substrates in plant tissues using Folin–Ciocalteu reagent. Nat Protoc 2, 875–877. https://doi.org/10.1038/nprot.2007.102

Albert, N.W., Lewis, D.H., Zhang, H., Irving, L.J., Jameson, P.E., Davies, K.M., 2009. Light-induced vegetative anthocyanin pigmentation in Petunia. Journal of Experimental Botany 60, 2191–2202. https://doi.org/10.1093/jxb/erp097

Araus, J.L., Cairns, J.E., 2014. Field high-throughput phenotyping: the new crop breeding frontier. Trends in Plant Science 19, 52–61. https://doi.org/10.1016/j.tplants.2013.09.008

Awlia, M., Nigro, A., Fajkus, J., Schmoeckel, S.M., Negrão, S., Santelia, D., Trtílek, M., Tester, M., Julkowska, M.M., Panzarová, K., 2016. High-Throughput Non-destructive Phenotyping of Traits that Contribute to Salinity Tolerance in *Arabidopsis thaliana*. Front. Plant Sci. 7. https://doi.org/10.3389/fpls.2016.01414

Baba, S.A., Malik, S.A., 2015. Determination of total phenolic and flavonoid content, antimicrobial and antioxidant activity of a root extract of *Arisaema jacquemontii* Blume. Journal of Taibah University for Science 9, 449–454. https://doi.org/10.1016/j.jtusci.2014.11.001

Bahadori, M.B., Zengin, G., Bahadori, S., Dinparast, L., Movahhedin, N., 2018. Phenolic composition and functional properties of wild mint ( *Mentha longifolia* var. *calliantha* (Stapf) Briq.). International Journal of Food Properties 21, 183–193. https://doi.org/10.1080/10942912.2018.1440238

Baker, N.R., 2008. Chlorophyll Fluorescence: A Probe of Photosynthesis In Vivo. Annu. Rev. Plant Biol. 59, 89–113. https://doi.org/10.1146/annurev.arplant.59.032607.092759

Baker, N.R., 2004. Applications of chlorophyll fluorescence can improve crop production strategies: an examination of future possibilities. Journal of Experimental Botany 55, 1607–1621. https://doi.org/10.1093/jxb/erh196

Bantis, F., Ouzounis, T., Radoglou, K., 2016. Artificial LED lighting enhances growth characteristics and total phenolic content of *Ocimum basilicum*, but variably affects transplant success. Scientia Horticulturae 198, 277–283. https://doi.org/10.1016/j.scienta.2015.11.014

Bauerle, W.L., McCullough, C., Iversen, M., Hazlett, M., 2020. Leaf Age and Position Effects on Quantum Yield and Photosynthetic Capacity in Hemp Crowns. Plants 9, 271. https://doi.org/10.3390/plants9020271

Beadle, C.L., Ludlow, M.M., Honeysett, J.L., 1985. Water Relations, in: Techniques in Bioproductivity and Photosynthesis. Elsevier, pp. 50–61. https://doi.org/10.1016/B978-0-08-031999-5.50015-7

Bethge, H., Winkelmann, T., Lüdeke, P., Rath, T., 2023. Low-cost and automated phenotyping system “Phenomenon” for multi-sensor in situ monitoring in plant in vitro culture. Plant Methods 19, 42. https://doi.org/10.1186/s13007-023-01018-w

Bowyer, J.R., Leegood, R.C., 1997. Photosynthesis, in: Plant Biochemistry. Elsevier, pp. 49-p4. https://doi.org/10.1016/B978-012214674-9/50003-5

Burkholder, P.R., 1936. The rôle of light in the life of plants II. The influence of light upon growth and differentiation. Bot. Rev 2, 97–172. https://doi.org/10.1007/BF02872368

Camargo, M.A.B., Marenco, R.A., 2011. Density, size and distribution of stomata in 35 rainforest tree species in Central Amazonia. Acta Amaz. 41, 205–212.

https://doi.org/10.1590/S0044-59672011000200004

Cardona, T., Shao, S., Nixon, P.J., 2018. Enhancing photosynthesis in plants: the light reactions. Essays in Biochemistry 62, 85–94. https://doi.org/10.1042/EBC20170015

Casson, S.A., Franklin, K.A., Gray, J.E., Grierson, C.S., Whitelam, G.C., Hetherington, A.M., 2009. phytochrome B and PIF4 Regulate Stomatal Development in Response to Light Quantity. Current Biology 19, 229–234. https://doi.org/10.1016/j.cub.2008.12.046

Cerovic, Z.G., Ghozlen, N.B., Milhade, C., Obert, M., Debuisson, S., Moigne, M.L., 2015. Nondestructive Diagnostic Test for Nitrogen Nutrition of Grapevine (*Vitis vinifera* L.) Based on Dualex Leaf-Clip Measurements in the Field. J. Agric. Food Chem. 63, 3669–3680. https://doi.org/10.1021/acs.jafc.5b00304

Cerovic, Z.G., Masdoumier, G., Ghozlen, N.B., Latouche, G., 2012. A new optical leaf-clip meter for simultaneous non-destructive assessment of leaf chlorophyll and epidermal flavonoids. Physiologia Plantarum 146, 251–260. https://doi.org/10.1111/j.1399-3054.2012.01639.x

Chen, H.-J., Inbaraj, B.S., Chen, B.-H., 2011. Determination of Phenolic Acids and Flavonoids in Taraxacum formosanum Kitam by Liquid Chromatography-Tandem Mass Spectrometry Coupled with a Post-Column Derivatization Technique. IJMS 13, 260–285. https://doi.org/10.3390/ijms13010260

Chen, M., Blankenship, R.E., 2011. Expanding the solar spectrum used by photosynthesis. Trends in Plant Science 16, 427–431. https://doi.org/10.1016/j.tplants.2011.03.011

Chen, Z., Tao, X., Khan, A., Tan, D.K.Y., Luo, H., 2018. Biomass Accumulation, Photosynthetic Traits and Root Development of Cotton as Affected by Irrigation and Nitrogen-Fertilization. Front. Plant Sci. 9, 173. https://doi.org/10.3389/fpls.2018.00173

Childs, K.L., Miller, F.R., Cordonnier-Pratt, M.M., Pratt, L.H., Morgan, P.W., Mullet, J.E., 1997. The Sorghum Photoperiod Sensitivity Gene, Ma3, Encodes a Phytochrome B. Plant Physiology 113, 611–619. https://doi.org/10.1104/pp.113.2.611

Cho, W.-J., Yang, M., 2023. High-Throughput Plant Phenotyping System Using a Low-Cost Camera Network for Plant Factory. Agriculture 13, 1874. https://doi.org/10.3390/agriculture13101874

Coleman, H.D., Beamish, L., Reid, A., Park, J.-Y., Mansfield, S.D., 2010. Altered sucrose metabolism impacts plant biomass production and flower development. Transgenic Res 19, 269–283. https://doi.org/10.1007/s11248-009-9309-5

Constable, G., Rawson, H., 1980. Effect of Leaf Position, Expansion and Age on Photosynthesis, Transpiration and Water Use Efficiency of Cotton. Functional Plant Biol. 7, 89. https://doi.org/10.1071/PP9800089

Coombs, J., Hind, G., Leegood, R.C., Tieszen, L.L., Vonshak, A., 1985. Analytical Techniques, in: Techniques in Bioproductivity and Photosynthesis. https://doi.org/10.1016/B978-0-08-031999-5.50027-3

Craver, J.K., Nemali, K.S., Lopez, R.G., 2020. Acclimation of Growth and Photosynthesis in Petunia Seedlings Exposed to High-intensity Blue Radiation. J. Amer. Soc. Hort. Sci. 145, 152–161. https://doi.org/10.21273/JASHS04799-19

Dar, M.A., Masoodi, M.H., Wali, A.F., Mir, M.A., Shapoo, N.S., 2014. Antioxidant potential of methanol Root extract of *Mentha arvensis* L. from Kashmir Region. j app pharm sci 50–57. https://doi.org/10.7324/JAPS.2014.40311

Darko, E., Heydarizadeh, P., Schoefs, B., Sabzalian, M.R., 2014. Photosynthesis under artificial light: the shift in primary and secondary metabolism. Phil. Trans. R. Soc. B 369, 20130243. https://doi.org/10.1098/rstb.2013.0243

De Mello, F.P., Orçati, M.Z., Almeida-Junior, L.D.D., Di Stasi, L.C., 2023. Isolated bioactive

compounds, in: Natural Plant Products in Inflammatory Bowel Diseases. Elsevier, pp. 287–318. https://doi.org/10.1016/B978-0-323-99111-7.00005-2

De Vega, J.J., Peel, N., Purdy, S.J., Hawkins, S., Donnison, L., Dyer, S., Farrar, K., 2021. Differential expression of starch and sucrose metabolic genes linked to varying biomass yield in Miscanthus hybrids. Biotechnol Biofuels 14, 98. https://doi.org/10.1186/s13068-021-01948-4

Deng, B., Li, Y., Xu, D., Ye, Q., Liu, G., 2019. Nitrogen availability alters flavonoid accumulation in *Cyclocarya paliurus* via the effects on the internal carbon/nitrogen balance. Sci Rep 9, 2370. https://doi.org/10.1038/s41598-019-38837-8

Dou, H., Niu, G., Gu, M., 2019. Photosynthesis, Morphology, Yield, and Phytochemical Accumulation in Basil Plants Influenced by Substituting Green Light for Partial Red and/or Blue Light. horts 54, 1769–1776. https://doi.org/10.21273/HORTSCI14282-19

Driesen, E., Van Den Ende, W., De Proft, M., Saeys, W., 2020. Influence of Environmental Factors Light, CO2, Temperature, and Relative Humidity on Stomatal Opening and Development: A Review. Agronomy 10, 1975. https://doi.org/10.3390/agronomy10121975

Du, J., Lu, X., Fan, J., Qin, Y., Yang, X., Guo, X., 2020. Image-Based High-Throughput Detection and Phenotype Evaluation Method for Multiple Lettuce Varieties. Front. Plant Sci. 11, 563386. https://doi.org/10.3389/fpls.2020.563386

Dueck, T., Van Ieperen, W., Taulavuori, K., 2016. Light perception, signalling and plant responses to spectral quality and photoperiod in natural and horticultural environments. Environmental and Experimental Botany 121, 1–3. https://doi.org/10.1016/j.envexpbot.2015.06.012

Dwyer, L.M., Stewart, D.W., 1986. Effect of leaf age and position on net photosynthetic rates in maize (*Zea Mays* L.). Agricultural and Forest Meteorology 37, 29–46. https://doi.org/10.1016/0168-1923(86)90026-2

Ellis, N.K., 1960. Peppermint and spearmint production. Econ Bot 14, 280–285. https://doi.org/10.1007/BF02908037

Elser, J.J., Fagan, W.F., Kerkhoff, A.J., Swenson, N.G., Enquist, B.J., 2010. Biological stoichiometry of plant production: metabolism, scaling and ecological response to global change. New Phytologist 186, 593–608. https://doi.org/10.1111/j.1469-8137.2010.03214.x

Fahlén, A., Welander, M., Wennersten, R., 1997. Effects of Light-Temperature Regimes on Plant Growth and Essential Oil Yield of Selected Aromatic Plants. J. Sci. Food Agric. 73, 111–119. https://doi.org/10.1002/(SICI)1097-0010(199701)73

Fan, K., Li, F., Chen, X., Li, Z., Mulla, D., 2022. Nitrogen Balance Index Prediction of Winter Wheat by Canopy Hyperspectral Transformation and Machine Learning. Remote Sensing 14, 3504. https://doi.org/10.3390/rs14143504

Fan, X., Zang, J., Xu, Z., Guo, S., Jiao, X., Liu, X., Gao, Y., 2013. Effects of different light quality on growth, chlorophyll concentration and chlorophyll biosynthesis precursors of non-heading Chinese cabbage (*Brassica campestris* L.). Acta Physiol Plant 35, 2721–2726. https://doi.org/10.1007/s11738-013-1304-z

Fan, Y., Feng, H., Jin, X., Yue, J., Liu, Y., Li, Z., Feng, Z., Song, X., Yang, G., 2022. Estimation of the nitrogen content of potato plants based on morphological parameters and visible light vegetation indices. Front. Plant Sci. 13, 1012070. https://doi.org/10.3389/fpls.2022.1012070

Fang, L., Ma, Z., Wang, Q., Nian, H., Ma, Q., Huang, Q., Mu, Y., 2021. Plant Growth and Photosynthetic Characteristics of Soybean Seedlings Under Different LED Lighting Quality Conditions. J Plant Growth Regul 40, 668–678. https://doi.org/10.1007/s00344-020-10131-2

Fatih, B., Madani, K., Chibane, M., Duez, P., 2017. Chemical Composition and Biological

Activities of Mentha Species, in: El-Shemy, H.A. (Ed.), Aromatic and Medicinal Plants - Back to Nature. InTech. https://doi.org/10.5772/67291

Feduraev, P., Chupakhina, G., Maslennikov, P., Tacenko, N., Skrypnik, L., 2019. Variation in Phenolic Compounds Content and Antioxidant Activity of Different Plant Organs from *Rumex crispus* L. and *Rumex obtusifolius* L. at Different Growth Stages. Antioxidants 8, 237. https://doi.org/10.3390/antiox8070237

Ferreyra, M.L.F., Serra, P., Casati, P., 2021. Recent advances on the roles of flavonoids as plant protective molecules after UV and high light exposure. Physiologia Plantarum 173, 736–749. https://doi.org/10.1111/ppl.13543

Finlayson, S.A., Krishnareddy, S.R., Kebrom, T.H., Casal, J.J., 2010. Phytochrome Regulation of Branching in *Arabidopsis*. Plant Physiol. 152, 1914–1927. https://doi.org/10.1104/pp.109.148833

Fu, P., Montes, C.M., Siebers, M.H., Gomez-Casanovas, N., McGrath, J.M., Ainsworth, E.A., Bernacchi, C.J., 2022. Advances in field-based high-throughput photosynthetic phenotyping. Journal of Experimental Botany 73, 3157–3172. https://doi.org/10.1093/jxb/erac077

Furbank, R.T., Tester, M., 2011. Phenomics – technologies to relieve the phenotyping bottleneck. Trends in Plant Science 16, 635–644. https://doi.org/10.1016/j.tplants.2011.09.005

Groff, P.A., Kaplan, D.R., 1988. The relation of root systems to shoot systems in vascular plants. Bot. Rev 54, 387–422. https://doi.org/10.1007/BF02858417

Grouneva, I., Gollan, P.J., Kangasjärvi, S., Suorsa, M., Tikkanen, M., Aro, E.-M., 2013. Phylogenetic viewpoints on regulation of light harvesting and electron transport in eukaryotic photosynthetic organisms. Planta 237, 399–412. https://doi.org/10.1007/s00425-012-1744-5

Guo, N., Cheng, F., Wu, J., Liu, B., Zheng, S., Liang, J., Wang, X., 2014. Anthocyanin biosynthetic genes in *Brassica rapa*. BMC Genomics 15, 426. https://doi.org/10.1186/1471-2164-15-426

Hamdani, S., Khan, N., Perveen, S., Qu, M., Jiang, J., Govindjee, Zhu, X.-G., 2019. Changes in the photosynthesis properties and photoprotection capacity in rice (*Oryza sativa*) grown under red, blue, or white light. Photosynth Res 139, 107–121. https://doi.org/10.1007/s11120-018-0589-6

Han, G.D., Jang, G., Kim, J., Kim, D.-W., Rodrogues, R., Kim, S.-H., Kim, H.-J., Chung, Y.S., 2021. RGB images-based vegetative index for phenotyping kenaf (*Hibiscus cannabinus* L.). PLoS ONE 16, e0256978. https://doi.org/10.1371/journal.pone.0256978

Hardwick, K., Wood, M., Woolhouse, H.W., 1968. Photosynthesis and Respiration in Relation to Leaf Age in *Perilla Frutescens* (L.) Britt. New Phytol 67, 79–86. https://doi.org/10.1111/j.1469-8137.1968.tb05456.x

Hasan, Md.M., Bashir, T., Ghosh, R., Lee, S.K., Bae, H., 2017. An Overview of LEDs' Effects on the Production of Bioactive Compounds and Crop Quality. Molecules 22, 1420. https://doi.org/10.3390/molecules22091420

Haworth, M., Marino, G., Centritto, M., 2018. An introductory guide to gas exchange analysis of photosynthesis and its application to plant phenotyping and precision irrigation to enhance water use efficiency. Journal of Water and Climate Change 9, 786–808. https://doi.org/10.2166/wcc.2018.152

Heo, J., Lee, C., Chakrabarty, D., Paek, K., 2002. Growth responses of marigold and salvia bedding plants as affected by monochromic or mixture radiation provided by a Light-Emitting Diode (LED). Plant Growth Regulation 38, 225–230. https://doi.org/10.1023/A:1021523832488

Heo, J.-W., Kang, D.-H., Bang, H.-S., Hong, S.-G., Chun, C.-H., Kang, K.-K., 2012. Early Growth, Pigmentation, Protein Content, and Phenylalanine Ammonia-lyase Activity of Red

Curled Lettuces Grown under Different Lighting Conditions. Korean Journal of Horticultural Science and Technology 30, 6–12. https://doi.org/10.7235/hort.2012.11118

Hernández, R., Kubota, C., 2016. Physiological responses of cucumber seedlings under different blue and red photon flux ratios using LEDs. Environmental and Experimental Botany 121, 66–74. https://doi.org/10.1016/j.envexpbot.2015.04.001

Hind, G., 1985. Photosynthetic Energy Conversion, in: Techniques in Bioproductivity and Photosynthesis. Elsevier, pp. 133–138. https://doi.org/10.1016/B978-0-08-031999-5.50020-0

Hogewoning, S.W., Trouwborst, G., Maljaars, H., Poorter, H., Van Ieperen, W., Harbinson, J., 2010. Blue light dose-responses of leaf photosynthesis, morphology, and chemical composition of *Cucumis sativus* grown under different combinations of red and blue light. Journal of Experimental Botany 61, 3107–3117. https://doi.org/10.1093/jxb/erq132

Holalu, S.V., Finlayson, S.A., 2017. The ratio of red light to far red light alters *Arabidopsis* axillary bud growth and abscisic acid signalling before stem auxin changes. EXBOTJ erw479. https://doi.org/10.1093/jxb/erw479

Hu, H., Xu, K., He, L., Wang, G., 2021. A model for the relationship between plant biomass and photosynthetic rate based on nutrient effects. Ecosphere 12, e03678. https://doi.org/10.1002/ecs2.3678

Hu, J., Dai, X., Sun, G., 2016. Morphological and Physiological Responses of *Morus alba* Seedlings under Different Light Qualities. Not Bot Horti Agrobo 44, 382–392. https://doi.org/10.15835/nbha44210486

Hung, C.D., Hong, C.-H., Kim, S.-K., Lee, K.-H., Park, J.-Y., Nam, M.-W., Choi, D.-H., Lee, H.-I., 2016. LED light for in vitro and ex vitro efficient growth of economically important highbush blueberry (*Vaccinium corymbosum* L.). Acta Physiol Plant 38, 152. https://doi.org/10.1007/s11738-016-2164-0

Hunt, S., 2003. Measurements of photosynthesis and respiration in plants. Physiologia Plantarum 117, 314–325. https://doi.org/10.1034/j.1399-3054.2003.00055.x

Jewiss, O.R., Woledge, J., 1967. The Effect of Age on the Rate of Apparent Photosynthesis in Leaves of Tall Fescue (*Festuca arundinacea* Schreb.). Annals of Botany 31, 661–671. https://doi.org/10.1093/oxfordjournals.aob.a084171

Johkan, M., Shoji, K., Goto, F., Hashida, S., Yoshihara, T., 2010. Blue Light-emitting Diode Light Irradiation of Seedlings Improves Seedling Quality and Growth after Transplanting in Red Leaf Lettuce. horts 45, 1809–1814. https://doi.org/10.21273/HORTSCI.45.12.1809

Johnson, M.P., 2016. Photosynthesis. Essays in Biochemistry 60, 255–273. https://doi.org/10.1042/EBC20160016

Jou, J.-H., Lin, C.-C., Li, T.-H., Li, C.-J., Peng, S.-H., Yang, F.-C., Thomas, K., Kumar, D., Chi, Y., Hsu, B.-D., 2015. Plant Growth Absorption Spectrum Mimicking Light Sources. Materials 8, 5265–5275. https://doi.org/10.3390/ma8085240

Jung, C., Arar, M., 2023. Natural vs. Artificial Light: A Study on the Influence of Light Source on Chlorophyll Content and Photosynthetic Rates on Indoor Plants. Buildings 13, 1482. https://doi.org/10.3390/buildings13061482

Jung, W.-S., Chung, I.-M., Hwang, M.H., Kim, S.-H., Yu, C.Y., Ghimire, B.K., 2021. Application of Light-Emitting Diodes for Improving the Nutritional Quality and Bioactive Compound Levels of Some Crops and Medicinal Plants. Molecules 26, 1477. https://doi.org/10.3390/molecules26051477

Kalaji, H.M., Schansker, G., Brestic, M., Bussotti, F., Calatayud, A., Ferroni, L., Goltsev, V., Guidi, L., Jajoo, A., Li, P., Losciale, P., Mishra, V.K., Misra, A.N., Nebauer, S.G., Pancaldi, S., Penella, C., Pollastrini, M., Suresh, K., Tambussi, E., Yanniccari, M., Zivcak, M., Cetner, M.D., Samborska, I.A., Stirbet, A., Olsovska, K., Kunderlikova, K., Shelonzek, H., Rusinowski, S.,

Bąba, W., 2017. Frequently asked questions about chlorophyll fluorescence, the sequel. Photosynth Res 132, 13–66. https://doi.org/10.1007/s11120-016-0318-y

Kaniszewski, S., Kowalski, A., Dysko, J., Agati, G., 2021. Application of a Combined Transmittance/Fluorescence Leaf Clip Sensor for the Nondestructive Determination of Nitrogen Status in White Cabbage Plants. Sensors 21, 482. https://doi.org/10.3390/s21020482

Kapoor, S., Raghuvanshi, R., Bhardwaj, P., Sood, H., Saxena, S., Chaurasia, O.P., 2018. Influence of light quality on growth, secondary metabolites production and antioxidant activity in callus culture of *Rhodiola imbricata* Edgew. Journal of Photochemistry and Photobiology B: Biology 183, 258–265. https://doi.org/10.1016/j.jphotobiol.2018.04.018

Karimi, M., Ahmadi, N., Ebrahimi, M., 2022. Red LED light promotes biomass, flowering and secondary metabolites accumulation in hydroponically grown *Hypericum perforatum* L. (cv. Topas). Industrial Crops and Products 175, 114239. https://doi.org/10.1016/j.indcrop.2021.114239

Kebrom, T.H., Burson, B.L., Finlayson, S.A., 2006. Phytochrome B Represses *Teosinte Branched1* Expression and Induces Sorghum Axillary Bud Outgrowth in Response to Light Signals. Plant Physiology 140, 1109–1117. https://doi.org/10.1104/pp.105.074856

Kim, S.-J., Hahn, E.-J., Heo, J.-W., Paek, K.-Y., 2004. Effects of LEDs on net photosynthetic rate, growth and leaf stomata of chrysanthemum plantlets in vitro. Scientia Horticulturae 101, 143–151. https://doi.org/10.1016/j.scienta.2003.10.003

Kim, T.-H., Böhmer, M., Hu, H., Nishimura, N., Schroeder, J.I., 2010. Guard Cell Signal Transduction Network: Advances in Understanding Abscisic Acid, $CO_2$, and $Ca^{2+}$ Signaling. Annu. Rev. Plant Biol. 61, 561–591. https://doi.org/10.1146/annurev-arplant-042809-112226

Kitao, M., Yasuda, Y., Kodani, E., Harayama, H., Awaya, Y., Komatsu, M., Yazaki, K., Tobita, H., Agathokleous, E., 2021. Integration of electron flow partitioning improves estimation of photosynthetic rate under various environmental conditions based on chlorophyll fluorescence. Remote Sensing of Environment 254, 112273. https://doi.org/10.1016/j.rse.2020.112273

Kitao, S., Sekine, H., 1994. α-D-Glucosyl Transfer to Phenolic Compounds by Sucrose Phosphorylase from Leuconostoc mesenteroides and Production of α-Arbutin. Bioscience, Biotechnology, and Biochemistry 58, 38–42. https://doi.org/10.1271/bbb.58.38

Kong, Y., Stasiak, M., Dixon, M.A., Zheng, Y., 2018. Blue light associated with low phytochrome activity can promote elongation growth as shade-avoidance response: A comparison with red light in four bedding plant species. Environmental and Experimental Botany 155, 345–359. https://doi.org/10.1016/j.envexpbot.2018.07.021

Kozai, T., Niu, G., Takagaki, M. (Eds.), 2016. Plant factory: an indoor vertical farming system for efficient quality food production. Elsevier/AP, Academic Press is an imprint of Elsevier, Amsterdam ; Boston.

Kramer, D.M., Evans, J.R., 2011. The Importance of Energy Balance in Improving Photosynthetic Productivity. Plant Physiology 155, 70–78. https://doi.org/10.1104/pp.110.166652

Kuleshova, T.E., Likhachev, A.I., Pavlova, E.S., Kuleshov, D.O., Nashchekin, A.V., Gall, N.R., 2018. Interrelation of Absorption Spectra of Plant Pigments and LED Lighting with Different Spectral Compositions. Tech. Phys. 63, 1243–1247. https://doi.org/10.1134/S1063784218090104

Kusuma, P., Pattison, P.M., Bugbee, B., 2020. From physics to fixtures to food: current and potential LED efficacy. Hortic Res 7, 56. https://doi.org/10.1038/s41438-020-0283-7

Lawson, T., 2009. Guard cell photosynthesis and stomatal function. New Phytologist 181, 13–34. https://doi.org/10.1111/j.1469-8137.2008.02685.x

Leduc, N., Roman, H., Barbier, F., Péron, T., Huché-Thélier, L., Lothier, J., Demotes-

Mainard, S., Sakr, S., 2014. Light Signaling in Bud Outgrowth and Branching in Plants. Plants 3, 223–250. https://doi.org/10.3390/plants3020223

Lejeune, P., Fratamico, A., Bouché, F., Huerga-Fernández, S., Tocquin, P., Périlleux, C., 2022. LED color gradient as a new screening tool for rapid phenotyping of plant responses to light quality. GigaScience 11, giab101. https://doi.org/10.1093/gigascience/giab101

Li, H., Testerink, C., Zhang, Y., 2021. How roots and shoots communicate through stressful times. Trends in Plant Science 26, 940–952. https://doi.org/10.1016/j.tplants.2021.03.005

Li, Q., Kubota, C., 2009. Effects of supplemental light quality on growth and phytochemicals of baby leaf lettuce. Environmental and Experimental Botany 67, 59–64. https://doi.org/10.1016/j.envexpbot.2009.06.011

Lillo, C., 1994. Light regulation of nitrate reductase in green leaves of higher plants. Physiologia Plantarum 90, 616–620. https://doi.org/10.1111/j.1399-3054.1994.tb08822.x

Liu, J., Van Iersel, M.W., 2021. Photosynthetic Physiology of Blue, Green, and Red Light: Light Intensity Effects and Underlying Mechanisms. Front. Plant Sci. 12, 619987. https://doi.org/10.3389/fpls.2021.619987

Liu, Y., Wang, J., Xiao, Y., Shi, X., Zeng, Y., 2021. Diversity Analysis of Chlorophyll, Flavonoid, Anthocyanin, and Nitrogen Balance Index of Tea Based on Dualex. Phyton 90, 1549–1558. https://doi.org/10.32604/phyton.2021.015557

Luo, W., Elser, J.J., Lü, X., Wang, Z., Bai, E., Yan, C., Wang, C., Li, M., Zimmermann, N.E., Han, X., Xu, Z., Li, H., Wu, Y., Jiang, Y., 2015. Plant nutrients do not covary with soil nutrients under changing climatic conditions. Global Biogeochemical Cycles 29, 1298–1308. https://doi.org/10.1002/2015GB005089

Luo, W., Li, M., Sardans, J., Lü, X., Wang, C., Peñuelas, J., Wang, Z., Han, X., Jiang, Y., 2017. Carbon and nitrogen allocation shifts in plants and soils along aridity and fertility gradients in grasslands of China. Ecology and Evolution 7, 6927–6934. https://doi.org/10.1002/ece3.3245

Ma, Y., Xu, A., Cheng, Z.-M. (Max), 2021. Effects of light emitting diode lights on plant growth, development and traits a meta-analysis. Horticultural Plant Journal 7, 552–564. https://doi.org/10.1016/j.hpj.2020.05.007

Maddison, A.L., Camargo-Rodriguez, A., Scott, I.M., Jones, C.M., Elias, D.M.O., Hawkins, S., Massey, A., Clifton-Brown, J., McNamara, N.P., Donnison, I.S., Purdy, S.J., 2017. Predicting future biomass yield in *Miscanthus* using the carbohydrate metabolic profile as a biomarker. GCB Bioenergy 9, 1264–1278. https://doi.org/10.1111/gcbb.12418

Maffei, M., Scannerini, S., 1999. Photomorphogenic and Chemical Responses to Blue Light in *Mentha piperita*. Journal of Essential Oil Research 11, 730–738. https://doi.org/10.1080/10412905.1999.9712007

Matthews, J.S.A., Vialet-Chabrand, S., Lawson, T., 2020. Role of blue and red light in stomatal dynamic behaviour. Journal of Experimental Botany 71, 2253–2269. https://doi.org/10.1093/jxb/erz563

Matysiak, B., 2021. The Effect of Supplementary LED Lighting on the Morphological and Physiological Traits of *Miniature* Rosa × Hybrida 'Aga' and the Development of Powdery Mildew (Podosphaera pannosa) under Greenhouse Conditions. Plants 10, 417. https://doi.org/10.3390/plants10020417

Matysiak, B., Kaniszewski, S., Dyśko, J., Kowalczyk, W., Kowalski, A., Grzegorzewska, M., 2021. The Impact of LED Light Spectrum on the Growth, Morphological Traits, and Nutritional Status of '*Elizium*' Romaine Lettuce Grown in an Indoor Controlled Environment. Agriculture 11, 1133. https://doi.org/10.3390/agriculture11111133

Meng, X., Wang, Z., He, S., Shi, L., Song, Y., Lou, X., He, D., 2019. LED-Supplied Red and

Blue Light Alters the Growth, Antioxidant Status, and Photochemical Potential of in Vitro-Grown *Gerbera jamesonii* Plantlets. H.S.T. 37, 473–489. https://doi.org/10.7235/HORT.20190048

Miao, Y., Chen, Q., Qu, M., Gao, L., Hou, L., 2019. Blue light alleviates 'red light syndrome' by regulating chloroplast ultrastructure, photosynthetic traits and nutrient accumulation in cucumber plants. Scientia Horticulturae 257, 108680. https://doi.org/10.1016/j.scienta.2019.108680

Miao, Y., Wang, X., Gao, L., Chen, Q., Qu, M., 2016. Blue light is more essential than red light for maintaining the activities of photosystem II and I and photosynthetic electron transport capacity in cucumber leaves. Journal of Integrative Agriculture 15, 87–100. https://doi.org/10.1016/S2095-3119(15)61202-3

Mickens, M.A., Skoog, E.J., Reese, L.E., Barnwell, P.L., Spencer, L.E., Massa, G.D., Wheeler, R.M., 2018. A strategic approach for investigating light recipes for '*Outredgeous*' red romaine lettuce using white and monochromatic LEDs. Life Sciences in Space Research 19, 53–62. https://doi.org/10.1016/j.lssr.2018.09.003

Morisette, J.T., Baret, F., Privette, J.L., Myneni, R.B., Nickeson, J.E., Garrigues, S., Shabanov, N.V., Weiss, M., Fernandes, R.A., Leblanc, S.G., Kalacska, M., Sanchez-Azofeifa, G.A., Chubey, M., Rivard, B., Stenberg, P., Rautiainen, M., Voipio, P., Manninen, T., Pilant, A.N., Lewis, T.E., Iiames, J.S., Colombo, R., Meroni, M., Busetto, L., Cohen, W.B., Turner, D.P., Warner, E.D., Petersen, G.W., Seufert, G., Cook, R., 2006. Validation of global moderate-resolution LAI products: a framework proposed within the CEOS land product validation subgroup. IEEE Trans. Geosci. Remote Sensing 44, 1804–1817. https://doi.org/10.1109/TGRS.2006.872529

Mott, K.A., Sibbernsen, E.D., Shope, J.C., 2008. The role of the mesophyll in stomatal responses to light and $CO_2$. Plant Cell & Environment 31, 1299–1306. https://doi.org/10.1111/j.1365-3040.2008.01845.x

Muneer, S., Kim, E., Park, J., Lee, J., 2014. Influence of Green, Red and Blue Light Emitting Diodes on Multiprotein Complex Proteins and Photosynthetic Activity under Different Light Intensities in Lettuce Leaves (*Lactuca sativa* L.). IJMS 15, 4657–4670. https://doi.org/10.3390/ijms15034657

Murchie, E.H., Burgess, A.J., 2022. Casting light on the architecture of crop yield. Crop and Environment 1, 74–85. https://doi.org/10.1016/j.crope.2022.03.009

Naeem, M., Idrees, Mohd., Aftab, T., Khan, M.M.A., Moinuddin, Varshney, L., 2012. Depolymerised carrageenan enhances physiological activities and menthol production in *Mentha arvensis* L. Carbohydrate Polymers 87, 1211–1218. https://doi.org/10.1016/j.carbpol.2011.09.002

Naznin, M., Lefsrud, M., Gravel, V., Azad, M., 2019. Blue Light added with Red LEDs Enhance Growth Characteristics, Pigments Content, and Antioxidant Capacity in Lettuce, Spinach, Kale, Basil, and Sweet Pepper in a Controlled Environment. Plants 8, 93. https://doi.org/10.3390/plants8040093

Nguyen, T.L., Saleh, M.A., 2019. Effect of exposure to light emitted diode (LED) lights on essential oil composition of sweet mint plants. Journal of Environmental Science and Health, Part A 54, 435–440. https://doi.org/10.1080/10934529.2018.1562810

Nishioka, N., Nishimura, T., Ohyama, K., Sumino, M., Malayeri, S.H., Goto, E., Inagaki, N., Morota, T., 2008. Light Quality Affected Growth and Contents of Essential Oil Components of Japanese Mint Plants. Acta Hortic. 431–436. https://doi.org/10.17660/ActaHortic.2008.797.62

Noguchi, A., Amaki, W., 2016. Effects of light quality on the growth and essential oil production in Mexican mint. Acta Hortic. 239–244. https://doi.org/10.17660/ActaHortic.2016.1134.32

Olle, M., Viršile, A., 2013. The effects of light-emitting diode lighting on greenhouse plant growth and quality. AFSci 22, 223–234. https://doi.org/10.23986/afsci.7897

O'Neill, E.J., Batey, T., Cresser, M.S., 1984. Effect of nitrogen supply on barley pigment concentrations. Plant Soil 77, 315–326. https://doi.org/10.1007/BF02182934

Ouzounis, T., Fretté, X., Ottosen, C., Rosenqvist, E., 2015. Spectral effects of LEDs on chlorophyll fluorescence and pigmentation in *Phalaenopsis* 'Vivien' and 'Purple Star.' Physiologia Plantarum 154, 314–327. https://doi.org/10.1111/ppl.12300

Palacio, S., Maestro, M., Montserrat-Martí, G., 2007. Relationship between Shoot-rooting and Root-sprouting Abilities and the Carbohydrate and Nitrogen Reserves of Mediterranean Dwarf Shrubs. Annals of Botany 100, 865–874. https://doi.org/10.1093/aob/mcm185

Paradiso, R., Proietti, S., 2022. Light-Quality Manipulation to Control Plant Growth and Photomorphogenesis in Greenhouse Horticulture: The State of the Art and the Opportunities of Modern LED Systems. J Plant Growth Regul 41, 742–780. https://doi.org/10.1007/s00344-021-10337-y

Park, C., Kim, N., Park, J., Lee, S., Lee, J.-W., Park, S., 2019. Effects of Light-Emitting Diodes on the Accumulation of Glucosinolates and Phenolic Compounds in Sprouting Canola (*Brassica napus* L.). Foods 8, 76. https://doi.org/10.3390/foods8020076

Park, W.T., Yeo, S.K., Sathasivam, R., Park, J.S., Kim, J.K., Park, S.U., 2020. Influence of light-emitting diodes on phenylpropanoid biosynthetic gene expression and phenylpropanoid accumulation in *Agastache rugosa*. Appl Biol Chem 63, 25. https://doi.org/10.1186/s13765-020-00510-4

Parry, C., Blonquist, J.M., Bugbee, B., 2014. In situ measurement of leaf chlorophyll concentration: analysis of the optical/absolute relationship. Plant Cell & Environment 37, 2508–2520. https://doi.org/10.1111/pce.12324

Peat, W.E., 1970. Relationships between Photosynthesis and Light Intensity in the Tomato. Annals of Botany 34, 319–328. https://doi.org/10.1093/oxfordjournals.aob.a084372

Qiu, R., Wei, S., Zhang, M., Li, H., Sun, H., Liu, G., Li, M., 2015. Sensors for measuring plant phenotyping: A review. International Journal of Agricultural and Biological Engineering 11, 1–17. https://doi.org/10.25165/j.ijabe.20181102.2696

Rabinowitch, E.I., Govindjee, 1965. The Role of Chlorophyll in Photosynthesis. Sci Am 213, 74–83. https://doi.org/10.1038/scientificamerican0765-74

Rabinowitch, E.I., Livingston, R., 1946. Photosynthesis and Related Processes. Volume I: Chemistry of Photosynthesis, Chemosynthesis, and Related Processes in Vitro and in Vivo. J. Phys. Chem. 50, 72–72. https://doi.org/10.1021/j150445a011

Rahman, M.M., Field, D.L., Ahmed, S.M., Hasan, M.T., Basher, M.K., Alameh, K., 2021. LED Illumination for High-Quality High-Yield Crop Growth in Protected Cropping Environments. Plants 10, 2470. https://doi.org/10.3390/plants10112470

Rao, B.R.R., 1999. Biomass and essential oil yields of cornmint (*Mentha arvensis* L. f. piperascens Malinvaud ex Holmes) planted in different months in semi-arid tropical climate. Industrial Crops and Products 10, 107–113.

Rashid, W., Asim, S., Rashid, S., Rafique, S., Aziz, R.S., Iftikhar, S., Rashid, M., Arfat, Y., 2023. Antioxidant and Anti-Mutagenic Potential of Mint (*Mentha arvensis*) and its Chemical Characterization by HPLC. PJMHS 17, 514–518. https://doi.org/10.53350/pjmhs2023174514

Rehman, M., Fahad, S., Saleem, M.H., Hafeez, M., Ur Rahman, M.H., Liu, F., Deng, G., 2020. Red light optimized physiological traits and enhanced the growth of ramie (*Boehmeria nivea* L.). Photosynt. 58, 922–931. https://doi.org/10.32615/ps.2020.040

Rehman, R., Hanif, M.A., Mushtaq, Z., Al-Sadi, A.M., 2016. Biosynthesis of essential oils in aromatic plants: A review. Food Reviews International 32, 117–160.

https://doi.org/10.1080/87559129.2015.1057841

Roni, M.Z.K., Islam, M.S., Shimasaki, K., 2017. Response of Eustoma Leaf Phenotype and Photosynthetic Performance to LED Light Quality. Horticulturae 3, 50. https://doi.org/10.3390/horticulturae3040050

Sawhney, S.K., Naik, M.S., 1972. Role of light in the synthesis of nitrate reductase and nitrite reductase in rice seedlings. Biochemical Journal 130, 475–485. https://doi.org/10.1042/bj1300475

Schindelin, J., Arganda-Carreras, I., Frise, E., Kaynig, V., Longair, M., Pietzsch, T., Preibisch, S., Rueden, C., Saalfeld, S., Schmid, B., Tinevez, J.-Y., White, D.J., Hartenstein, V., Eliceiri, K., Tomancak, P., Cardona, A., 2012. Fiji: an open-source platform for biological-image analysis. Nat Methods 9, 676–682. https://doi.org/10.1038/nmeth.2019

Schneider, A., Godin, C., Boudon, F., Demotes-Mainard, S., Sakr, S., Bertheloot, J., 2019. Light Regulation of Axillary Bud Outgrowth Along Plant Axes: An Overview of the Roles of Sugars and Hormones. Front. Plant Sci. 10, 1296. https://doi.org/10.3389/fpls.2019.01296

Seif, M., Aliniaeifard, S., Arab, M., Mehrjerdi, M.Z., Shomali, A., Fanourakis, D., Li, T., Woltering, E., 2021. Monochromatic red light during plant growth decreases the size and improves the functionality of stomata in chrysanthemum. Functional Plant Biol. 48, 515. https://doi.org/10.1071/FP20280

Shapiro, S.S., Wilk, M.B., 1965. An Analysis of Variance Test for Normality (Complete Samples). Biometrika 52, 591–611.

Sheibani, F., Bourget, M., Morrow, R.C., Mitchell, C.A., 2023. Close-canopy lighting, an effective energy-saving strategy for overhead sole-source LED lighting in indoor farming. Front. Plant Sci. 14, 1215919. https://doi.org/10.3389/fpls.2023.1215919

Shimazaki, K., Doi, M., Assmann, S.M., Kinoshita, T., 2007. Light Regulation of Stomatal Movement. Annu. Rev. Plant Biol. 58, 219–247. https://doi.org/10.1146/annurev.arplant.57.032905.105434

Son, K.-H., Park, J.-H., Kim, D., Oh, M.-M., 2012. Leaf Shape Index, Growth, and Phytochemicals in Two Leaf Lettuce Cultivars Grown under Monochromatic Light-emitting Diodes. Korean Journal of Horticultural Science and Technology 30, 664–672. https://doi.org/10.7235/hort.2012.12063

Soufi, H.R., Roosta, H.R., Stępień, P., Malekzadeh, K., Hamidpour, M., 2023. Manipulation of light spectrum is an effective tool to regulate biochemical traits and gene expression in lettuce under different replacement methods of nutrient solution. Sci Rep 13, 8600. https://doi.org/10.1038/s41598-023-35326-x

Spaninks, K., Van Lieshout, J., Van Ieperen, W., Offringa, R., 2020. Regulation of Early Plant Development by Red and Blue Light: A Comparative Analysis Between *Arabidopsis thaliana* and *Solanum lycopersicum*. Front. Plant Sci. 11, 599982. https://doi.org/10.3389/fpls.2020.599982

Stanford, A.L., Tanner, J.M., 1985. Early Quantum Physics, in: Physics for Students of Science and Engineering. Elsevier, pp. 691–716. https://doi.org/10.1016/B978-0-12-663380-1.50026-4

Stirbet, A., Lazár, D., Guo, Y., Govindjee, G., 2020. Photosynthesis: basics, history and modelling. Annals of Botany 126, 511–537. https://doi.org/10.1093/aob/mcz171

Stutte, G.W., Edney, S., Skerritt, T., 2009. Photoregulation of Bioprotectant Content of Red Leaf Lettuce with Light-emitting Diodes. horts 44, 79–82. https://doi.org/10.21273/HORTSCI.44.1.79

Tajima, R., 2021. Importance of individual root traits to understand crop root system in agronomic and environmental contexts. Breed. Sci. 71, 13–19.

https://doi.org/10.1270/jsbbs.20095

Trejo-Téllez, L.I., Estrada-Ortiz, E., Gómez-Merino, F.C., Becker, C., Krumbein, A., Schwarz, D., 2019. Flavonoid, Nitrate and Glucosinolate Concentrations in Brassica Species Are Differentially Affected by Photosynthetically Active Radiation, Phosphate and Phosphite. Front. Plant Sci. 10, 371. https://doi.org/10.3389/fpls.2019.00371

Ueda, T., Murata, M., Yokawa, K., 2021. Single Wavelengths of LED Light Supplement Promote the Biosynthesis of Major Cyclic Monoterpenes in Japanese Mint. Plants 10, 1420. https://doi.org/10.3390/plants10071420

Valin, H., Sands, R.D., Van Der Mensbrugghe, D., Nelson, G.C., Ahammad, H., Blanc, E., Bodirsky, B., Fujimori, S., Hasegawa, T., Havlik, P., Heyhoe, E., Kyle, P., Mason-D'Croz, D., Paltsev, S., Rolinski, S., Tabeau, A., Van Meijl, H., Von Lampe, M., Willenbockel, D., 2014. The future of food demand: understanding differences in global economic models. Agricultural Economics 45, 51–67. https://doi.org/10.1111/agec.12089

Van Bel, A.J.E., Offler, C.E., Patrick, J.W., 2003. PHOTOSYNTHESIS AND PARTITIONING | Sources and Sinks, in: Encyclopedia of Applied Plant Sciences. Elsevier, pp. 724–734. https://doi.org/10.1016/B0-12-227050-9/00089-2

W. Patrick, J., C. Botha, F., G. Birch, R., 2013. Metabolic engineering of sugars and simple sugar derivatives in plants. Plant Biotechnology Journal 11, 142–156. https://doi.org/10.1111/pbi.12002

Wang, J., Lu, W., Tong, Y., Yang, Q., 2016. Leaf Morphology, Photosynthetic Performance, Chlorophyll Fluorescence, Stomatal Development of Lettuce (*Lactuca sativa* L.) Exposed to Different Ratios of Red Light to Blue Light. Front. Plant Sci. 7. https://doi.org/10.3389/fpls.2016.00250

Wang, S., Liu, Xiaoting, Liu, Xiaoning, Xue, J., Ren, X., Zhai, Y., Zhang, X., 2022. The red/blue light ratios from light-emitting diodes affect growth and flower quality of *Hippeastrum hybridum* 'Red Lion.' Front. Plant Sci. 13, 1048770. https://doi.org/10.3389/fpls.2022.1048770

Wang, X.-Q., Zeng, Z.-L., Shi, Z.-M., Wang, J.-H., Huang, W., 2023. Variation in Photosynthetic Efficiency under Fluctuating Light between Rose Cultivars and its Potential for Improving Dynamic Photosynthesis. Plants 12, 1186. https://doi.org/10.3390/plants12051186

Xin, P., Li, B., Zhang, H., Hu, J., 2019. Optimization and control of the light environment for greenhouse crop production. Sci Rep 9, 8650. https://doi.org/10.1038/s41598-019-44980-z

Yahia, E.M., Carrillo-López, A., Barrera, G.M., Suzán-Azpiri, H., Bolaños, M.Q., 2019. Photosynthesis, in: Postharvest Physiology and Biochemistry of Fruits and Vegetables. Elsevier, pp. 47–72. https://doi.org/10.1016/B978-0-12-813278-4.00003-8

Yang, B., Zhou, X., Xu, R., Wang, J., Lin, Y., Pang, J., Wu, S., Zhong, F., 2016. Comprehensive Analysis of Photosynthetic Characteristics and Quality Improvement of Purple Cabbage under Different Combinations of Monochromatic Light. Front. Plant Sci. 7. https://doi.org/10.3389/fpls.2016.01788

Yang, W., Feng, H., Zhang, X., Zhang, J., Doonan, J.H., Batchelor, W.D., Xiong, L., Yan, J., 2020. Crop Phenomics and High-Throughput Phenotyping: Past Decades, Current Challenges, and Future Perspectives. Molecular Plant 13, 187–214. https://doi.org/10.1016/j.molp.2020.01.008

Yang, X.-C., Hwa, C.-M., 2008. Genetic modification of plant architecture and variety improvement in rice. Heredity 101, 396–404. https://doi.org/10.1038/hdy.2008.90

Yue, C., Wang, Z., Yang, P., 2021. Review: the effect of light on the key pigment compounds of photosensitive etiolated tea plant. Bot Stud 62, 21. https://doi.org/10.1186/s40529-021-00329-2

Zhang, H., Wang, L., Jin, X., Bian, L., Ge, Y., 2023. High-throughput phenotyping of plant

leaf morphological, physiological, and biochemical traits on multiple scales using optical sensing. The Crop Journal 11, 1303–1318. https://doi.org/10.1016/j.cj.2023.04.014

Zhang, J., Wang, X., Wang, J., Wang, W., 2014. Carbon and Nitrogen Contents in Typical Plants and Soil Profiles in Yanqi Basin of Northwest China. Journal of Integrative Agriculture 13, 648–656. https://doi.org/10.1016/S2095-3119(13)60723-6

Zhang, P., Zhang, Z., Li, B., Zhang, H., Hu, J., Zhao, J., 2020a. Photosynthetic rate prediction model of newborn leaves verified by core fluorescence parameters. Sci Rep 10, 3013. https://doi.org/10.1038/s41598-020-59741-6

Zhang, X., Bian, Z., Yuan, X., Chen, X., Lu, C., 2020b. A review on the effects of light-emitting diode (LED) light on the nutrients of sprouts and microgreens. Trends in Food Science & Technology 99, 203–216. https://doi.org/10.1016/j.tifs.2020.02.031

Zhang, Yuqi, Kaiser, E., Zhang, Yating, Yang, Q., Li, T., 2019. Red/blue light ratio strongly affects steady-state photosynthesis, but hardly affects photosynthetic induction in tomato (*Solanum lycopersicum*). Physiologia Plantarum 167, 144–158. https://doi.org/10.1111/ppl.12876

Zhao, D., Xie, D., Zhou, H., Jiang, H., An, S., 2012. Estimation of Leaf Area Index and Plant Area Index of a Submerged Macrophyte Canopy Using Digital Photography. PLoS ONE 7, e51034. https://doi.org/10.1371/journal.pone.0051034

Zheng, L., Van Labeke, M.-C., 2017. Long-Term Effects of Red- and Blue-Light Emitting Diodes on Leaf Anatomy and Photosynthetic Efficiency of Three Ornamental Pot Plants. Front. Plant Sci. 8, 917. https://doi.org/10.3389/fpls.2017.00917

Zheng, Z.-L., 2009. Carbon and nitrogen nutrient balance signaling in plants. Plant Signaling & Behavior 4, 584–591. https://doi.org/10.4161/psb.4.7.8540

Zhu, H., Li, X., Zhai, W., Liu, Y., Gao, Q., Liu, J., Ren, L., Chen, H., Zhu, Y., 2017. Effects of low light on photosynthetic properties, antioxidant enzyme activity, and anthocyanin accumulation in purple pak-choi (*Brassica campestris* ssp. Chinensis Makino). PLoS ONE 12, e0179305. https://doi.org/10.1371/journal.pone.0179305

Zhu, H., Zhang, T.J., Zheng, J., Huang, X.D., Yu, Z.C., Peng, C.L., Chow, W.S., 2018. Anthocyanins function as a light attenuator to compensate for insufficient photoprotection mediated by nonphotochemical quenching in young leaves of *Acmena acuminatissima* in winter. Photosynt. 56, 445–454. https://doi.org/10.1007/s11099-017-0740-1

**Supplementary**

**Table S1.** The normality tests of Wild Mint plant height under different LED sources, over time.

| Light treatment | | Shapiro-Wilk test | | | | | | | | Levene test (According to the time) | |
|---|---|---|---|---|---|---|---|---|---|---|---|
| | | 1st week | | 2nd week | | 3rd week | | 4th week | | | |
| | | W | p-value | W | p-value | W | p-value | W | p-value | F value | Pr(>F) |
| B | | 0.921 | 0.029 | 0.896 | 0.007 | 0.972 | 0.597 | 0.924 | 0.034 | 48.683 | 2.200e-16 *** |
| B3R7 | | 0.949 | 0.160 | 0.954 | 0.214 | 0.940 | 0.088 | 0.944 | 0.114 | 13.911 | 8.267e-08 *** |
| R | | 0.926 | 0.038 | 0.943 | 0.109 | 0.957 | 0.256 | 0.938 | 0.079 | 16.883 | 3.636e-09 *** |
| W | | 0.978 | 0.775 | 0.953 | 0.200 | 0.965 | 0.417 | 0.946 | 0.135 | 21.964 | 2.467e-11 *** |
| Levene test | F value | 2.831 | | 7.4885 | | 13.609 | | 9.4567 | | | |
| (According to the experiment) | Pr(>F) | 0.041 * | | 0.126 e-03 *** | | 1.145e-07 *** | | 1.221e-05 *** | | | |

** and *** Significant at the 0.05 and 0.001 probability level.*

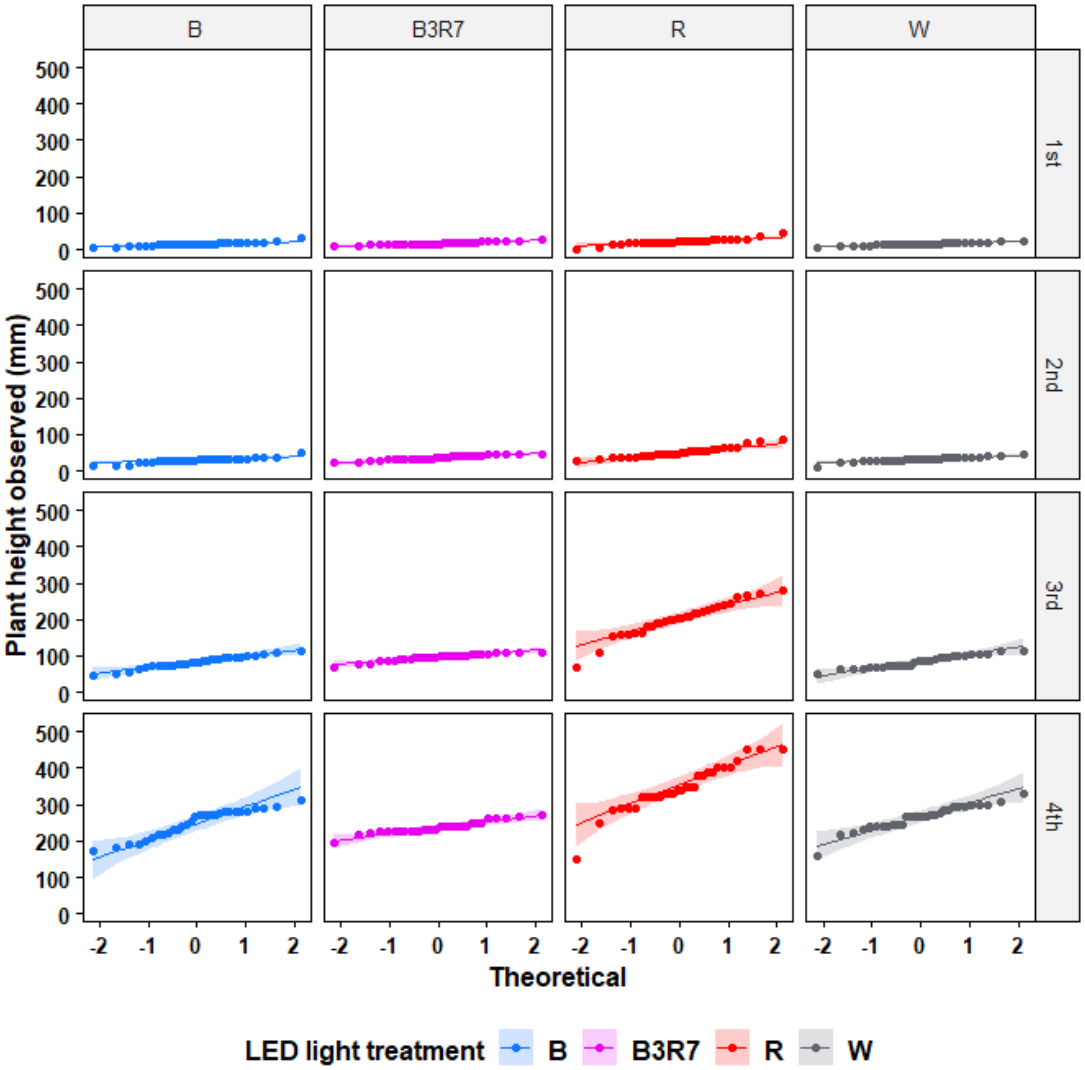


**Figure S1.** The quantile-quantile plots of Wild Mint plant height under different LED sources, over time.

Evidence suggests unequal variances among treatments. Therefore, the non-parametric Kruskal-Wallis's test was used to compare the results of LED light treatments. For the post hoc test, the Dunn test with Benjamini-Hochberg correction was employed.

**Table S2.** The normality tests of the number of Wild Mint leaves under different LED sources, over time.

| Light treatment | | Shapiro-Wilk test | | | | | | | | Levene test (According to the time) | |
|---|---|---|---|---|---|---|---|---|---|---|---|
| | | 1st week | | 2nd week | | 3rd week | | 4th week | | | |
| | | W | p-value | W | p-value | W | p-value | W | p-value | F value | Pr(>F) |
| B | | 0.765 | 1.623e-05 | 0.826 | 2.019e-04 | 0.863 | 1.184e-03 | 0.909 | 0.014 | 1.989 | 0.120 |
| B3R7 | | 0.818 | 1.401e-04 | 0.830 | 2.470 e-04 | 0.852 | 6.939e-04 | 0.869 | 1.602e-03 | 1.115 | 0.346 |
| R | | 0.818 | 1.401e-04 | 0.852 | 6.877e-04 | 0.794 | 5.028e-05 | 0.909 | 0.014 | 3.381 | 0.021 * |
| W | | 0.680 | 8.192e-07 | 0.721 | 3.201e-06 | 0.860 | 1.014e-03 | 0.866 | 1.336 e-03 | 4.363 | 0.006 ** |
| Levene test (According to the experiment) | F value | 1.049 | | 2.145 | | 0.610 | | 1.720 | | | |
| | Pr(>F) | 0.374 | | 0.098 | | 0.610 | | 0.167 | | | |

** and ** Significant at the 0.05 and 0.01 probability level.*

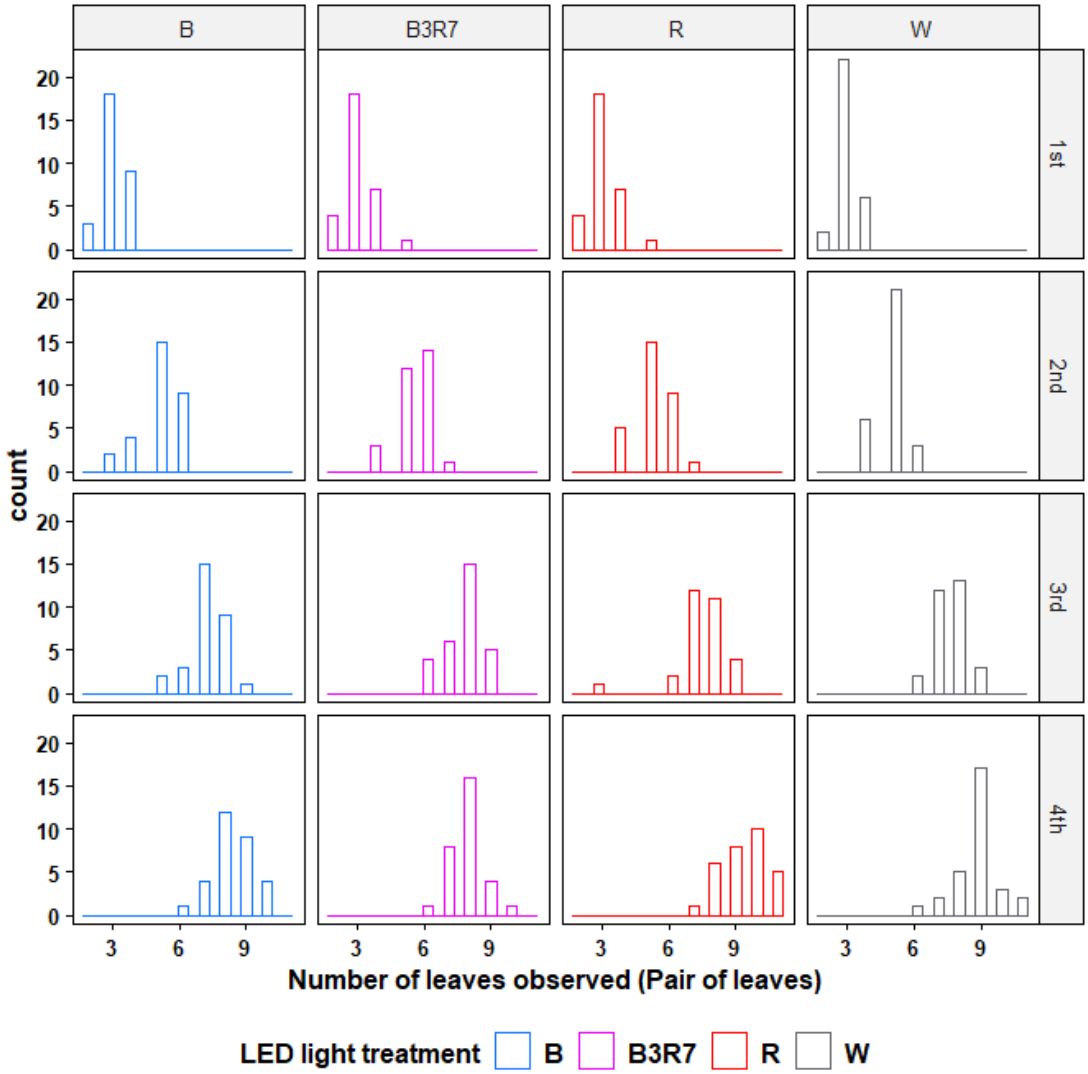


**Figure S2.** The histogram plots of the number of Wild Mint leaves under different LED sources, over time.

Evidence suggests unequal variances among treatments. Therefore, the non-parametric Kruskal-Wallis's test was used to compare the results of LED light treatments. For the post hoc test, the Dunn test with Benjamini-Hochberg correction was employed.

**Table S3.** The normality tests of the number of Wild Mint axillary bud under different LED sources, over time.

| Light treatment | | Shapiro-Wilk test | | | | | | | | Levene test (According to the time) | |
|---|---|---|---|---|---|---|---|---|---|---|---|
| | | 1st week | | 2nd week | | 3rd week | | 4th week | | | |
| | | W | p-value | W | p-value | W | p-value | W | p-value | F value | Pr(>F) |
| B | | - | - | 0.896 | 0.007 | 0.855 | 0.001 | 0.877 | 0.003 | 14.888 | 2.907e-08 *** |
| B3R7 | | - | - | 0.886 | 0.004 | 0.753 | 1.031e-05 | 0.810 | 9.879e-05 | 9.761 | 8.575e-06 *** |
| R | | - | - | 0.851 | 0.001 | 0.890 | 0.005 | 0.881 | 0.003 | 13.973 | 7.726e-08 *** |
| W | | - | - | 0.918 | 0.024 | 0.846 | 0.001 | 0.810 | 0.001 | 12.187 | 5.457e-07 *** |
| Levene test (According to the experiment) | F value | - | | 0.770 | | 1.385 | | 1.504 | | | |
| | Pr(>F) | - | | 0.513 | | 0.251 | | 0.2173 | | | |

*** *Significant at the 0.001 probability level.*

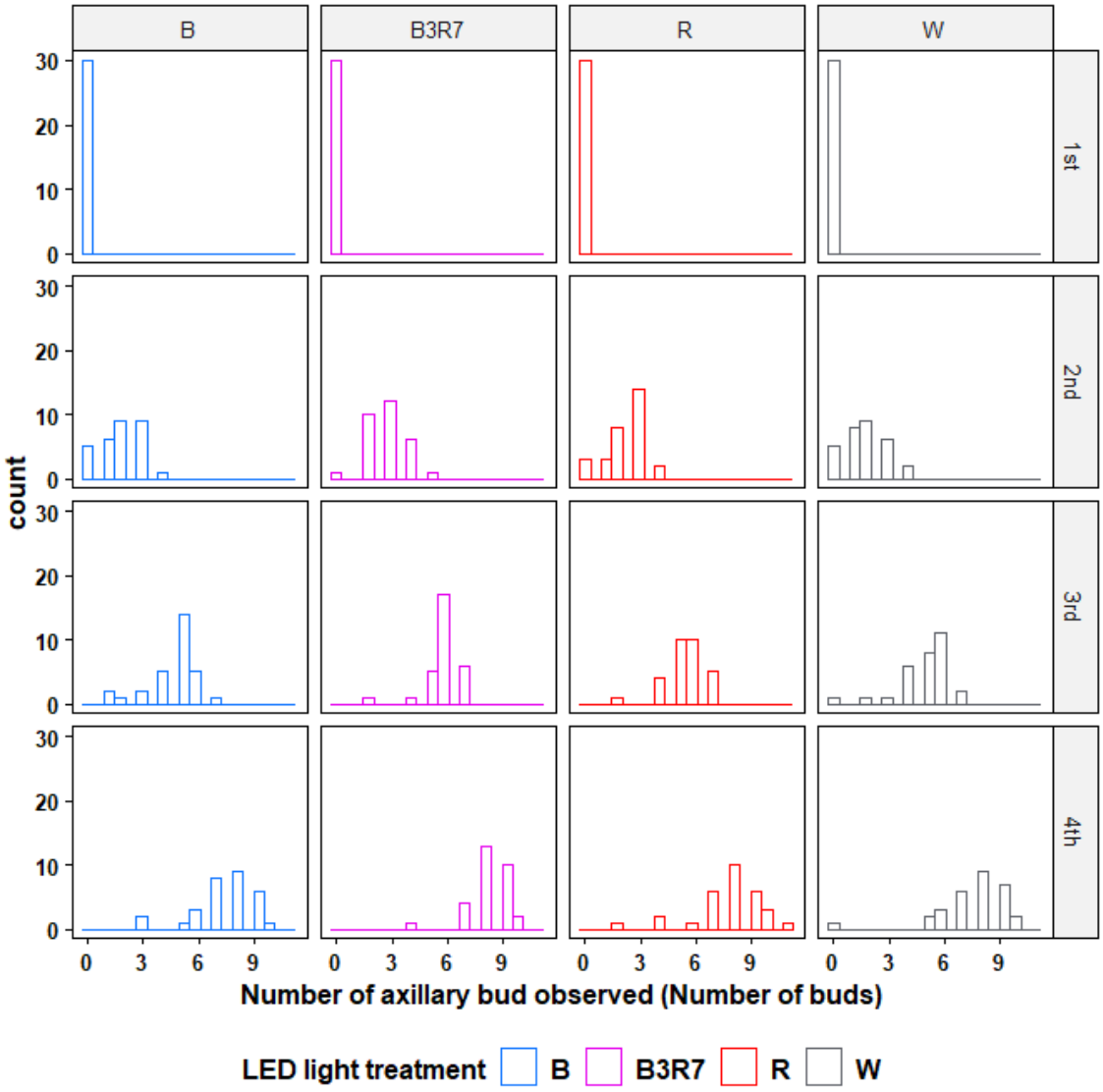


**Figure S3.** The histogram plots of the number of Wild Mint axillary bud under different LED sources, over time.

Evidence suggests unequal variances among treatments. Therefore, the non-parametric Kruskal-Wallis's test was used to compare the results of LED light treatments. For the post hoc test, the Dunn test with Benjamini-Hochberg correction was employed.

**Table S4.** The normality tests of Wild Mint fresh weight under different LED sources.

| Light treatment | | Shapiro-Wilk test | | | | | | | |
|---|---|---|---|---|---|---|---|---|---|
| | | Root | | Stem | | Leaves | | Total plant | |
| | | W | p-value | W | p-value | W | p-value | W | p-value |
| B | | 0.8834 | 0.3534 | 0.8323 | 0.1737 | 0.8165 | 0.1352 | 0.7072 | 0.0141 |
| B3R7 | | 0.8350 | 0.1812 | 0.9325 | 0.6094 | 0.9591 | 0.7735 | 0.9646 | 0.8080 |
| R | | 0.7432 | 0.0333 | 0.8314 | 0.1716 | 0.7530 | 0.0420 | 0.8650 | 0.2821 |
| W | | 0.9205 | 0.5400 | 0.79500 | 0.0935 | 0.7735 | 0.0626 | 0.8961 | 0.4118 |
| Levene test | F value | 4.5617 | | 35.236 | | 4.6684 | | 4.383 | |
| (According to the experiment) | Pr(>F) | 0.0236 * | | 3.145e-06 *** | | 0.0220 * | | 0.0266 * | |

** and *** Significant at the 0.05 and 0.001 probability level.*

**Table S5.** Normal distribution test of 6-week-old Wild Mint leaves data, at different locations.

| Leaf position | | Shapiro-Wilk test | | | | | | | |
|---|---|---|---|---|---|---|---|---|---|
| | | Fresh weight | | Dry weight | | Leaves area | | Chlorophyll content index | |
| | | W | p-value | W | p-value | W | p-value | W | p-value |
| 2 | | 0.9492 | 0.5112 | 0.9433 | 0.4260 | 0.8737 | 0.0382 | - | - |
| 3 | | 0.9346 | 0.3190 | 0.9550 | 0.5994 | 0.8390 | 0.0122 | 0.9434 | 0.4274 |
| 4 | | 0.9521 | 0.5586 | 0.9901 | 0.9995 | 0.7213 | 0.0004 | 0.9510 | 0.5401 |
| 5 | | 0.9550 | 0.6062 | 0.9552 | 0.6104 | 0.8181 | 0.0063 | 0.9189 | 0.1854 |
| 6 | | 0.9464 | 0.4693 | 0.9670 | 0.8110 | 0.9384 | 0.3623 | 0.9149 | 0.1611 |
| 7 | | 0.9684 | 0.8343 | 0.9606 | 0.7035 | 0.9603 | 0.6969 | 0.9263 | 0.2397 |
| 8 | | 0.9205 | 0.1960 | 0.9065 | 0.1195 | 0.9356 | 0.3297 | 0.9563 | 0.6290 |
| 9 | | 0.9350 | 0.3234 | 0.8939 | 0.0768 | 0.9683 | 0.8324 | 0.8774 | 0.0434 |
| Levene test | F value | 3.5358 | | 4.8405 | | 1.2761 | | 1.9743 | |
| | Pr(>F) | 0.0018 ** | | 8.564e-05 *** | | 0.2686 | | 0.0766 | |

*** and **** Significant at the 0.01 and 0.001 probability level.*

Evidence suggests unequal variances among treatments. Therefore, the non-parametric Kruskal-Wallis's test was used to compare the results of LED light treatments. For the post hoc test, the Dunn test with Benjamini-Hochberg correction was employed.

**Table S6.** The normality tests of Chlorophyll Content Index (CCI) value in Wild Mint leaves under different LED sources.

| Light treatment | Shapiro-Wilk test | | Levene test | |
|---|---|---|---|---|
| | W | p-value | F value | Pr(>F) |
| B | 0.96067 | 0.8165 | 1.7526 | 0.1791 |
| B3R7 | 0.97067 | 0.9032 | | |
| R | 0.90642 | 0.3295 | | |
| W | 0.89406 | 0.2552 | | |

** Significant at the 0.05 probability level*

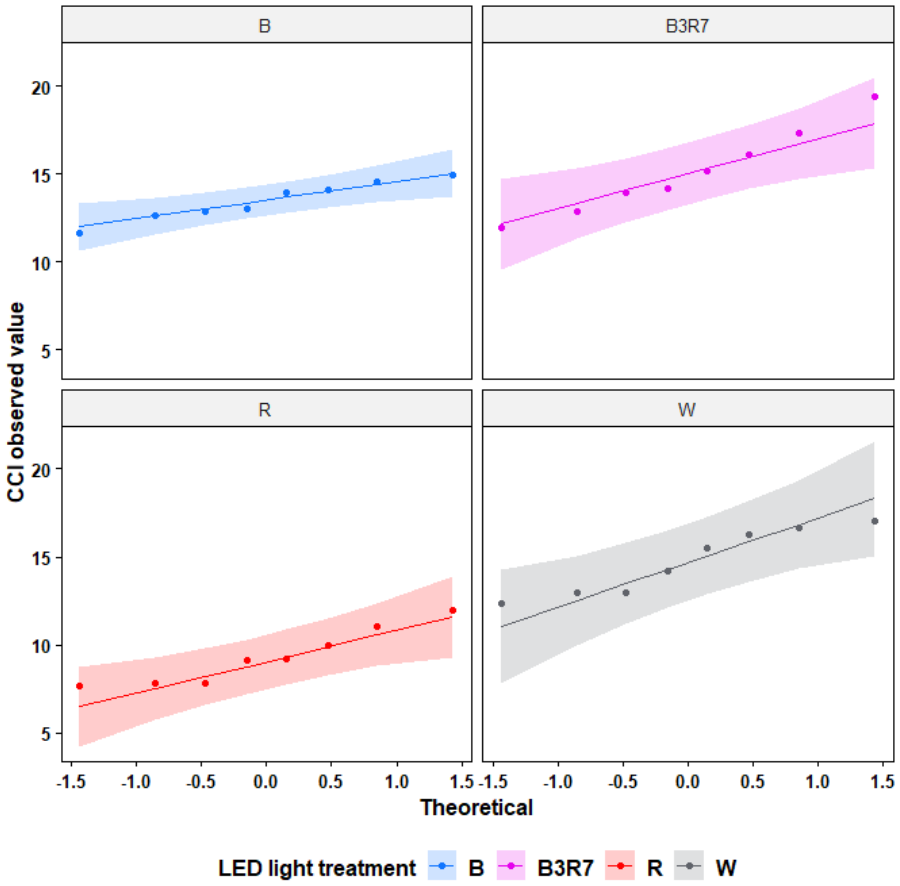


**Figure S4.** The quantile-quantile plots of Chlorophyll Content Index (CCI) in Wild Mint leaves under different LEDs sources.

Since the data satisfy the normal distribution condition, the parametric analysis of variance (ANOVA) test was used to compare the results of LED light treatments. For the post hoc test, Tukey's test correction was applied.

**Table S7.** The normality tests of Anthocyanins content in Wild Mint leaves under different LED sources.

| Light treatment | Shapiro-Wilk test | | Levene test | |
|---|---|---|---|---|
| | W | p-value | F value | Pr(>F) |
| B | 0.9419 | 0.6302 | 1.9866 | 0.1388 |
| B3R7 | 0.8712 | 0.1547 | | |
| R | 0.9471 | 0.6816 | | |
| W | 0.9281 | 0.4989 | | |

** Significant at the 0.05 probability level*

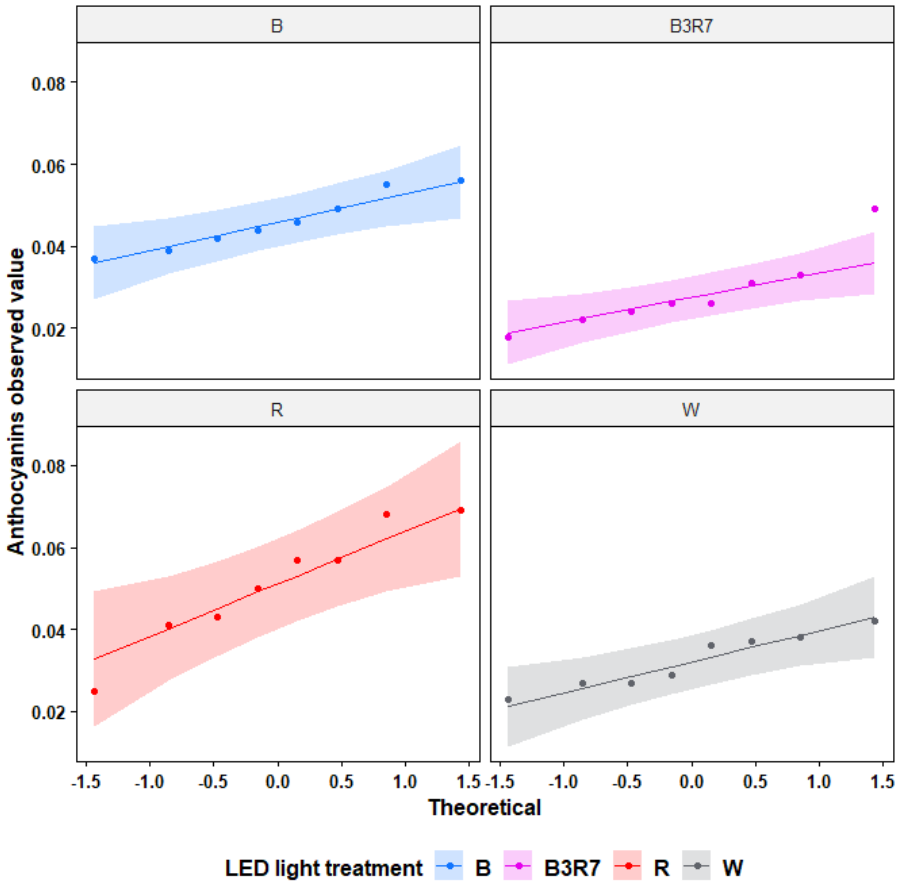


**Figure S5.** The quantile-quantile plots of Anthocyanins content in Wild Mint leaves under different LEDs sources.

Since the data satisfy the normal distribution condition, the parametric analysis of variance (ANOVA) test was used to compare the results of LED light treatments. For the post hoc test, Tukey's test correction was applied.

**Table S8.** The normality tests of Flavonoids content in Wild Mint leaves under different LED sources.

| Light treatment | Shapiro-Wilk test | | Levene test | |
|---|---|---|---|---|
| | W | p-value | F value | Pr(>F) |
| B | 0.9051 | 0.3207 | 2.6353 | 0.0693 |
| B3R7 | 0.9570 | 0.7810 | | |
| R | 0.9442 | 0.6529 | | |
| W | 0.8018 | 0.0299 | | |

** Significant at the 0.05 probability level*

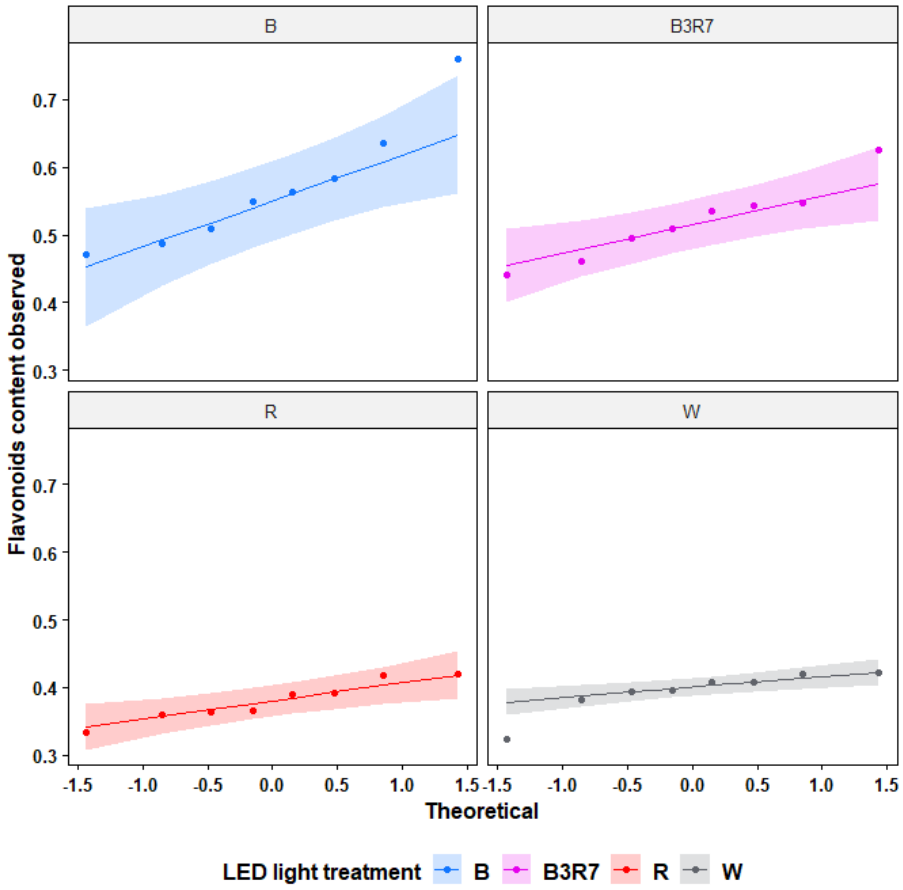


**Figure S6.** The quantile-quantile plots of Flavonoids content in Wild Mint leaves under different LEDs sources.

Evidence suggests that the data did not satisfy the normal distribution condition. As a result, the non-parametric Kruskal-Wallis's test was used to compare the results of LED light treatments. For the post hoc test, the Wilcoxon test with correction was applied.

**Table S9.** The normality tests of Nitrogen Balance Index (NBI) value in Wild Mint leaves under different LED sources.

| Light treatment | Shapiro-Wilk test | | Levene test | |
|---|---|---|---|---|
| | W | p-value | F value | Pr(>F) |
| B | 0.8995 | 0.2862 | 2.369 | 0.0920 |
| B3R7 | 0.9787 | 0.9562 | | |
| R | 0.9667 | 0.8709 | | |
| W | 0.9236 | 0.4600 | | |

** Significant at the 0.05 probability level*

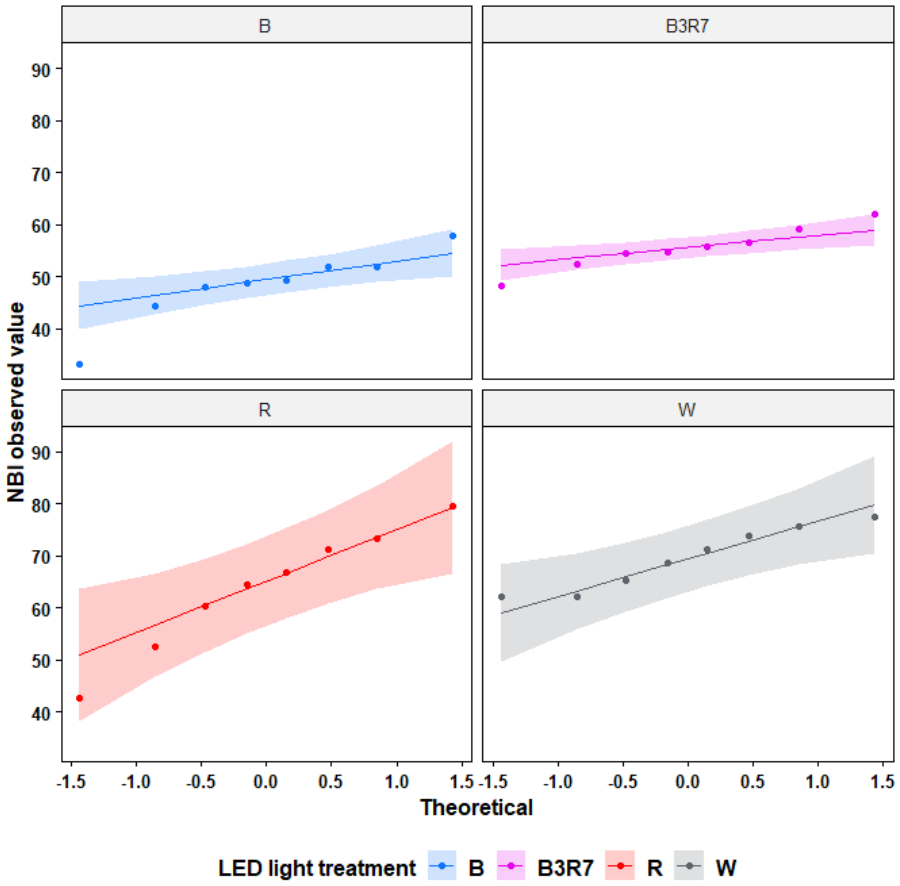


**Figure S7.** The quantile-quantile plots of Nitrogen Balance Index (NBI) in Wild Mint leaves under different LEDs sources.

Since the data satisfy the normal distribution condition, the parametric analysis of variance (ANOVA) test was used to compare the results of LED light treatments. For the post hoc test, Tukey's test correction was applied.

**Table S10.** The normality tests of $F_v/F_m$ value in Wild Mint leaves under different LED sources.

| Light treatment | Shapiro-Wilk test | | Levene test | |
|---|---|---|---|---|
| | W | p-value | F value | Pr(>F) |
| B | 0.9198 | 0.4283 | 6.5781 | 0.0017 ** |
| B3R7 | 0.8600 | 0.1199 | | |
| R | 0.8130 | 0.0394 | | |
| W | 0.7230 | 0.0041 | | |

*** Significant at the 0.01 probability level*

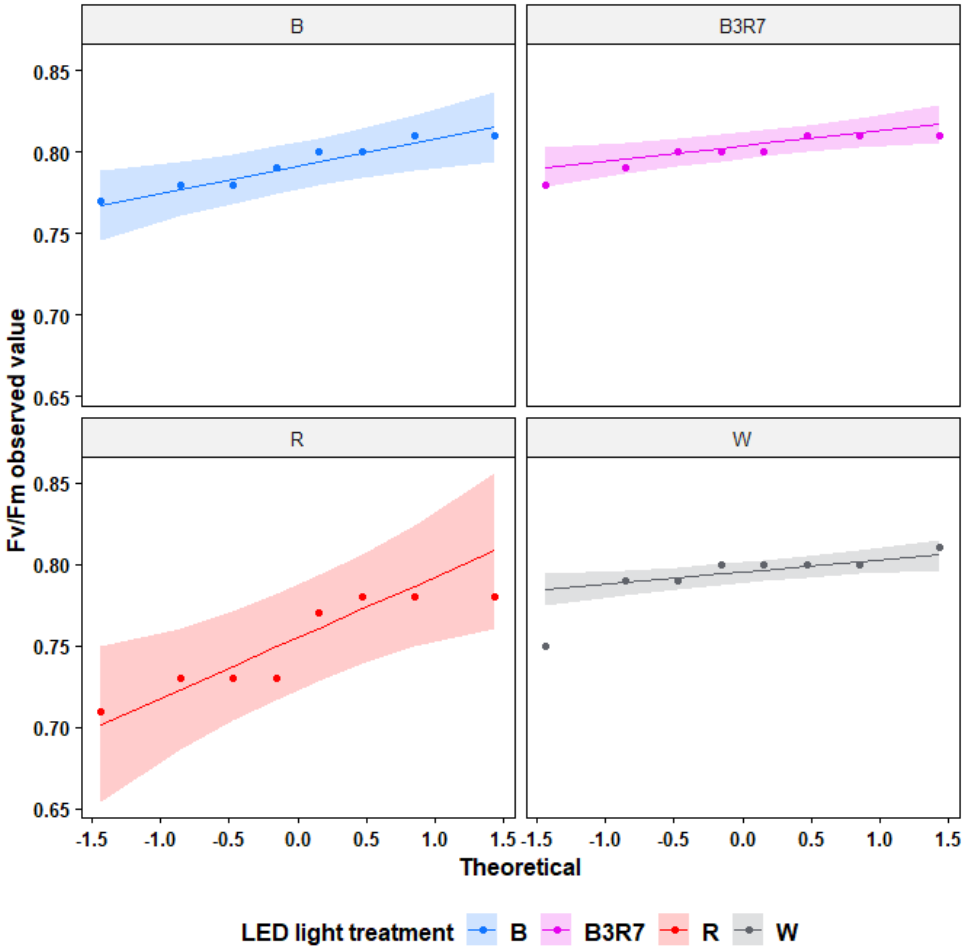


**Figure S8.** The quantile-quantile plots of maximal quantum yield of PSII ($F_v/F_m$) in Wild Mint leaves under different LEDs sources.

Evidence suggests that the data did not satisfy the normal distribution condition. As a result, the non-parametric Kruskal-Wallis's test was used to compare the results of LED light treatments. For the post hoc test, the Wilcoxon test with correction was applied.

**Table S11.** The normality tests of qP value in Wild Mint leaves under different LED sources.

| Light treatment | Shapiro-Wilk test | | Levene test | |
|---|---|---|---|---|
| | W | p-value | F value | Pr(>F) |
| B | 0.8846 | 0.2083 | 1.1627 | 0.3415 |
| B3R7 | 0.9551 | 0.7620 | | |
| R | 0.89700 | 0.2713 | | |
| W | 0.9221 | 0.4470 | | |

** Significant at the 0.05 probability level*

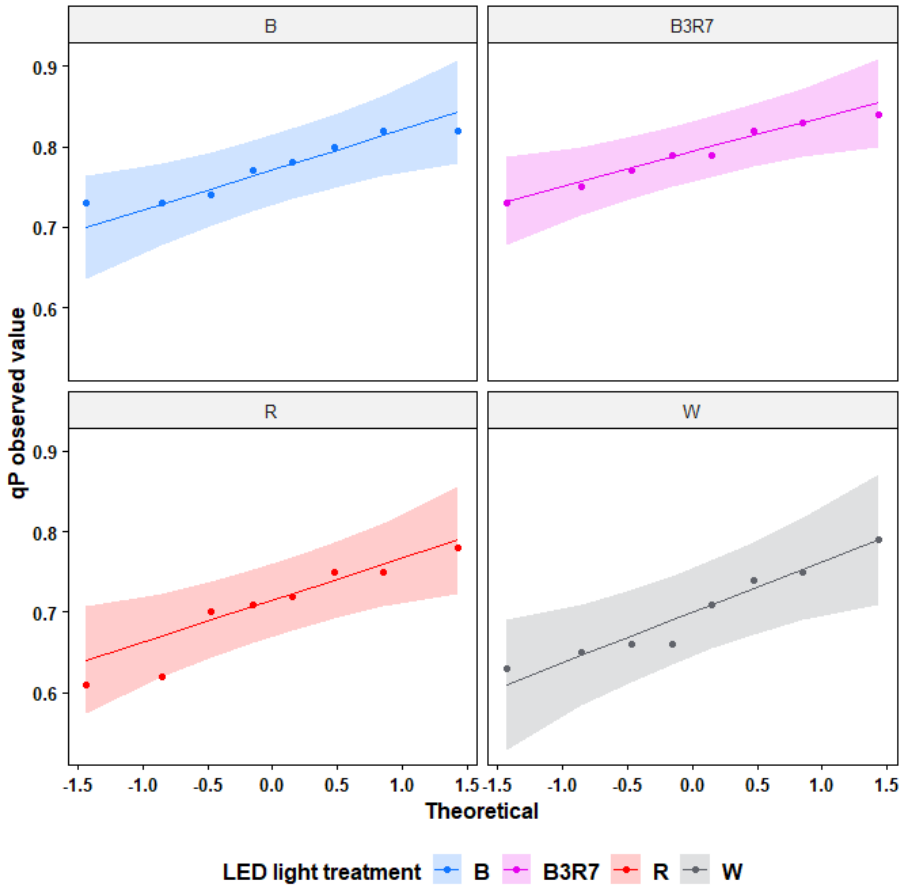


**Figure S9.** The quantile-quantile plots of photochemical fluorescence quenching coefficient (qP) in Wild Mint leaves under different LEDs sources.

Since the data satisfy the normal distribution condition, the parametric analysis of variance (ANOVA) test was used to compare the results of LED light treatments. For the post hoc test, Tukey's test correction was applied.

**Table S12.** The normality tests of qN value in Wild Mint leaves under different LED sources.

| Light treatment | Shapiro-Wilk test | | Levene test | |
|---|---|---|---|---|
| | W | p-value | F value | Pr(>F) |
| B | 0.9206 | 0.4345 | 0.9053 | 0.451 |
| B3R7 | 0.9205 | 0.4337 | | |
| R | 0.9478 | 0.6886 | | |
| W | 0.8920 | 0.2440 | | |

** Significant at the 0.05 probability level*

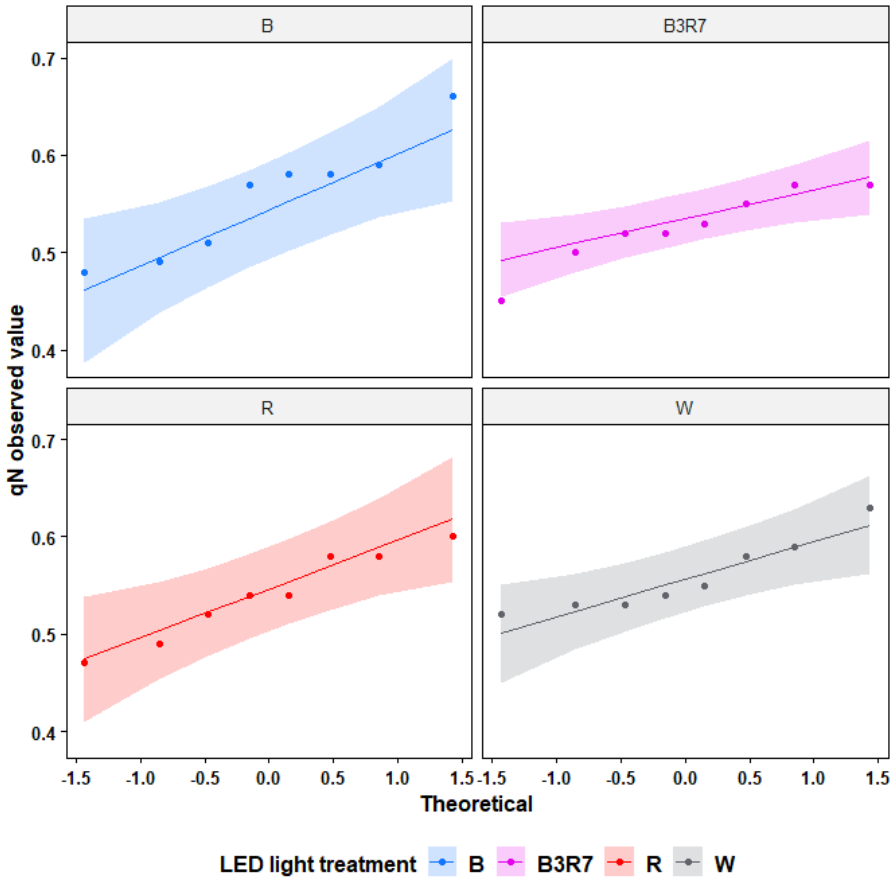


**Figure S10.** The quantile-quantile plots of non-photochemical fluorescence quenching coefficient (qN) in Wild Mint leaves under different LEDs sources.

Since the data satisfy the normal distribution condition, the parametric analysis of variance (ANOVA) test was used to compare the results of LED light treatments. For the post hoc test, Tukey's test correction was applied.

**Table S13.** The normality tests of ETR value in Wild Mint leaves under different LED sources.

| Light treatment | Shapiro-Wilk test | | Levene test | |
|---|---|---|---|---|
| | W | p-value | F value | Pr(>F) |
| B | 0.8730 | 0.1613 | 1.2785 | 0.3009 |
| B3R7 | 0.9348 | 0.5612 | | |
| R | 0.9200 | 0.4301 | | |
| W | 0.9111 | 0.3622 | | |

** Significant at the 0.05 probability level*

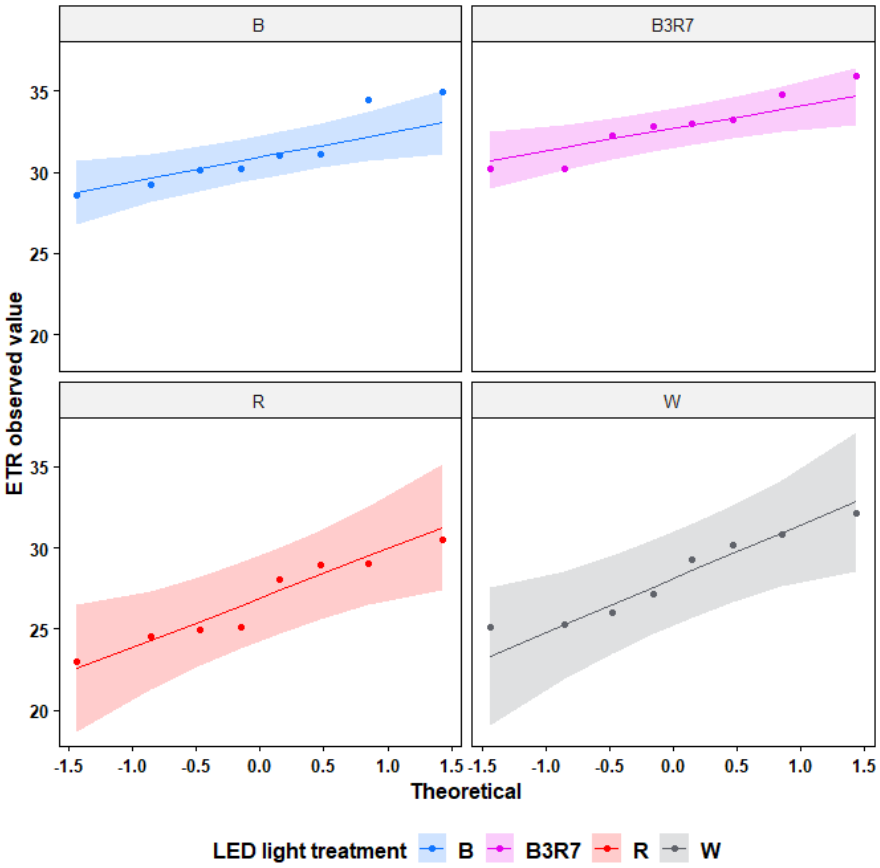


**Figure S11.** The quantile-quantile plots of electron transfer rate (ETR) in Wild Mint leaves under different LEDs sources.

Since the data satisfy the normal distribution condition, the parametric analysis of variance (ANOVA) test was used to compare the results of LED light treatments. For the post hoc test, Tukey's test correction was applied.

**Table S14.** The normality tests of Wild Mint leaves and plant area under different LED sources.

| Light treatment | | Shapiro-Wilk test | | | | | | | |
|---|---|---|---|---|---|---|---|---|---|
| | | $5^{th}$ leaves area | | Total leaves area | | Plant area | | Plant convex hull | |
| | | W | p-value | W | p-value | W | p-value | W | p-value |
| B | | 0.8383 | 0.1261 | 0.9794 | 0.9313 | 0.78567 | 0.0789 | 0.8836 | 0.3543 |
| B3R7 | | 0.9615 | 0.8309 | 0.8387 | 0.1614 | 0.8170 | 0.1364 | 0.7987 | 0.0999 |
| R | | 0.9593 | 0.8139 | 0.9030 | 0.4266 | 0.9643 | 0.806 | 0.9395 | 0.6513 |
| W | | 0.9376 | 0.6401 | 0.9168 | 0.5097 | 0.9704 | 0.844 | 0.8908 | 0.3868 |
| Levene test | F value | 2.1468 | | 0.1262 | | 1.8481 | | 0.9197 | |
| (According to the experiment) | Pr(>F) | 5.1054 | | 0.1144 | | 0.1922 | | 0.4607 | |

**Acknowledgements**

With all due respect, I would like to express my sincere gratitude to my advisor, Prof. Yong-Suk Chung, who gave me this wonderful opportunity to pursue a Ph.D. in his lab. During this journey, he guided me to raise hypotheses and carry out a research project. He also instilled in me a love for science and helped shape my attitude to be humbler and more responsible. I extend my heartfelt gratitude to him for his excellent advice, patience, guidance, and vast knowledge.

I would also like to express my deepest gratitude to Prof. Dong-soon Kim, Prof. Ju-Sung Kim, Prof. Won-Pyo Park, and Prof. Yong-Chull Jeun, who imparted invaluable knowledge to me and enriched my understanding through their lectures. I am also grateful to my thesis defense committee members, including Prof. Yong-Chull Jeun, Prof. In-Jung Kim, Prof. Jin-Hyun Anh, Prof. Jong-Eun Park for their invaluable advice in reviewing my thesis.

My sincere thanks go to Prof. Gyung-Deok Han, Dr. Thanh-Tuan Thai, and Dr. Sheikh Mansoor, who taught me about statistics analysis, image processing, and scientific report writing. Thanks to their valuable advice, support, and kind nature.

I extend my acknowledgments to my labmates: Dr. Ji-Eun Park, Ki-Bon Ku, E.M.B.M.Karunathilake, Jeong Min Choi, and Ji-Hyeon Jung, for their support in various ways during my academic journey.

A special note of gratitude goes to all Vietnamese student members, with particular thanks to Phan Phuong Thao Doan and Nguyen-Chuong Nguyen for standing by my side through both good and challenging times.

Last but certainly not least, I wish to convey my profound gratitude and appreciation to my family and Dr. Van-Ve Le for their unconditional love and care throughout my extended period of study. Your constant encouragement, belief in me, and allowing me to pursue my own path have made my achievements meaningful.